



Universität Hamburg

DER FORSCHUNG | DER LEHRE | DER BILDUNG

FACULTY

OF MATHEMATICS, INFORMATICS  
AND NATURAL SCIENCES

University of Hamburg

Faculty of Mathematics, Informatics and Natural Sciences

---

# **Generation and analysis of anti-ganglioside antibodies for the immunotherapeutic treatment of high-risk neuroblastoma**

---

Dissertation submitted to the University of Hamburg by

Laura Rekowski

A thesis submitted for the degree of  
Doctor of Natural Sciences (Dr. rer. nat.)

Hamburg 2023

Submitted on September 18, 2023

Supervisor:

Prof. Dr. Ingo Müller

Department of Pediatric Hematology and Oncology, Pediatric Stem Cell Transplantation and Immunology; University Medical Center, Hamburg-Eppendorf

Co-Supervisor:

Prof. Dr. Wolfram Brune

Department of Virus-Host Interactions, Leibniz-Institute of Virology, Hamburg

Thesis defense on 24<sup>th</sup> November 2023

Committee members

1. Prof. Dr. Wolfgang Maison

2. Prof. Dr. Ingo Müller

3. Prof. Dr. Michael Kolbe

The experimental research for this thesis was conducted between October 2019 and May 2023 within the research group of Prof. Dr. Ingo Müller at the Research Institute Children's Cancer Center Hamburg. The research group is affiliated with the UKE (University Medical Center Hamburg-Eppendorf) and is part of the Department of Pediatric Hematology and Oncology, specifically within the Division of Pediatric Stem Cell Transplantation and Immunology.

## List of Publications

Kruchen, A., Johann, P. D., Rekowski, L., & Müller, I. (2023). Epigenetic Modification of Mesenchymal Stromal Cells Derived from Bone Marrow and Embryonal Tumors to Facilitate Immunotherapeutic Approaches in Pediatric Malignancies. *Current issues in molecular biology*, 45(3), 2121–2135. <https://doi.org/10.3390/cimb45030136>

## I. Table of contents

<b>1</b>	<b>ABSTRACT</b> .....	<b>1</b>
<b>2</b>	<b>GERMAN ABSTRACT</b> .....	<b>2</b>
<b>3</b>	<b>INTRODUCTION</b> .....	<b>4</b>
3.1	NEUROBLASTOMA .....	4
3.1.1	<i>Epidemiology and classification</i> .....	4
3.1.2	<i>Clinical manifestation</i> .....	5
3.1.3	<i>Molecular characteristics</i> .....	6
3.1.4	<i>Treatment options</i> .....	7
3.2	IMMUNOGLOBULINS AND THEIR ROLE IN IMMUNITY .....	9
3.2.1	<i>Structure of immunoglobulins</i> .....	9
3.2.2	<i>Functions of immunoglobulins in the adaptive immune response</i> .....	11
3.2.3	<i>Immunotherapeutic approaches against cancer</i> .....	13
3.3	GANGLIOSIDES .....	13
3.3.1	<i>Classification and biosynthesis</i> .....	14
3.3.2	<i>General function and their role in disease</i> .....	16
3.3.3	<i>Discovery of GM2 as potential antigen for neuroblastoma immunotherapy</i> .....	17
<b>4</b>	<b>AIMS OF THE WORK</b> .....	<b>18</b>
<b>5</b>	<b>RESULTS</b> .....	<b>20</b>
5.1	GANGLIOSIDE EXPRESSION ON TUMOR CELLS .....	20
5.2	EXPRESSION OF GD2 AND GM2 IN CLINICAL SPECIMENS FROM NEUROBLASTOMA PATIENTS .....	21
5.3	GENERATION OF NEUROBLASTOMA CELL LINES DEPLETED FROM GM2 AND GD2 .....	23
5.4	IDENTIFICATION OF ANTIBODY SEQUENCES RECOGNIZING THE TUMOR ANTIGEN GM2 .....	25
5.5	EXPRESSION AND STABILITY OF ANTI-GM2 ANTIBODIES .....	29
5.6	BINDING OF ANTI-GM2 ANTIBODIES TO GANGLIOSIDE TEST STRIPES AND CELL LINES .....	32
5.7	EVALUATION OF <i>IN VITRO</i> EFFECTOR FUNCTIONS OF ANTI-GM2 ANTIBODIES .....	36
5.8	<i>IN VIVO</i> TESTING OF GM2-AB3 IGG .....	40
<b>6</b>	<b>DISCUSSION</b> .....	<b>44</b>
6.1	ANALYSIS OF GD2 AND GM2 EXPRESSION ON TUMOR CELL LINES <i>IN VITRO</i> .....	44
6.1.1	<i>Variability of ganglioside expression on neuroblastoma cell lines</i> .....	44
6.1.2	<i>Changes in ganglioside composition on neuroblastoma cells following B4GALNT1 knockout</i> ..	46
6.2	RELEVANCE OF <i>IN VIVO</i> GM2 EXPRESSION FOR THE TREATMENT OF NEUROBLASTOMA .....	47
6.2.1	<i>Different isoforms of GM2 complicate the detection by antibodies with different specificities</i> ...	47
6.2.2	<i>The ganglioside composition is influenced by extrinsic and intrinsic factors</i> .....	48
6.2.3	<i>Limitations in the detection of gangliosides in human samples</i> .....	50
6.3	PERFORMANCE ANALYSIS OF DIFFERENT ANTI-GM2 ANTIBODIES .....	51
6.3.1	<i>Differential expression and stability of anti-GM2 antibodies and isotypes</i> .....	51
6.3.2	<i>The recognition of GM2 varied between the different anti-GM2 antibodies</i> .....	54
6.3.3	<i>GM2-AB3 IgG showed superior cytotoxic potential</i> .....	57
6.3.4	<i>Suppression of tumor growth through treatment with GM2-AB3 IgG in a humanized mice</i> .....	60
6.4	CONCLUSION .....	61
<b>7</b>	<b>OUTLOOK</b> .....	<b>63</b>
<b>8</b>	<b>MATERIAL</b> .....	<b>64</b>
8.1	INSTRUMENTS .....	64

8.2	LABORATORY CONSUMABLES.....	64
8.3	CHEMICALS, REAGENTS, AND SOLUTIONS .....	65
8.4	CELL CULTURE MEDIA AND BUFFER.....	66
8.5	CELL LINES .....	67
8.6	KITS .....	68
8.7	ENZYMES AND BUFFERS.....	68
8.8	OLIGONUCLEOTIDES .....	69
8.9	PLASMIDS.....	71
8.10	ANTIBODIES.....	72
8.11	SOFTWARE AND TOOLS .....	73
<b>9</b>	<b>METHODS.....</b>	<b>74</b>
9.1	CELL CULTURE.....	74
9.2	CLONING.....	74
9.2.1	<i>Generation of plasmids for the expression of anti-GM2 IgG and IgM antibodies .....</i>	<i>75</i>
9.2.2	<i>Plasmid construction for CRISPR/Cas9-based knockout strategy.....</i>	<i>77</i>
9.3	PRODUCTION OF LENTIVIRAL PARTICLES AND TRANSDUCTION.....	78
9.4	ISOLATION OF HUMAN CD34 <sup>+</sup> STEM CELLS FROM BONE MARROW BLOOD.....	79
9.5	ANTIBODY PRODUCTION AND PURIFICATION .....	80
9.6	ANTIBODY VALIDATION <i>IN VITRO</i> .....	81
9.6.1	<i>Western Blot .....</i>	<i>81</i>
9.6.2	<i>Enzyme-linked immunosorbent assay (ELISA).....</i>	<i>81</i>
9.6.3	<i>Tycho stability measurement.....</i>	<i>82</i>
9.6.4	<i>Flow cytometry.....</i>	<i>82</i>
9.6.5	<i>Ganglioside test stripes.....</i>	<i>82</i>
9.6.6	<i>Complement-dependent cytotoxicity assay .....</i>	<i>83</i>
9.6.7	<i>Antibody-dependent cellular cytotoxicity assay.....</i>	<i>83</i>
9.7	MOUSE EXPERIMENTS.....	84
9.7.1	<i>Animal maintenance, husbandry, and care.....</i>	<i>84</i>
9.7.2	<i>Treatment with the monoclonal anti-GM2 antibody .....</i>	<i>84</i>
9.8	STATISTICAL ANALYSIS.....	85
<b>10</b>	<b>REFERENCES.....</b>	<b>86</b>
<b>11</b>	<b>LIST OF FIGURES .....</b>	<b>102</b>
<b>12</b>	<b>LIST OF TABLES .....</b>	<b>103</b>
<b>13</b>	<b>APPENDIX .....</b>	<b>104</b>
13.1	APPENDIX A: SUPPLEMENTARY DATA.....	104
13.2	APPENDIX B: PLASMID GENE CARDS.....	108
13.3	APPENDIX C: HAZARDOUS SUBSTANCES.....	111
<b>14</b>	<b>ACKNOWLEDGEMENT.....</b>	<b>113</b>
<b>15</b>	<b>DECLARATION OF AUTHORSHIP .....</b>	<b>115</b>

## II. List of abbreviations

Abbreviation	Meaning
°C	Degree Celsius
µg	Microgram
µL	Microliter
µM	Micromolar
µm	Micrometer
2D	Two-dimensional
3D	Three-dimensional
A	Adenine
AB	Antibody
ADC	Antibody drug conjugates
ADCC	Antibody-dependent cellular cytotoxicity
ALK	Anaplastic lymphoma kinase
ALP	Alkaline phosphatase
amp	Ampicillin
APC	Allophycocyanine
AF647	Alexa Fluor 647
<i>B4GALNT1</i>	β-1,4-N-Acetyl-Galactosaminyltransferase 1 gene
B7-H3	B7 Homolog 3
BiTE	Bispecific T-cell engagers
BM	Bone marrow
bp	Base pair
BSA	Bovine serum albumin
BV	Brilliant Violet
C	Cytosine
C1q	Complement component 1q
CaCl <sub>2</sub>	Calcium chloride
CAR	Chimeric antigen receptor
Cas9	CRISPR-associated protein 9
Cat	Catalogue
CCTop	CRISPR / Cas9 target online predictor
CD	Cluster of differentiation
CDC	Complement-dependent cytotoxicity
cDNA	Complementary DNA
CDR	Complementary determining region
cGy	Centigray
CH	Constant heavy
CHO	Chinese Hamster Ovary
CL	Constant light
CO <sub>2</sub>	Carbon Dioxide
CRISPR	Clustered Regularly Interspaced Short Palindromic Repeats
Ctrl	Control

Abbreviation	Meaning
DMEM	Dulbecco's Modified Eagle Medium
DMSO	Dimethyl sulfoxide
DNA	Deoxyribonucleic acid
dNTP	Deoxynucleoside triphosphate
dTom	dTomato
DTT	Dithiothreitol
<i>E. coli</i>	Escherichia coli
E:T	Effector to target ratio
EBV	Epstein-Barr virus
EDTA	Ethylene diamine tetra acetate
EF-1α	Elongation factor 1 alpha
EFS	Event-free survival
ELISA	Enzyme-linked immunosorbent assay
ER	Endoplasmic reticulum
F	Female
F <sub>ab</sub>	Fragment antigen binding
FACS	Fluorescence Activated Cell Sorting
FBS	Fetal Bovine Serum
F <sub>c</sub>	Crystallisable fragment
F <sub>c</sub> R	Crystallisable fragment receptor
FITC	Fluorescein isothiocyanate
fw	Forward
G	Guanine
GalNAc	N-acetyl galactosamine
gDNA	Genomic DNA
GFP	Green fluorescent protein
GM-CSF	Granulocyte-macrophage colony-stimulating factor
GM2-AB	Anti-GM2 antibody
gMFI	Geometric mean fluorescence intensity
GPC2	Glypican 2
GT	Glycosyltransferase
h	Hours
H	Heavy chain
H <sub>2</sub> O	Water
HBS	HEPES-Buffered Saline
HEK	Human embryonic kidney
HEPES	4-(2-hydroxyethyl)-1-piperazineethanesulfonic acid
hHSC	Human hematopoietic stem cells
h.i.	Heat inactivated
HLA-I	Human leukocyte antigen class I

Abbreviation	Meaning
HRP	Horseradish peroxidase
ID	Initial diagnosis
i.v.	intravenously
Ig	Immunoglobulin
IL	Interleukin
indels	Insertions and deletions
INPS	International Neuroblastoma Pathology Classification
INRGSS	International Neuroblastoma Risk Group Staging System
INSS	International Neuroblastoma Staging System
IRES	Internal ribosome entry site
IU	International unit
IV	Individually ventilated
IVIS	<i>In vivo</i> imaging system
kb	Kilo base
kDa	Kilodaltons
KLD	Kinase, Ligase, Dpnl
KO	Knockout
L	Light chain
LacCer	Lactosylceramide
LB	Luria-Bertani
LDH	Lactate dehydrogenase
M	Molar mass
M	Months
mA	Milliampere
MAC	Membrane attack complex
MEM	Minimum Essential Medium Eagle
MES	2-(N-morpholino) ethanesulfonic acid
min	Minutes
mL	Milliliter
mM	Millimolar
MNC	Mononuclear cells
MOI	Multiplicity of infection
mRNA	Messenger ribonucleic acid
MWCO	Molecular weight cut off
NB	Neuroblastoma
NCAM	Neural cell adhesion molecule
Neu5Ac	N-acetyl-neuraminic acid
Neu5Gc	N-glycolyl-neuraminic acid
NH	Ammonium Sulfate
NK	Natural killer
No	Number
NSG-SGM3	NOD.Cg- <i>Prkdc<sup>scid</sup>Il2rg<sup>tm1Wjl</sup>Tg(CMV-IL3,CSF2,KITLG)1Eav/MloySz</i> J

Abbreviation	Meaning
nTPM	Normalized Transcripts per million
OS	Overall Survival
PBMC	Peripheral blood mononuclear cells
PBS	Phosphate Buffered Saline
PCR	Polymerase Chain Reaction
PD	Patient-derived
PE	Phycoerythrin
Pen/Step	Penicillin/Streptomycin
PFA	Paraformaldehyde
pH	Potentia hydrogenii
<i>PHOX2B</i>	Paired-like homeobox 2B
PI	Propidium Iodide
PIPE	Polymerase Incomplete Primer Extension
pmol	Picomol
PNK	Polynucleotide 5'-hydroxylkinase
pNPP	Para-nitrophenylphosphate
RNA	Ribonucleic acid
rpm	Revolutions per minute
RPMI Medium	Roswell Park Memorial Institute Medium
RT	Room temperature
rv	Reverse
s	Seconds
s.c.	subcutaneously
SD	Standard deviation
SDS	Sodium dodecyl sulfate
SDS-PAGE	Sodium dodecyl sulfate polyacrylamide gel electrophoresis
SEM	Standard error of the mean
sgRNA	Single guide RNA
SOC	Super Optimal broth with Catabolite repression
<i>ST8SIA1</i>	$\alpha$ -N-Acetylneuraminide $\alpha$ -2,8-Sialyltransferase gene
T	Thymine
TAE	Tris-acetate EDTA
Taq	<i>Thermus aquaticus</i>
TB	Tumor biopsy
TBS	Tris-buffered saline
TBS-T	Tris-buffered saline with 0.1% Tween20
TGF- $\beta$ RIII	Transforming growth factor receptor III
T <sub>i</sub>	Inflection temperature
TIDE	Tracking of Indels by DEcomposition

<b>Abbreviation</b>	<b>Meaning</b>
Tris	Tris(hydroxymethyl)aminomethane
UDP	Uridine diphosphate
UV	Ultraviolet
V	Volt
VH	Variable heavy
VL	Variable light

<b>Abbreviation</b>	<b>Meaning</b>
VSV-G	Vesicular stomatitis virus glycoprotein envelope
w/o	Without
WT	Wild type
x g	Standard acceleration due to gravity at the earth's surface
$\kappa$	Kappa
$\lambda$	Lambda

### 1 Abstract

Neuroblastoma (NB), originating from early neural crest cells, is the most prevalent solid cancer in children outside the brain and is characterized by a high clinical heterogeneity. It accounts for 6-10% of pediatric malignancies and causes 15% of childhood cancer-related mortality. Current treatment options for NB patients include surgery, chemotherapy, radiotherapy, autologous hematopoietic stem cell transplantation, and immunotherapy with the chimeric monoclonal antibody Dinutuximab, which targets the ganglioside GD2. Despite treatment advancements with Dinutuximab, high-risk patients still face a 5-year survival rate below 60%, and many patients still relapse. Additionally, severe side effects such as neuropathic pain, hypersensitivity reactions, and capillary leak syndrome often occur during Dinutuximab treatment and require additional medication. For this, there is an urgent need for new therapeutic approaches to improve prognosis and outcomes for NB patients.

Hence, we aimed to target gangliosides that are highly expressed on the surface of NB cells. After the discovery of naturally occurring antibodies recognizing the ganglioside GM2, this study focused on generating recombinant anti-GM2 antibodies and evaluating their potential for immunotherapeutic application in NB. We utilized five different available B cell receptor sequences (HuCAL, L55-81, KM966, US2011, DMF10.167.4) which were successfully cloned into expression plasmids. These antibodies were examined *in vitro* and compared based on their stability, antigen binding properties, and cytotoxic activity to determine their suitability as candidates for NB treatment. It was shown that the antibody clones exhibited varying degrees of stability, resulting in different binding specificities. While some antibodies failed to recognize the antigen, others successfully bound to NB and other tumor cell lines, as confirmed through flow cytometric analysis and with the help of knockout cell lines. Among the five antibodies tested, the GM2-AB3 IgG variant with the variable sequence KM966 showed superior antigen recognition and demonstrated potent and specific complement-dependent and antibody-dependent cell-mediated cytotoxicity against various NB cell lines, making it the most promising candidate. *In vivo* tests in a humanized mouse model further confirmed the antibody's effectiveness in inhibiting tumor growth and improving survival rates.

In conclusion, this research project highlights the potential of antibody-targeted attack on the ganglioside GM2 as an immunotherapeutic approach for NB. The study successfully identified a promising antibody clone, namely GM2-AB3 IgG with the variable sequence KM966. This antibody exhibited remarkable efficacy in eliminating NB cells expressing the target antigen and thereby provides new perspectives for enhancing NB treatment.

### 2 German abstract

Das Neuroblastom (NB), das aus Vorläuferzellen der Neuralleiste entsteht, ist die häufigste solide Krebsentität außerhalb des Gehirns bei Kindern und zeichnet sich durch eine hohe klinische Heterogenität aus. Es macht 6-10% der pädiatrischen Krebserkrankungen aus und verursacht 15% der krebisbedingten Sterblichkeit bei Kindern. Die derzeitigen Behandlungsmöglichkeiten für NB-Patienten umfassen Operationen, Chemo- und Strahlentherapien, autologe hämatopoetische Stammzelltransplantationen und eine Immuntherapie mit dem chimären monoklonalen Antikörper Dinutuximab, der das Gangliosid GD2 erkennt. Trotz der Behandlungsfortschritte mit Dinutuximab haben Hochrisiko-Patienten immer noch eine 5-Jahres-Überlebensrate von unter 60% und viele Patienten erleiden Rückfälle. Während der Behandlung treten außerdem häufig schwere Nebenwirkungen wie neuropathische Schmerzen, Überempfindlichkeitsreaktionen und das Kapillarleck-Syndrom auf, die mit zusätzlichen Medikamenten behandelt werden müssen. Deshalb besteht ein dringender Bedarf an neuen Therapieansätzen, um die Prognose und Ergebnisse für NB-Patienten zu verbessern.

Unser Ziel ist es daher Ganglioside, die auf der Oberfläche von NB-Zellen stark exprimiert werden, als Zielstrukturen für eine immuntherapeutische Behandlung mit Antikörpern anzugreifen. Basierend auf der Entdeckung von natürlich vorkommenden Antikörpern, die das Gangliosid GM2 erkennen, konzentrierte sich diese Studie darauf, rekombinante Antikörper gegen GM2 zu generieren und ihre potenzielle immuntherapeutische Anwendung beim NB zu evaluieren. Wir verwendeten fünf verschiedene verfügbare B-Zellrezeptorsequenzen (HuCAL, L55-81, KM966, US2011, DMF10.167.4), die erfolgreich in Expressionsplasmide kloniert wurden. Diese Antikörper wurden *in vitro* untersucht und hinsichtlich ihrer Stabilität, Antigenbindung und zytotoxischen Aktivität verglichen, um ihre Eignung als Kandidaten für die NB-Behandlung zu ermitteln. Es zeigte sich, dass die Antikörperklone unterschiedliche Stabilitätsgrade und Bindungsspezifitäten aufwiesen. Während einige Antikörper das Antigen nicht erkannten, konnten andere es erfolgreich auf NB- und anderen Tumorzelllinien binden, wie durch die durchflusszytometrische Analyse und mithilfe von *Knockout*-Zelllinien bestätigt wurde. Von den fünf getesteten Antikörpern zeigte die Antikörpervariante GM2-AB3 IgG mit der variablen Sequenz KM966 eine überlegene Antigenerkennung und eine starke sowie spezifische komplementvermittelte und antikörperabhängige zellvermittelte zytotoxische Wirkung gegen verschiedene NB-Zelllinien, wodurch dieser Antikörper zum vielversprechendsten Kandidaten wurde. Die *in vivo* Tests in einem humanisierten Mausmodell bestätigten zusätzlich die Wirksamkeit des Antikörpers bei der Hemmung des Tumorwachstums und der Verbesserung der Überlebensraten.

Zusammenfassend zeigt dieses Forschungsprojekt das Potenzial der zielgerichteten Antikörpertherapie gegen das Gangliosid GM2 beim NB. Die Studie konnte erfolgreich einen vielversprechenden Antikörperklon identifizieren, nämlich GM2-AB3 IgG, welcher die variable

Sequenz KM966 enthält. Dieser Antikörper zeigte eine sehr starke Wirksamkeit bei der Eliminierung von NB-Zellen, die das Zielantigen exprimieren und eröffnet somit neue Perspektiven für die Verbesserung der NB-Behandlung.

### 3 Introduction

#### 3.1 Neuroblastoma

The German physician Dr. Rudolf Virchow was the first to describe neuroblastoma (NB) in 1864. He initially referred to the tumor as a glioma occurring in the abdominal cavity of children. In 1910, James Homer Wright further elucidated the origin and characteristic features of the tumor and henceforth named it neuroblastoma [1].

##### 3.1.1 Epidemiology and classification

NB is the most common extracranial solid tumor in the pediatric population. It comprises 6-10% of all childhood cancers and is responsible for 15% of childhood cancer-related deaths [2]. The median disease onset is 15 months and 40% of the patients are younger than one year at diagnosis [3]. Usually, NB occurs sporadically but also familial cases are observed [4].

Due to the high clinical heterogeneity, NB patients are stratified into risk groups prior to treatment using the 'International Neuroblastoma Risk Group Staging System' (INRGSS). This staging system relies on statistical analysis of clinical criteria and tumor imaging to classify patients into low-, intermediate-, or high-risk pretreatment groups. The classification includes factors such as age, histological category, tumor differentiation grade, *MYCN* status, presence or absence of 11q aberrations, and tumor cell ploidy [5–7]. Patients with a 5-year event-free survival (EFS) prognosis exceeding 75% are categorized as low-risk patients. Those with a 5-year EFS rate between 50% and 75% are classified as intermediate-risk, while those with a 5-year EFS rate below 50% are considered high-risk. Locoregional tumors are staged as L1 and L2, while metastatic tumors are designated as stage M and MS. In stage MS, metastases are restricted to the skin, liver, and/or bone marrow in children younger than 18 months [5].

In addition to the INRGSS staging system, NB is classified into four different stages according to the 'International Neuroblastoma Staging System' (INSS). Unlike the INRGSS, the INSS takes into account the postsurgical status of the patient. Stage 1 and 2A are characterized by a localized tumor without involvement of lymph nodes, which can be completely or partially removed through surgery. In stage 2B, the tumor remains localized, but tumor cells are infiltrating the nearby lymph nodes. Stage 3 is characterized by an unresectable tumor infiltrating across the vertebral column or a localized tumor with metastasis in lymph nodes. When the tumor disseminates to distant lymph nodes and metastasis occur in different organs it is classified as stage 4 which is analogous to INRGSS stage M. An exceptional subgroup is stage 4S, a localized tumor with metastasis restricted to the skin, liver, and bone marrow, and typically occurring in infants under 12 months of age [8]. Tumors in this

group can undergo spontaneous regression without any treatment. A long-term clinical survey conducted by Tas *et al.* summarized the 5-year overall survival (OS) for patients across all stages, based on a cohort of 585 cases in the Netherlands (Figure 1). For patients with stages 1, 2 and 4S the 5-year OS was over 84%. For patients grouped in stage 3 or stage 4 it was 70% or 35%, respectively [9].

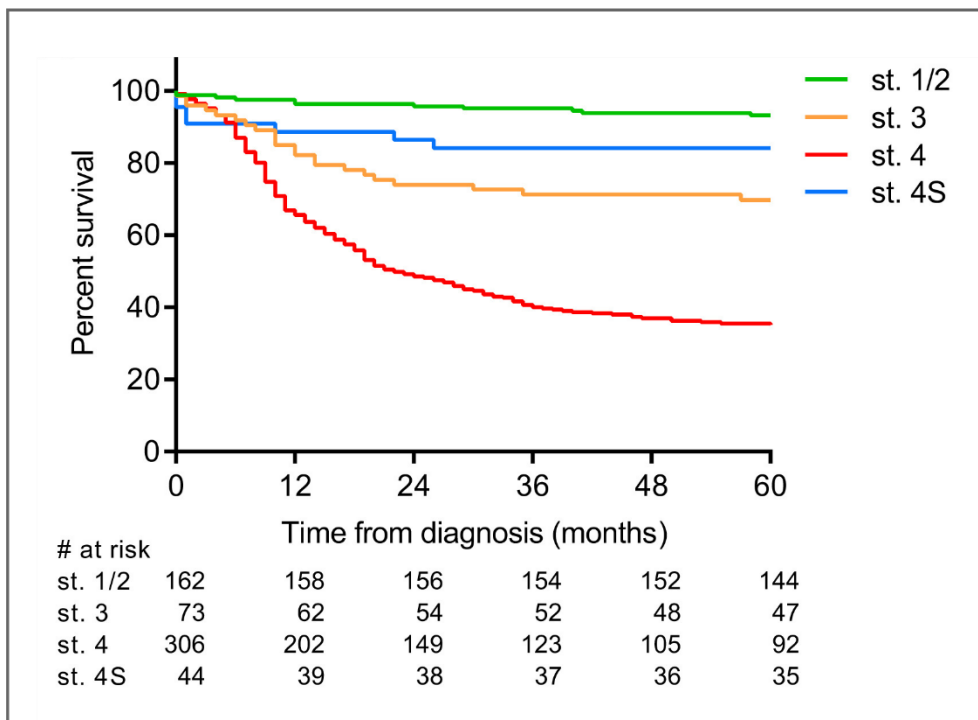


**Figure 1:** The illustration adapted from Tas *et al.* shows the Kaplan-Meier curves of the 5-year overall survival of neuroblastoma patients at different stages in the Netherlands between 1990 and 2014 [9].

A histopathological classification is made by the ‘International Neuroblastoma Pathology Classification’ (INPC) which groups neuroblastic tumors based on the patients’ age and morphologic characteristics of the tumors. This takes into account factors such as the differentiation grade of the neuroblasts, the cellular turnover index (mitosis-karyorrhexis index) and the presence of Schwannian stroma. NB is defined as a Schwannian stroma poor tumor and can be further grouped into undifferentiated, poorly differentiated, or differentiating subtype. Additionally, the INPC subtypes NB into two groups: a favorable histology group or an unfavorable histology group [10]. It has been shown that patients with tumors classified as having favorable histology had a 90% EFS, whereas those with tumors categorized as having unfavorable histology exhibit a lower EFS of 31% [11].

### 3.1.2 Clinical manifestation

NB is a malignancy of the sympatico-adrenal lineage that arises from neural crest progenitor cells, which are normally destined to develop into sympathetic ganglion and adrenal medulla cells [12]. This tumor type manifests alongside the sympathetic nervous system. Approximately, 65% of primary

NB originate within the abdomen, with the majority originating in the adrenal medulla [6]. Other primary tumor sites include paraspinal ganglia (25%), thorax (20%), pelvis (4%), or cervix (1%) [13]. At the time point of diagnosis, 51% of patients have a localized or regional NB (stage 1-3), while 38% are categorized as stage 4 with disseminated disease and 11% as stage 4S. Among stage 4 patients, metastasis to the bone marrow occur in 89% of cases. Further localizations of metastasis include bones (65%), lymph nodes (21%), liver (13%) and intracranial sites (6%) [3,6].

The clinical presentation of NB is very heterogeneous ranging from spontaneous regression to aggressive growth and metastasis. The underlying mechanisms behind spontaneous regression remain elusive. Depending on the tumor location and tumor burden, the manifestation of symptoms in patients varies. Children with localized disease typically present minimal symptoms, while those with bone metastases, for instance, may experience bone pain, limping, or irritability. The presence of a primary tumor often leads to visible abdominal swelling, which can be accompanied by difficulties in breathing or swallowing. Further symptoms may include weight loss and problems related to bowel movements or urination [14].

Due to the lack of specific symptoms and its heterogeneity, NB is often detected incidentally or through routine screenings [6]. Abdominal tumors are primarily identified by computer tomography. Diagnosis relies on multiple biological and genetic markers and histopathological analysis of tumor biopsies. In case of disseminated disease, bilateral bone marrow aspirates are examined to check the presence of tumor cells. Furthermore, blood and urine samples are analyzed to detect increased concentrations of catecholamine metabolites [6]. More than 90% of NB patients show elevated levels of those metabolites in urine samples. Elevated serum levels of lactate dehydrogenase (LDH) and ferritin can also be detected in approximately 60% and 36% of all NB patients, respectively.

#### 3.1.3 Molecular characteristics

NB is caused by the aberrant expression and dysregulation of developmental proteins which are normally epigenetically silenced in normal tissues after birth [15]. The mutational burden in NB is generally low but there are some common genetic alterations. More than half of the primary tumors exhibit hyperdiploidy or triploidy, characterized by a chromosome count ranging from 58 to 80. The *MYCN* oncogene, for instance, is amplified in 40% of patients under the age of 18 months with stage 4 NB, whereas in patients with localized NB, approximately 9% of tumors show *MYCN* amplification. *MYCN* amplification is associated with an unfavorable disease prognosis and poor outcome as implicated in Figure 1. Moreover, it is also linked to adrenal and nonthoracic tumor sites, an unfavorable histology, diploidy, 1p deletion and poorly differentiated tumors [16]. Another characteristic of advanced stage NB is the downregulation of transforming growth factor receptor III (TGF- $\beta$ RIII). Iolascon *et al.* demonstrated that TGF- $\beta$ RIII expression was present in 89%

of stage 1 NB samples and in 29% of stage 4 NB samples [17]. As observed in the majority of human tumors, NB is characterized by the absence of human leukocyte antigen class I (HLA-I) molecules. This downregulation is known to play a key role in evading CD8<sup>+</sup> T cell-mediated immune responses [18]. Deletion of 1p and loss of 11q are also associated with NB, occurring in approximately 28% and 40% of cases, respectively. Allelic loss of 11q can be found in tumors without *MYCN* amplification and is associated with a poor prognosis [19]. Furthermore, tyrosine kinase receptors which are involved in the development of the sympathetic nervous system play a role in NB pathogenesis. For instance, mutations in tropomyosin receptor kinase (Trk) A and TrkC are associated with a favorable disease outcome, whereas mutations in TrkB are usually expressed in advanced disease stages and tumors with *MYCN* amplification [20,21].

With 1-2% of all cases, familial NB is very rare and only a few inherited mutations are known. Examples for these are three germline missense mutations (G1128A, R1192P and R1275Q) located in the receptor tyrosine kinase anaplastic lymphoma kinase (*ALK*) oncogene on the short arm of chromosome 2. *ALK* is expressed in neural crest progenitor cells and regulates the balance between proliferation and differentiation. In 14% of NB patients, mutations in key genes lead to amplification or constitutive activation of the signaling pathway, which is associated with a poor prognosis in high-risk patients [22,23]. Also, two germline missense mutations (R100L and R141G) in the paired-like homeobox 2B (*PHOX2B*) or a disruption on chromosome 16p were reported in hereditary cases [4,24].

Next to aberrations, an increased cell surface expression of the disialoganglioside GD2 is characteristic for NB and distinguishes it from related but more differentiated neural tumors such as ganglioneuroma or ganglioneuroblastoma [25]. It is also highly expressed on other neuroectoderm-derived tumors such as retinoblastoma, melanoma, small cell lung cancer as well as on sarcomas like rhabdomyosarcoma, osteosarcoma, and Ewing sarcoma, or brain tumors like glioblastoma [26,27]. Normally, GD2 is expressed on neural and mesenchymal stem cells, but after birth, it is primarily detectable on neurons, peripheral nerve fibers, and melanocytes in the skin [28]. It plays a pivotal role in the immunotherapeutic treatment of NB. Additionally, NB cells exhibit high expression of other surface molecules that serve as potential immunotherapeutic targets, including the immune checkpoint molecule B7 Homolog 3 (B7-H3), neural cell adhesion molecule (NCAM), and Glypican 2 (GPC2). The characterization of tumor-specific markers like *MYCN* or GD2 is essential for treatment planning and prognosis assessment.

#### 3.1.4 Treatment options

Therapy of NB is often a multimodal treatment and depends on the disease stage and risk group. Treatment includes surgery, chemo- and radiotherapy, autologous hematopoietic stem cell

transplantation and immunotherapy. In some cases, such as for patients with 4S NB, observation alone is sufficient. Localized tumors can mostly be successfully removed surgically, whereas treating disseminated NB, as for instance stage 4 disease, is challenging, and patients often relapse [6]. Metastatic disease is typically first treated by a combination of resection and chemotherapy, using chemotherapeutic agents like cisplatin, etoposide, doxorubicin, cyclophosphamide and vincristine [29].

The final stage of treatment, referred to as maintenance, focusses on addressing minimal residual disease. During this phase, NB patients with relapsed or resistant disease receive immunotherapy with a human-murine chimeric anti-GD2 monoclonal antibody along with cis-retinoic acid (isotretinoin). This combination is sometimes supplemented with cytokines like Interleukin-2 (IL-2) and granulocyte-macrophage colony-stimulating factor (GM-CSF) [30]. Several variants of anti-GD2 monoclonal antibodies are available, but among them, Dinutuximab and Dinutuximab beta are the specific variants that have been evaluated in randomized studies and are usually used. A phase III clinical study demonstrated an increased EFS of high-risk NB patients treated with Dinutuximab to 66% after five years, compared to the standard therapy with isotretinoin which achieved an EFS of 46% [30]. Dinutuximab is a monoclonal antibody that consists of the murine fragment antigen binding ( $F_{ab}$ ) moiety of the murine 14G2a antibody fused to the human constant fragment ( $F_c$ ) region of an immunoglobulin (Ig) G1 [26]. Originally, the antibody was produced in the murine myeloma cells SP2/0 and approved as Unituximab (ch14.18/SP2/0) in 2015 but allergic and hypersensitivity reactions associated with the glycosylation pattern were observed in patients. To enhance the glycosylation profile and minimize adverse effects, the production was shifted to Chinese hamster ovary (CHO) cells resulting in the development of Dinutuximab beta (ch14.18/CHO) which was approved in 2016 under the trade name Qarziba as a first-line therapy for children over one year of age with a high-risk NB [31]. The antibody is administered as an infusion for five to ten days every 35 days for a total of five cycles with a total dose of  $100 \text{ mg/m}^2$  body surface per course [26]. Immunotherapy with Dinutuximab beta may lead to common side effects in patients. For example, seven out of ten patients experience fever and neuropathic pain. In addition, hypersensitivity reactions, diarrhea, vomiting, capillary leak syndrome, and hypotension may occur [26,31]. The risk of developing these side effects is particularly increased when co-administering IL-2 [32]. Neuropathic pain is mediated by the binding of Dinutuximab beta to GD2 on the surface of peripheral nerve fibers leading to an activation of the complement cascade [33]. The pain usually begins within an hour after the start of the infusion and subsides shortly after its completion. As the pain can be severe, continuous administration of analgesics such as gabapentin, non-opioid analgesics or opioids is necessary throughout the antibody infusion [26]. In the case of pain uncontrollable with analgesics, discontinuation of the treatment may be required.

Although the use of Dinutuximab beta has shown improvements in EFS of high-risk NB patients, certain challenges remain. One of these challenge is that some patients relapse and show a downregulation of the targeted antigen [34]. Moreover, the presence of severe neuropathic pain limits the administration of the anti-GD2 antibody. Consequently, it is important to search for new antigens as potential targets for immunotherapeutic approaches. B7-H3, *ALK* or GPC2 which were mentioned in chapter 3.1.3 are currently under investigation due to their strong expression on the surface of NB cells. Further investigative therapeutic options include cytotoxic agents such as the topoisomerase inhibitors topotecan and irinotecan, which are often used in early relapse treatment, or angiogenesis inhibitors and tyrosine kinase inhibitors which have already been tested in pre-clinical trials. Targeted and localized delivery of radionuclides or immunocytokines attached to anti-GD2 antibodies is another strategy being explored [6].

## 3.2 Immunoglobulins and their role in immunity

Immunoglobulins (Ig), also known as antibodies (AB), are a class of proteins playing a crucial role in the immune system's defense against harmful pathogens such as bacteria, viruses, and other foreign substances. The production of antibodies by B or plasma cells occurs after the initial exposure to a particular antigen and is an essential component of the humoral immune response, which is a part of the adaptive immune response [35]. Antibodies provide targeted recognition and elimination of specific antigens in cooperation with the complement system or immune cells. They can occur in two different forms – attached to the B cell surface as part of the B cell receptor or soluble in blood, tissue fluids, and secretions [36].

### 3.2.1 Structure of immunoglobulins

Immunoglobulins are heterodimeric glycoproteins that have a Y-shaped structure composed of four polypeptide chains. Each antibody consists of two identical heavy (H) chains and two identical light (L) chains linked by disulfide bonds between conserved cysteine residues as illustrated in Figure 2A [37,38]. The heavy chains have a molecular weight of approximately 55 kDa, while the light chains, which can be either  $\kappa$  or  $\lambda$  chains, have a molecular weight of approximately 25 kDa. Both, H and L chains consist of variable (V) and constant (C) regions. Specifically, the light chain consists of one variable and one constant chain, while the heavy chain is composed of one variable and three to four constant regions depending on the antibody isotype. Each V or C chain has a total length of 110-130 amino acids and has a similar structure, characterized by seven  $\beta$ -strands for the constant domains and nine  $\beta$ -strands for the variable domains, forming two  $\beta$ -sheets [37,38]. Based on the type of  $C_H$  region they possess, Igs are classified into different isotypes. The isotypes include IgA, IgD, IgE, IgG, and IgM, which correspond to the constant regions  $\alpha$ ,  $\delta$ ,  $\epsilon$ ,  $\gamma$ , and  $\mu$ , respectively (Figure 2B) [39]. IgA has two subtypes (IgA1 and IgA2), while IgG has four subclasses (IgG1 to

IgG4) [37]. Depending on their class, immunoglobulins can exist in different forms. IgD, IgE, and IgG are found as monomers, IgA antibodies can be monomers or dimers, and IgM antibodies are usually pentamers.

Functionally, an antibody can be divided into two main fragments: the antigen-binding fragments ( $F_{ab}$ ) and the crystallizable fragment ( $F_c$ ). The  $F_{ab}$  region, formed by the pairing of  $V_H$  and  $V_L$  chains with the  $C_{H1}$  and  $C_L$  domains, resembles the arms of the Y-shaped structure. The  $F_c$  fragment, composed of the  $C_{H2}$  to  $C_{H4}$  regions, forms the trunk of the Y. The three complementary-determining regions (CDRs) of the  $F_{ab}$  region are responsible for antigen recognition and binding. This region is hypervariable and highly diverse in its amino acid sequence. On the other hand, the  $F_c$  region is responsible for the interaction with other components of the immune system and can activate the complement cascade or bind to  $F_c$  receptors ( $F_cR$ ) on effector cells. The hinge region, located between the  $F_{ab}$  and  $F_c$  regions, provides flexibility and independent movement of the two  $F_{ab}$  fragments, allowing the antibody to adapt to different antigens and engage in various immune responses [37,38]. An Ig can recognize more than one antigen that has similar epitopes which is referred to as cross-reactivity [37].

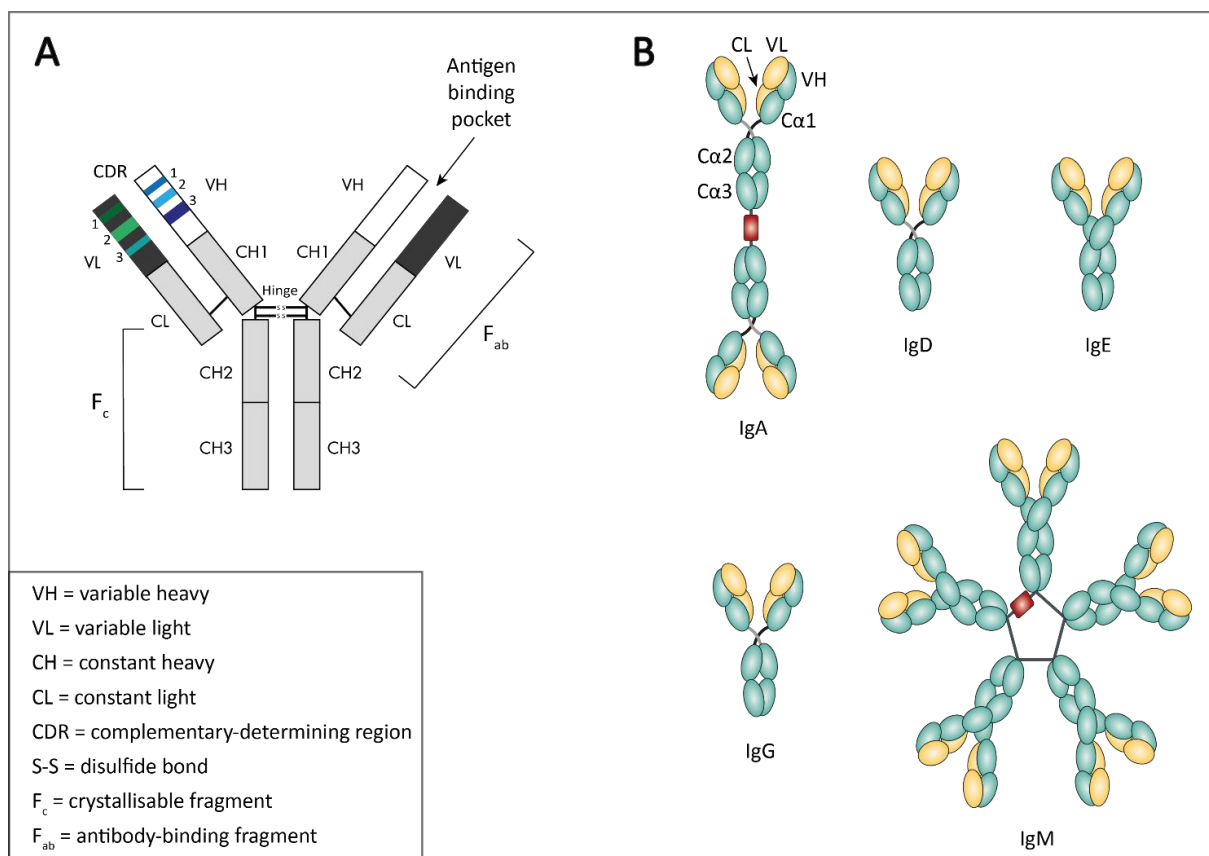


**Figure 2: Structural components of an antibody and different antibody isotypes.** The Y-shaped form of an IgG antibody with its structural and functional components was adopted from Smith *et al.* [40]. It shows two identical heavy and light chains linked by disulfide bonds and the complementary determining regions for antigen recognition highlighted in the variable region of each chain (A). Different antibody isotypes determined by different constant regions exist in various forms, as shown in the figure adopted from Duarte *et al.* [40,41] (B).

Antibody isotypes show distinct glycosylation profiles that impact the solubility, stability, conformation, and interaction with the  $F_cR$ , ultimately influencing their effector functions. N-glycosylation occurs most frequently in the  $F_c$  region but can also be present in the  $F_{ab}$  region, affecting antibody binding. For instance, the IgG isotype, which is the most abundant antibody in serum at 10-15 mg/ml, has one conserved N-glycosylation site at Asn297 in each  $C_H2$  domain [39]. In contrast, IgE is the most glycosylated antibody having seven N-linked glycosylation sites in the  $F_c$  [39,42]. Furthermore, O-glycosylation can occur in the hinge region, specifically in IgD and IgA isotypes. This O-glycosylation protects the region from protease digestion, facilitates pathogen binding, and modulates conformation as well as dynamics [39]. The attached glycans are essential for  $F_cR$  binding on leucocytes, contributing to thermostability and the quaternary antibody structure [43–45]. The composition and structure of glycans can vary depending on factors such as the cell type used for antibody production, cell culture conditions, disease state, and aging. Abnormal glycosylation can be a diagnostic marker for diseases. Changes in IgG glycosylation, for example, occur in rheumatoid arthritis, where an increased number of IgGs lack sialic acid and galactose residues, leading to inflammation [46].

#### 3.2.2 Functions of immunoglobulins in the adaptive immune response

IgG play a crucial role in the adaptive immune response through various mechanisms. One important function is the opsonization of pathogens, where antibodies bind to pathogens or toxins, enhancing phagocytosis or neutralization, or obstructing their attachment and entry into phagocytosing cells [47]. Complement-dependent cytotoxicity (CDC) is another mechanism involving antibodies. Igs bound to surface antigens attract complement component 1q (C1q) through specific sugar residues in their  $F_c$  region and initiate the complement cascade. This leads to the formation of a membrane attack complex and lysis of the antigen-presenting cell [37,48]. Next to CDC antibodies can mediate antibody-dependent cell-mediated cytotoxicity (ADCC). In this process, antibodies act as a bridge between target cells expressing the antigen and the appropriate  $F_cR$  on effector cells. Binding of the antibody's  $F_c$  domain to the  $F_cR$  on effector cells such as phagocytes, mast cells, neutrophils, or natural killer (NK) leads to destruction of the target cell [47]. Different  $F_cRs$  have been identified on human effector cells each recognizing specific antibody isotypes. For example, IgG binds to  $F_{c\gamma}R$ , IgE to  $F_{c\epsilon}R$ , IgD to  $F_{c\delta}R$ , and IgA can interact with  $F_{c\alpha}R$ . Both IgA and IgM can bind to  $F_{c\alpha/\mu}R$  [49]. This interaction is highly dependent from the glycosylation pattern of the  $F_c$  region [37,50]. Furthermore, antibodies can modulate inflammation by inducing the secretion of cytokines or chemokines [47].

Antibodies can be engineered to enhance their effector functions and optimize their therapeutic potential. This can be achieved through modifications in the amino acid sequences or alterations in the carbohydrate composition of the  $F_c$  region. For example, CDC can be improved by shuffling the  $C_H$  regions of IgG1 and IgG3 antibodies, resulting in enhanced binding to C1q [51]. Furthermore, a triple mutated S298A/E333A/K334A IgG1 antibody engineered by Shields *et al.* displayed superior

binding to  $F_{c\gamma}R$ , leading to increased ADCC [52]. Amino acid substitutions can also increase CDC and ADCC activity simultaneously as exemplified by the E345K or E340G mutations in an anti-CD20 IgG1 antibody [53]. Examples for antibodies with a modified oligosaccharide composition are IgG1 antibodies depleted from fucose at Asn297 in the  $F_c$  part, enabling an enhanced  $F_{c\gamma}R$  binding and ADCC by mononuclear effector cells, but not by granulocytes [50,51,54,55]. Obinutuzumab, for instance, is a non-fucosylated anti-CD20 antibody, which was approved in 2013 for treatment of chronic lymphocytic leukemia and follicular lymphoma [56,57]. On the other hand, IgG1 antibodies completely lacking Asn297-linked carbohydrates showed reduced binding to  $F_{c\gamma}R$ . Moreover, deglycosylated IgG3 antibodies showed a shorter half-life [58]. Modifications targeting both ADCC and CDC can be implemented simultaneously, resulting in synergistic effects. Engineered antibodies can offer advantages such as improved pharmacokinetics, stability, and the ability to overcome clinical resistance exhibited by tumor cells.

Each Ig isotype plays a distinct role in the immune response and is found in different parts of the body in varying amounts. The first line of defense in the human body is mediated by IgM antibodies secreted from immature B lymphocytes. As they do not undergo antigen stimulation and somatic mutation, they show a low affinity and therefore can react with a variety of antigens. IgMs predominantly act by antigen opsonization and show a strong complement activation due to their high avidity. In addition to the secreted form, there is also membrane-bound monomeric IgM and IgD expressed on B cells as part of the B cell receptor [59]. Both, IgM and IgD are associated with B cell activation. Due to its sensitivity to proteolysis, IgD is rarely present in the soluble form, but can be found in small amounts in the circulation where it plays a role in recognizing bacteria in the respiratory mucosa and binding to basophils and mast cells [60]. Following the primary immune response, affinity maturation and isotype switching occur, leading to the production of more specific IgG, IgA and IgE antibodies during the secondary immune response [61]. IgG is the most abundant isotype in the human body and has the longest half-life in serum. It mediates its functions through either complement fixation or binding to  $F_{c\gamma}R$  on effector cells. Among the IgG subclasses, IgG3 has the strongest C1q binding and, along with IgG1, exhibits the highest  $F_cR$  affinity, while IgG4 has weaker binding to  $F_cR$  and does not activate the complement cascade [37]. Different IgG subclasses respond to different types of antigens, such as protein antigens for IgG1 and IgG3, and polysaccharide antigens for IgG2 and IgG4 [37,62]. Additionally, IgG antibodies also play a role in the neutralization of toxins and pathogens. The significance of IgA antibodies lies in their ability to safeguard mucosal surfaces against toxins, viruses, and bacteria by neutralizing them or preventing their binding to the mucosal surface. The dimeric form of IgA is the secretory form and most abundant on mucosal surfaces of the gastrointestinal tract or in mucous secretions such as tears, saliva, and breast milk. Monomeric IgA circulates in the serum [63]. IgA antibodies primarily exert their effector functions by activating neutrophils through  $F_cR$  binding [37,64]. IgE, the Ig with the lowest serum concentrations, is primarily involved in

hypersensitivity reactions, allergy, and asthma. It also plays a role in immune protection against parasitic worms. The functional mechanism of this antibody isotype is based on an extremely high binding affinity to the FcR on mast cells, basophils, macrophages and eosinophils, triggering a rapid release of inflammatory mediators [65].

#### **3.2.3 Immunotherapeutic approaches against cancer**

In recent times, immunotherapeutic strategies have emerged as new approaches to address the limitations of conventional therapies in treating various diseases like autoimmune disorders or cancer [66]. The principle of immunotherapies is to strengthen the body's own machinery of the immune system to combat foreign cells. Diverse forms of immunotherapy exist, each involving the modulation of immune system activity, either by activating cytotoxic T cells or by overcoming immune checkpoint inhibition. These approaches involve the application of monoclonal antibodies, chimeric antigen receptor (CAR)-T cells, and the use of cytokines and interleukins. Additionally, targeting immune checkpoint proteins such as PD-1 or CTLA-4 was focused by James P. Allison and Tasuku Honjo who were awarded the 'Nobel Prize in Physiology or Medicine' in 2018 for their work on overcoming the immune system blockade in cancer treatment [67,68]. Examples for immunotherapeutic approaches encompass the use of the anti-CD20 antibody Rituximab for the treatment of hematopoietic malignancies like chronic lymphocytic leukemia and lymphoma. In the context of solid tumors, apart from Trastuzumab employed to address HER2-overexpressing breast cancer, the anti-GD2 antibody Dinutuximab is an exemplar of an approved immunotherapeutic intervention for NB therapy [31,69,70]. However, despite advances in immunotherapy, challenges remain. Tumor heterogeneity, the emergence of mechanisms that facilitate immune evasion, the potential for autoimmune responses, and the limited availability of appropriate targets that are restricted exclusively to tumor cells rather than normal tissues are all obstacles [71]. Nevertheless, the ability of immunotherapy to harness the body's defenses and elicit a durable immune response is a promising approach against a broad spectrum of diseases.

#### **3.3 Gangliosides**

Gangliosides belong to the group of glycosphingolipids and are composed of a hydrophobic ceramide linked to one or more hydrophilic sialic acid residues [72]. So, broadly speaking, gangliosides contain a complex oligosaccharide, a long-chain fatty acid, and a sphingosine backbone. They are found in nearly all vertebrates and are located on the extracellular surface, anchored in the outer leaflet of the plasma membrane through their lipophilic ceramide part. Gangliosides exhibit high diversity, with over 200 different ganglioside structures identified [73]. The composition of gangliosides differs based on the number, order and linkage of glycosyl and sialyl residues [74]. Ganglioside expression is cell type specific and depends on developmental stage [72]. In normal tissue for example, predominantly

monosialogangliosides are present, while the nervous system contains more complex gangliosides [75]. The latter are primarily present during embryogenesis and their expression becomes restricted to the nervous system postnatally [76,77]. The highest levels of gangliosides are present in the central and peripheral nervous system, especially in the brain, where they are 10 to 30 times more abundant compared to other tissues [78]. The major gangliosides in the adult human brain are GM1, GD1a, GD1b, and GT1b [79]. In contrast, GM3 is reported to be the major extraneural ganglioside in vertebrates and is also present on human peripheral blood lymphocytes along with some other gangliosides [80]. GD2, for example, is found on dermal melanocytes, mesenchymal stem cells, lymphocytes, and peripheral sensory nerve fibers [81].

#### 3.3.1 Classification and biosynthesis

Gangliosides are classified and named based on the number and position of the sialic acid residues. They can be designated as O, M, D, T, Q, or P gangliosides, depending on the number of sialic acids they contain. The a-, b-, or c-series classification is used when the internal galactose residue carries one, two, or three sialic acid residues [75,82].

The biosynthesis of gangliosides starts with the synthesis of the hydrophobic ceramide tail in the endoplasmic reticulum (ER). Subsequent biosynthesis steps take place in the Golgi apparatus. Firstly, Uridine diphosphate (UDP) glucose is transferred to the ceramide by glycosyltransferases (GTs), resulting in the intermediate product glycosylceramide (GlcCer). After this, lactosylceramide (LacCer) is synthesized which serves as the precursor for most gangliosides. In addition, GM3, GD3, and GT3 are the precursors of the more complex gangliosides of the a-, b-, and c-series as depicted in Figure 3. Through successive addition of further monosaccharides and sialic acids to the scaffold, the complexity of the gangliosides is increased. Various GTs are involved in these processes such as the  $\alpha$ -2,8-sialyltransferase 8A (GD3 synthase), responsible for the synthesis of GD3, and the  $\beta$ -1,4-N-acetyl-galactosaminyltransferase 1 (GM2/GD2 synthase). It catalyzes the synthesis of all gangliosides harboring two terminal sialic acid residues like GM2 and GD2 [76]. Sialic acids can undergo various modifications, including N- or O-acetylation, de-N-acetylation, sulfation, or lactonization [74]. The most common types of sialic acids found in gangliosides are N-acetylneuraminic acid (Neu5Ac) and N-glycolylneuraminic acid (Neu5Gc) which differ by one oxygen atom. Humans cannot synthesize Neu5Gc due to genetic mutations that prevent the expression of the enzyme cytidine monophosphate-N-acetylneuraminic acid hydroxylase, responsible for its hydroxylation [83,84]. However, it can be expressed in human malignant tissues due to the metabolic incorporation of dietary Neu5Gc [74,84,85].

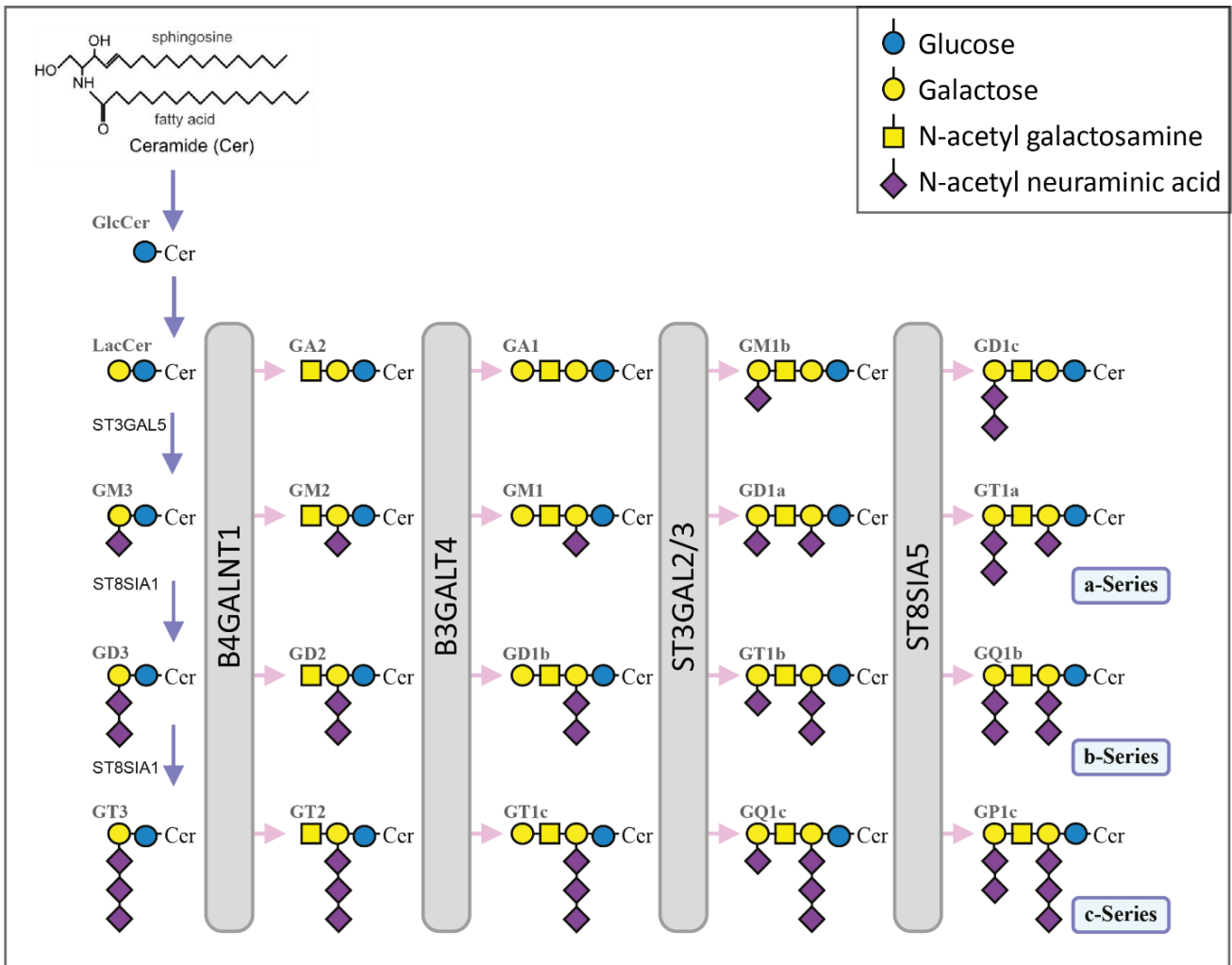


**Figure 3: In the biosynthesis pathway of gangliosides, monosaccharides and sialic acids are successively added to lactosylceramide by glycosyltransferases.** The diagram modified from *Inokuchi et al.* illustrates the grouping, nomenclature, and molecular relationship between different gangliosides [86]. GlcCer: glycosylceramide; LacCer: lactosylceramide; ST3GAL5: GM3 synthase; ST8SIA1: GD3 synthase; B4GALNT1: GM2/GD2 synthase; B3GALT4: GD1b synthase; ST3GAL2/3: GD1a synthase; ST8SIA5: GT1a synthase.

Once synthesized, gangliosides are transported from the luminal surface of the Golgi apparatus to the outer leaflet or the plasma membrane via exocytosis. There, they are anchored in the plasma membrane by their hydrophobic ceramide tail, with the hydrophilic carbohydrate residues exposed to the extracellular environment. Gangliosides can undergo endocytosis and be transported back to the Golgi apparatus in endosomes for reglycosylation. Degradation of gangliosides can take place in recycling endosomes or lysosomes, where glycohydrolases cleave off the monosaccharides under acidic conditions [72]. In some cases, degradation can also occur at the plasma membrane through the action of sialidases, particularly neuraminidase 3,  $\beta$ -galactosidase,  $\beta$ -glucosidase and  $\beta$ -hexosaminidase [87].

#### 3.3.2 General function and their role in disease

Gangliosides are involved in a number of biological processes such as cell growth, adhesion, proliferation, signal transduction, migration, and apoptosis. They can modulate cell signaling processes, cell-to-cell contacts as well as cell-to-matrix contacts [72,75]. Thereby they act as receptors for interferons, epidermal growth factors, nerve growth factors, or insulin [88,89]. In the nervous system, gangliosides play a role in myelination, axon and myelin integrity as well as nervous impulse transmission. These functions might be realized by interactions of the negatively charged sialic acid residues of the gangliosides with calcium ions [88]. In embryonic developmental processes and differentiation of certain tissues, the presence of glycosphingolipids has been shown to be crucial, as mice with an impaired glycosphingolipid synthesis were lethal [77].

Under pathological conditions, the composition and structures of gangliosides can change. In particular, the upregulation of b-series gangliosides is common in neuroectoderm-derived tumors. Tumor types such as neuroblastoma, melanoma, glioma, small-cell lung cancer, Ewing sarcoma, and retinoblastoma often show increased levels of GD2. Schulz *et al.* have demonstrated significantly elevated GD2 serum levels in NB patients compared to healthy children and children with other tumor types [90]. In cancer, gangliosides play a role in invasion, metastasis and cancer stem cell maintenance [91]. The expression pattern of gangliosides on tumors is associated with disease prognosis. Here, higher levels of circulating GD2 are linked to rapid tumor progression and poor survival [92,93]. In addition, GD2 is involved in tumor cell proliferation, motility, migration, adhesion, and invasion [81]. As mentioned in chapter 3.3.1, the Neu5Gc sialic acid residues on gangliosides, which accumulates in malignant tissues, is associated with tumor progression and metastasis. In NB and melanoma the incorporation of Neu5Gc-GM3 has been linked to more aggressive tumors and an immunosuppressive tumor environment due to a reduction in CD4<sup>+</sup> T lymphocytes [94,95]. Given their characteristic expression pattern in cancer and their role in tumor progression, gangliosides are an attractive target for immunotherapy.

In addition to their involvement in cancer, gangliosides also play significant roles in several other disorders. Most prominent ganglioside-related disorders are Tay-Sachs disease, Sandhoff disease, and the Guillain-Barré syndrome. In the recessive hereditary Tay-Sachs disease, patients harbor a mutation in the *HEXA* gene which encodes the enzyme hexosaminidase A. This enzyme is responsible for the lysosomal degradation of GM2. Insufficient enzyme activity results in the accumulation of GM2 in the lysosomes of ganglion cells, causing cell swelling and ultimately leading to destruction of nerve cells and eventually death. Similarly, Sandhoff disease is a recessively inherited disorder caused by a mutation in the *HEXB* gene that leads to a deficiency of hexosaminidases A and B [96]. Guillain-Barré syndrome is an example for an autoimmune disease characterized by the production of autoantibodies against various gangliosides such as GM1, GM2,

GD1a, GT1a, and GQ1b. These autoantibodies cause a muscle weakness due to the degradation of the myelin sheath of peripheral nerves. In some cases, Guillain-Barré syndrome is caused by infections such as gastroenteritis or cytomegalovirus infection. Further examples where anti-ganglioside antibodies play a major role are the Miller-Fisher Syndrome or the chronic idiopathic ataxic neuropathy [96]. Alzheimer's disease has also been associated with an impaired ganglioside metabolism. Specifically, GM1 has been linked to the aggregation of amyloid  $\beta$ -protein, a hallmark of Alzheimer's disease, which accumulates in the brain of affected individuals [97]. Gangliosides also play a role in viral infections, as certain viruses, including simian virus 40 and influenza virus, can enter cells by recognizing specific gangliosides on the cell surface. Additionally, gangliosides can serve as receptors for toxins (e.g. cholera, tetanus, botulinum toxins), lectins, and antibodies [72,96].

#### **3.3.3 Discovery of GM2 as potential antigen for neuroblastoma immunotherapy**

In a study conducted by Ollert *et al.* complement-mediated cytotoxicity against human NB cell lines was observed in sera from healthy adults. The cytotoxic components were identified as IgM antibodies and a 260 kDa antigen on the surface of NB cells was identified as target structure [98–100]. Further analysis of the antigen was performed in our working group, proving that the naturally occurring IgM antibodies from healthy individuals lysed NB cell lines through complement mediated mechanisms and inhibited growth of NB cell lines *in vitro*. Because there was no evidence of an isotype switch from IgM to IgG of the natural antibodies, the antigen targeted most likely is a thymus-independent antigen, specifically a carbohydrate structure rather than a protein. Molecular characterization of the epitope revealed that the antibody did not bind to GD2. This was confirmed in our working group by enzymatic treatment of NB cell lines with neuraminidase, which removed terminal sialic acids from carbohydrate structures and thereby degraded GD2 to GM2 (Figure 3). It has been shown that the binding to NB cells as well as the cytotoxic activity of IgM antibodies in positive donors' sera were not impaired after this enzymatic treatment of NB cells. Through systematic biochemical modifications of glycosylation pathways using inhibitors, more information about the biochemical characteristics of the target molecule was obtained. O-glycosylated molecules were excluded as target structures, and it has been shown that the target is an N-glycosylated carbohydrate. It was concluded that the antigen of these naturally occurring antibodies was a ganglioside synthesized by the GD2/GM2 synthase, as the cytotoxic effects had disappeared in GD2/GM2 synthase knockdown cell lines. Finally, among the possible gangliosides, GM2 was selected as the most promising candidate, as it had been previously associated with NB in the literature, although a clear link has not yet been demonstrated [101–104].

### 4 Aims of the work

Given the limited efficacy of existing therapeutic strategies for the treatment of high-risk NB, such as the immunotherapy with Dinutuximab, which is associated with severe side effects [26], and the limited access to suitable antigens, there is an urgent need for further therapeutic options. The discovery by members of our group that GM2 is the target of naturally occurring antibodies that effectively lysed NB cells has paved the way for the exploration of novel antibodies against gangliosides, particularly GM2, and the development of new immunotherapeutic strategies.

Previous publications have occasionally referenced GM2 in the context of NB, suggesting its potential overexpression [101,102], and suitability as an immunotherapeutic target. However, it has not been conclusively evaluated. The prevalence of healthy individuals carrying naturally occurring antibodies against GM2 with a specific lysis over 60% of NB cells is very low at 4.3% [105]. Hence, this study focused on engineering and comparing various recombinant antibodies using different available B cell receptor sequences against GM2 to assess their potential in combating NB.

Since there is currently no existing antibody that specifically targets the identified GM2 in NB and meets all the criteria for clinical application in patients – including human origin, high specificity, and the ability to efficiently eliminate NB cells – the main goal of this research was to find, modify, and characterize an antibody that meets these essential parameters.

To achieve this,

- available variable antibody sequences were incorporated into a human backbone to make them suitable as prospective candidates for future NB treatment
- the generated antibodies were evaluated and compared regarding the essential parameters for clinical application, covering the binding specificity and cytotoxic potential against NB cell lines *in vitro*
- following the identification of the most promising antibody candidate *in vitro*, a preclinical testing in a humanized mouse model should give insights into its efficacy *in vivo*.

The detailed steps of this study are illustrated in Figure 4 showing the objectives and different experimental setups of this work.

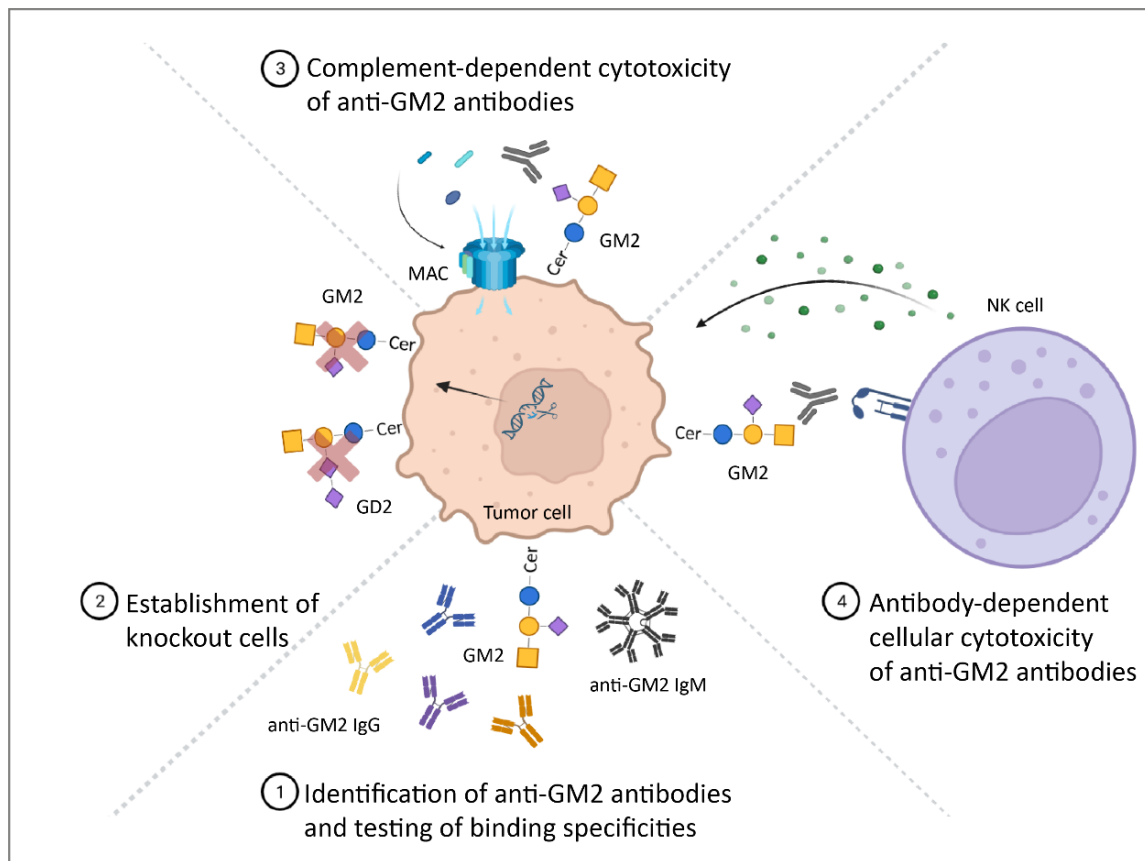


**Figure 4: Graphical summary of the objectives addressed in this work.** This included the identification and evaluation of a variety of anti-GM2 antibodies in different experimental setups.

Taken together, by engineering and evaluating different anti-GM2 antibodies, this research seeks to address the absence of existing antibodies that meet the clinical application criteria, potentially leading to more effective and targeted treatments for NB patients and serving as a model for the development of further therapeutic strategies.

### 5 Results

#### 5.1 Ganglioside expression on tumor cells

To assess the cell surface expression of GM2 on NB cells and some other tumor cell lines, flow cytometric analysis was performed by staining different cell lines with the murine anti-GM2 antibody clone MK1-16 IgM. Additionally, the expression of GD2, the target of the approved immunotherapy with Dinutuximab, was examined.

Upon investigation of ten NB cell lines, it was observed that GM2 was detectable to varying degrees on all NB cell lines except for SK-N-AS (Figure 5A). The geometric mean fluorescence intensity (gMFI) of GM2 expression was lowest in IMR32 with an average of 1.9 and highest in SH-SY5Y with 7.3. The expression levels of LAN-1, SK-N-BE(2), SK-N-SH, and SHEP were found to be very similar, with an average gMFI of 3.1. Kelly, LS, SK-N-LO, and SH-SY5Y showed GM2 expression higher than 5 on average. The average gMFI of GD2 varied from 3.2 for SK-N-BE(2) to 74.5 for LAN-1, indicating greater expression variability between NB cell lines compared to GM2 (Figure 5B). Some NB cell lines, such as SK-N-SH and its derived cell lines SHEP, did not show any GD2 expression, whereas the descendent SH-SY5Y showed low levels of GD2 with an average gMFI of 2.1. Both gangliosides exhibited variability in expression across most NB cell lines. This was exemplified by SH-SY5Y with a GM2 expression ranging from 2.7 to 11.7, and SK-N-LO where the results of nine independent measurements depicted a variability ranging from 2.3 to 9.3. An example for high GD2 expression variability was Kelly, showing gMFI from 17.9 to 45.0. No differences in GM2 expression were detectable depending on the *MYCN* status, but cell lines without *MYCN* amplification did not show any GD2 expression compared with cell lines in which *MYCN* is amplified. As all cell lines originated from patients with disseminated NB, it was not possible to establish any association between the expression of GM2 or GD2 and the disease stage.

In addition to NB cell lines, cell lines from other tumor types were also analyzed for their GM2 and GD2 expression. Again, the expression of GM2 was very variable within each cell line. Out of the twelve analyzed cell lines, five displayed high GM2 expression on their cell surface (Figure 5C). Among the cell lines tested, SJMM4 (medulloblastoma), showed the highest GM2 expression with an average gMFI of 10.5, surpassing the average expression observed on all NB cell lines. Furthermore, the rhabdomyosarcoma cell line RH-30, the medulloblastoma cell line DAOY, the cervix carcinoma cell line C33A, and the osteosarcoma cell line Saos-2 expressed GM2, with gMFI comparable to NB cell lines ranging from 1.2 for RH-30 to 5.9 for Saos-2. GM2 was not detectable on HeLa (cervix carcinoma), MCF7 and T47d (breast carcinoma), SK-MEL-2 and UACC62 (melanoma), HepG2 (hepatoblastoma), and U254 (glioblastoma) cells. GD2 was not detectable on any of the other tumor

cell lines (Figure 5D), indicating that GM2 might be a potential target for the treatment of various tumor entities beyond NB.

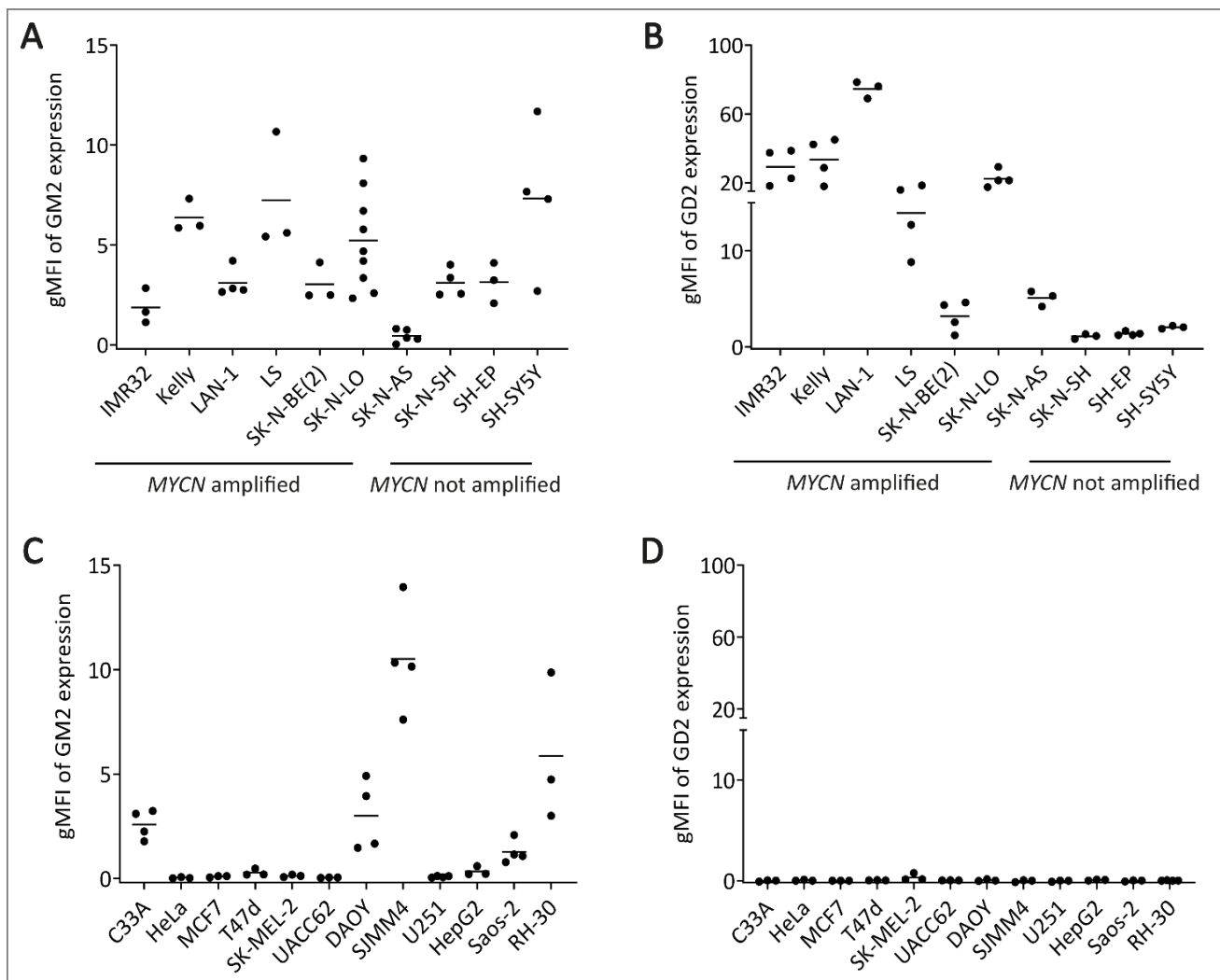


**Figure 5: Gangliosides GM2 and GD2 were expressed on the surface of neuroblastoma and various other tumor cell lines.** The cell surface expressions of GM2 (A,C) and GD2 (B,D) were analyzed on NB cell lines and various other tumor types by flow cytometric analysis. For GM2 staining the murine antibody clone MK1-16 IgM was used. GD2 was stained with the anti-GD2 antibody clone ch14.18 IgG. Appropriate APC-conjugated anti-murine IgM or anti-human IgG secondary antibodies were used for detection. Data show the gMFI of individual measurements normalized to the appropriate secondary antibody. Values represent gMFI of up to  $n=9$  independent representative experiments. Horizontal lines represent the mean values. gMFI: geometric mean fluorescence intensity.

## 5.2 Expression of GD2 and GM2 in clinical specimens from neuroblastoma patients

After the analysis of the ganglioside expression pattern on NB cell lines, six samples from NB patients were subjected to flow cytometric analysis to evaluate the expression levels of GD2 and GM2. The median age of patients was 10 months and as far as known all patients did not have a *MYCN* amplification. Among the five patients, four were classified as high-risk patients with stage 3 or stage 4 NB and one patient had a stage 4S NB. The samples originated from different sources at the

time point from the initial diagnosis (ID), including bone marrow (BM) and tumor biopsies (TB) (Table 1).

**Table 1: Neuroblastoma patient data and sample characteristics.**

No	Age	Sex	Tumor localization	Sampling time point	INSS	MYCN status	Sample type
1	6 m	M	Thoraco-abdominal with bone marrow infiltration and liver metastasis	ID	4	not amplified	BM
2	48 m	M	Abdominal with bone marrow infiltration and bone metastasis	ID	4	not amplified	BM
3	10 m	F	Abdominal with encasement of blood vessels	ID	3	not amplified	TB
4	3 m	F	Adrenal gland with minimal bone marrow involvement	ID	4S	not determined	TB
5	11 m	F	Abdominal with massive bone marrow infiltration and bone metastasis	ID	4	not amplified	BM
6	11 m	F	Abdominal with massive bone marrow infiltration and bone metastasis	ID	4	not amplified	BM

M: male; F: female; m: months; ID: initial diagnosis; BM: bone marrow; TB: tumor biopsy; INSS: International Neuroblastoma Staging System [106]. Sample 5 and 6 were obtained from the same patient. Samples 1, 2 and 6 were analyzed after culturing isolated cells from the original bone marrow samples.

Two different antibody clones against GM2, the murine MK1-16 IgM and the human KM966 IgG, were used for the analysis. All analyzed samples consistently exhibited a high expression of GD2, with over 70% of cells showing positive staining, irrespective of the sample type and cultivation conditions. In contrast, the expression of GM2 was found to be very heterogenous among the samples (Table 2). The murine antibody clone MK1-16 IgM did not recognize GM2 on the tumor cells in any specimen. However, when the human antibody KM966 IgG was used for staining, the percentage of GM2-positive cells varied widely, ranging from 1.7% to 84.9%. Interestingly, the sample from the 4S patient showed the highest expression of GM2. It was observed that the percentage of GM2<sup>+</sup> cells was influenced by the amount of antibody used for staining. In addition, slight differences in the expression were noticed after cultivation of the cells, showing a lower percentage of GD2<sup>+</sup> cells and a complete loss of GM2 expression.

**Table 2: GD2 and GM2 expression levels on cells from neuroblastoma patient samples.**

No	GD2 expression with 14G2a IgG (% positive cells)	GM2 expression with MK-16 IgM (% positive cells)	GM2 expression with KM966 IgG (% positive cells)
1	90.6	0.0	2.6
2	71.3	0.0	1.7
3	97.8	0.0	20.3
4	98.7	0.0	84.9
5	87.0	0.0	3.0
6	62.6	0.0	0.0

For the staining process, 0.2 µg of the APCFire750-labeled anti-GD2 antibody (clone 14G2a) and 1 µg of each anti-GM2 antibody clone, murine MK1-16 IgG or human KM966 IgG, were used, along with an APC-labeled anti-human IgG or anti-murine IgM antibody. In the case of sample 3 the amount of KM966 IgG antibody used was 3 µg.

### 5.3 Generation of neuroblastoma cell lines depleted from GM2 and GD2

NB cell lines with a knockout (KO) of *B4GALNT1* were generated using a CRISPR/Cas9-based approach to eliminate GM2 and GD2 on the cell surface. The corresponding enzyme  $\beta$ -1,4-N-acetyl-galactosaminyltransferase 1 (GM2/GD2 synthase), which is responsible for the synthesis of gangliosides containing N-acetyl galactosamine, was specifically targeted. Following the KO, only LacCer and the gangliosides GM3, GD3, and GT3 were expected to be synthesized (Figure 3). These KO cell lines could serve as controls to determine the specificity or potential cross-reactivity of the anti-GM2 antibodies to be tested in this work.

Quantitative assessment of genome editing was performed using the 'Tracking of Indels by Decomposition' (TIDE) method [107]. Knockouts were successfully generated for the NB cell lines LAN-1, LS, SK-N-LO, SK-N-AS, and SH-SY5Y, showing total KO efficiencies higher than 86% (Figure 6A). Furthermore, the KO of *B4GALNT1* was assessed using flow cytometric analysis. For this, the expression of the dTomato (dTom) reporter was examined to confirm the delivery of the plasmid containing the guide RNA (gRNA) and Cas9. The results for the SK-N-LO cells are exemplified and showed that more than 99.0% of the KO cells were positive for dTom reporter expression. Subsequently, staining with antibodies targeting GM2 and GD2 was conducted to validate the reduction of these two gangliosides on the cell surface of the KO cells compared to the wildtype (WT) cells. GM2 expression decreased from 23.1% to 0.4%. Furthermore, 93.3% of SK-N-LO WT cells were positive for GD2 and a reduction to 0.3% on SK-N-LO KO cells was detected (Figure 6B).

A quantitative analysis of insertions and deletions (indels) around the cut site was performed for the NB cell lines. The total editing efficiency and the percentage of indels which occurred due to non-homologous end joining repair of double-strand breaks are depicted for SK-N-LO cells (Figure 6C). The total editing efficiency in SK-N-LO KO was 91.1% and the most frequent genome editing event

observed was the insertion of 1 base pair (bp), accounting for 77.7% of SK-N-LO KO sequences. These results were also observed for all other NB cell lines analyzed (Appendix A-1). Additionally, a deletion of 5 bp was detected with a probability of 3.3%. Also, other indels occurred but with lower probabilities. The coefficient of determination  $R^2$ , indicating the suitability of independent variables, was high at 0.92. More detailed analysis revealed that adenine (A) was the most frequently incorporated nucleotide in sequences with a 1 bp insertion, accounting for 82.9% in SK-N-LO KO cells. Guanine (G) followed with an occurrence of 11.2%. The distribution of indels varied among the different NB cell lines, but a 1 bp insertion, resulting in an adenine incorporation was the most prominent event for all cell lines (Appendix A-1).

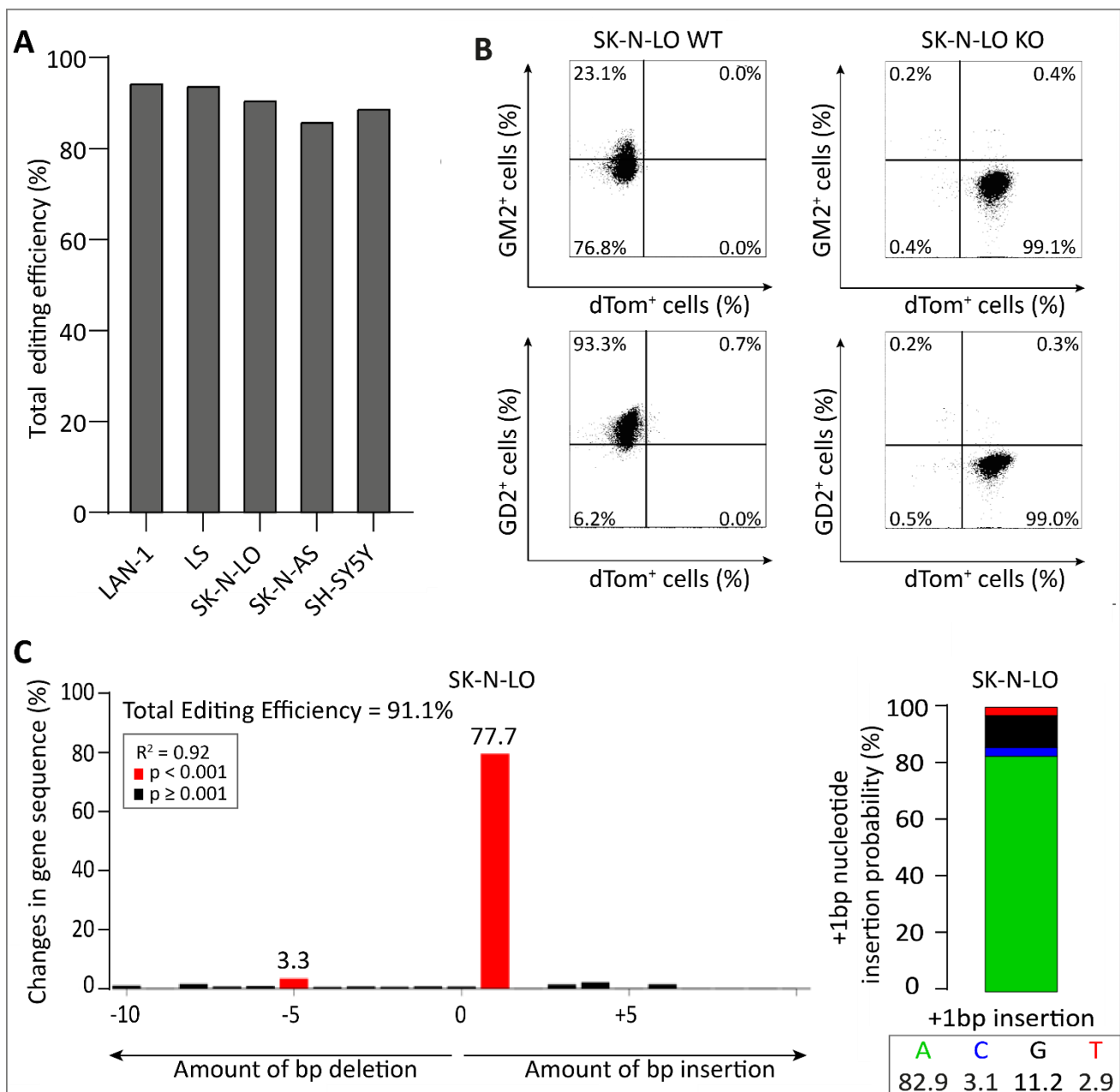


**Figure 6: Neuroblastoma cell lines with a knockout of *B4GALNT1* were depleted from GM2 and GD2.** The *B4GALNT1* gene, encoding the GM2/GD2 synthase, was targeted in several NB cell lines using the CRISPR/Cas9 system and resulted in a high total KO efficiency (A). DTomato reporter expression and the levels of GM2 and GD2 on SK-N-LO KO cells were assessed by flow cytometric analysis and compared to SK-N-LO WT cells. Staining was performed with the murine anti-GM2 antibody clone MK1-16 IgM in combination with an BV421-conjugated secondary anti-mouse IgM antibody as well as the anti-GD2 antibody clone 14G2a labeled with BV421 (B). TIDE analysis was conducted for quantitative evaluation and is exemplarily shown for the SK-N-LO cell line. The spectrum of genome editing is depicted as a percentage of indels and the probability of nucleotides at the +1bp insertion site (C). WT: wildtype; KO: knockout; indel: insertions and deletions; dTom: dTomato; bp: base pair.

#### 5.4 Identification of antibody sequences recognizing the tumor antigen GM2

In this work five different variable anti-GM2 antibody sequences, which originated from different sources, were analyzed. The variable heavy and light chain amino acid sequences were compared and are depicted in Figure 7, with the CDR underlined.



diverse human antibody repertoire. Combinations of seven VH and seven VL chain genes yield 49 distinct frameworks. Within each framework, human CDR sequences, composed of multiple trinucleotides, are inserted, representing a vast set of specificities from the theoretically human antibody repertoire, which is approximately  $10^9$ . Antibody selection was performed *in vitro* by phage display. For this, the HuCAL library fragments were attached to filamentous phages through a cleavable disulfide bond and incubated with the immobilized GM2 target antigen. Following several rounds of washing non-specifically binding phages were removed and specifically binding phages were eluted using a reducing reagent. Finally, the DNA encoding the specific antibody sequence was isolated, subcloned into an expression vector and sequenced [110–112]. In the context of this work, the antibody generated through this process on our behalf by Bio-Rad Laboratories, Inc. and incorporated into the pVITRO expression plasmids will be referred to as GM2-AB1.

The other antibody sequences analyzed in this work were either patented or published sequences that were supposed to bind GM2. The available selection of published anti-GM2 antibodies is limited, and often sequences are not available. Also, most available anti-GM2 antibodies are closely related or generated using similar approaches, making the choice of antibodies difficult. To ensure a pool of different antibody sequences, four were selected for this work. These included the monoclonal anti-GM2 antibody clone known as L55-81. This antibody was derived from peripheral blood B lymphocytes of a melanoma patient and were transformed by Epstein-Barr virus transformation technique. The original isotype of this antibody was IgM/k. No cross-reactivity with GM1, GM3, or GD2 has been shown and suggests that the epitope of L55-81 IgM/k must contain both N-acetyl galactosamine (GalNAc) and sialic acid residues bound to lactose [113]. This antibody will be referred to as GM2-AB2 in this work.

Furthermore, two closely related sequences referred to as KM966 and US2011 were used. The antibody clone KM966 is a chimeric human/mouse IgG1 antibody. It originated from a murine hybridoma which secreted the murine IgM/k antibody clone KM696. An IgG3 class-switch variant was generated by multiple enrichment cycles of antibody-secreting hybridomas after cultivation with the antigen and in the presence of mouse thymocytes which secreted cytokines and co-stimulating signals for the induction of a class-switch [114]. This resulted in the generation of the murine variant KM796, which was then converted to the chimeric clone KM966 [103,114]. The specific epitope of this antibody is not known, but it has been shown that the antibody was able to recognize two different forms of GM2, N-acetyl (Neu5Ac) and N-glycolyl (Neu5Gc) [115]. This antibody clone, which was expressed in this work using the pVITRO expression plasmid, is referred to as GM2-AB3 below. The sequence US2011 is an advanced version of the KM966 antibody with identical CDR regions as shown in Figure 7. Notably, the original backbone of the US2011 antibody has some modifications in the F<sub>c</sub> region, where the C<sub>H</sub>2 domain of the IgG1 antibody was replaced by the C<sub>H</sub>2 domain of IgG3,

demonstrating improved effector functions of the antibody [51,116]. The antibody clone, generated in this study is denoted as GM2-AB4 hereafter.

In addition to the human and murine derived antibodies, the sequence from the monoclonal antibody DMF10.167.4 was utilized, which was produced through hamster immunization with the murine cell line E710.2.3, originating from mouse thymic lymphoma [117–119]. The original format of this antibody was a hamster IgG/k, secreted from a hamster hybridoma cell line. The epitope of this antibody was identified to be the terminal galactose sugar with the sialic acid residue [119]. In this work, the generated humanized antibody was referred to as GM2-AB5 and the original hamster antibody was named DMF10.167.4 IgG.

The three-dimensional (3D) structures and interactions of the VH and VL chains of the utilized antibody sequences were modelled using the online prediction tool ABodyBuilder2. The analysis revealed very similar arrangements of amino acids in  $\alpha$ -helices and  $\beta$ -sheets for all five antibody sequences (Figure 8). The CDR regions showed only minor variations, with one exemplary difference observed in the uppermost CDR of L55-81, which displayed an additional loop compared to the other antibody models. It is essential to note that the structures were depicted in a single image, not reflecting the entire antibody from all sides. To ensure accurate comparison of the structures, an overall 3D view is necessary considering total conformations and orientations.

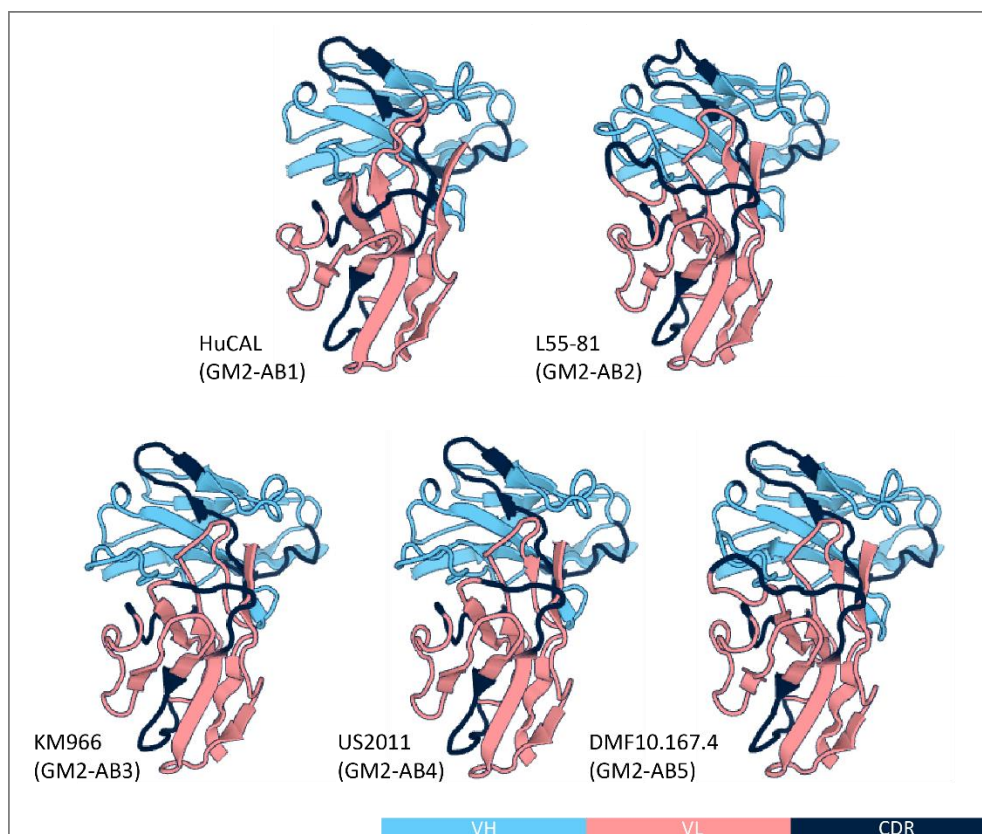


**Figure 8: Antibody structure models showing variable heavy and light chains with complementary determining regions were predicted using ABodyBuilder2 [120–122].**

### 5.5 Expression and stability of anti-GM2 antibodies

For the expression of the anti-GM2 antibodies, the different variable sequences outlined in chapter 5.4 were synthesized and inserted into expression plasmids for either IgG1 or IgM (see Appendix B-1 and Appendix B-2) following the procedure described in chapter 9.2.1. The antibodies were produced by transfecting human embryonal kidney cells (HEK) cells. The resulting antibodies were then harvested in the cell culture supernatant.

The expression of the produced anti-GM2 antibodies was assessed using western blot analysis, where the heavy and light chains were visualized (Figure 9A). All anti-GM2 antibodies were successfully expressed with the  $\gamma$  heavy chains consistently displaying a molecular weight of approximately 50 kDa, while the  $\kappa$  light chains showed slight differences in molecular weights, ranging from 25 to 30 kDa. Specifically, GM2-AB1 IgG and GM2-AB5 IgG light chains exhibited increased molecular weights compared to other antibodies. Additionally, for GM2-AB3, the production of IgM antibodies was also successful, showing the  $\mu$  heavy chain with a molecular weight of approximately 70 kDa, along with the  $\kappa$  light chain weighing 25 kDa (Figure 9B). It was observed that the quantity of heavy chains was generally higher than that of light chains, as indicated by stronger band signals. Moreover, the amount of light chains showed greater variability compared to the heavy chains. The ratios between heavy and light chains also varied strongly and ranged from 3:1 for Trastuzumab IgG to 15:1 for GM2-AB2 IgG (Figure 9C). Although, GM2-AB3 IgM was detectable in western blot, the amount of produced antibody was lower compared to GM2-AB3 IgG antibody, showing a H:L ratio of 38:1.

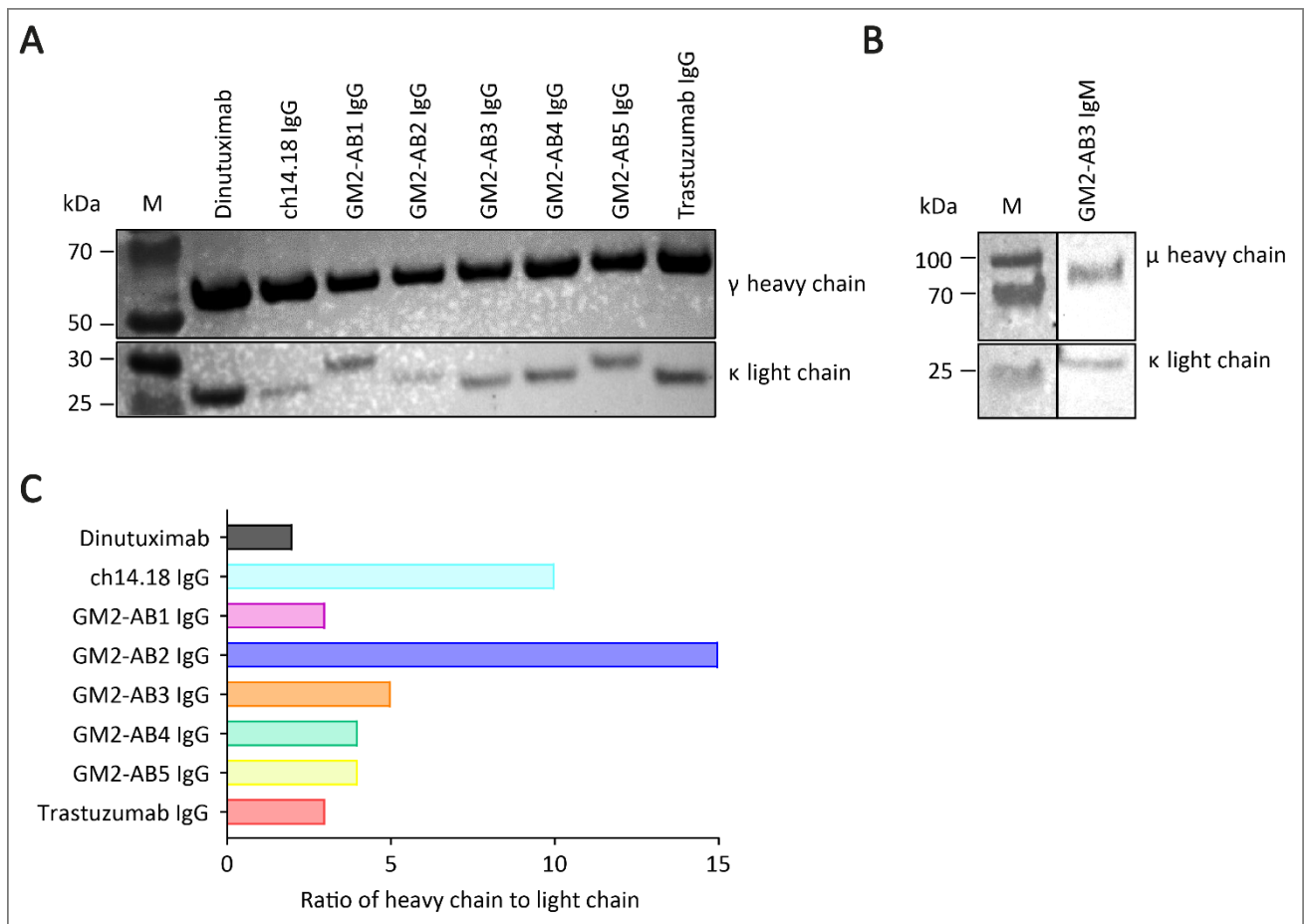


**Figure 9: Production of anti-GM2 antibodies by transfection of HEK293T cells was successful.** 2  $\mu$ g of Dinutuximab and the anti-GD2 antibody clone ch14.18, also produced in HEK cells as well as 2  $\mu$ g purified anti-GM2 IgG antibody samples (A) or 16,25  $\mu$ l of culture supernatant from HEK293T cells (B) were treated with dithiothreitol and loaded onto 4-12% Bis-Tris gels for SDS-PAGE. The molecular weight of the  $\gamma$  heavy chain was approximately 50 kDa, while the  $\mu$  heavy chain had a molecular weight of approximately 70 kDa, and the  $\kappa$  light chain had a molecular weight of 25 kDa. The ratios between the expression levels of heavy and light chains were calculated for each IgG antibody (C). M: marker, kDa: kilodaltons.

After demonstrating successful expression of all anti-GM2 antibodies after transfection of HEK293T cells, the next step was to evaluate antibody stability. Quality and stability are critical factors that determine the functionality of antibodies and are influenced by various factors such as the composition of the storage buffer (e.g. pH), storage temperature, and the number of freezing and thawing cycles. To assess the thermal stability of the tested antibodies, thermal unfolding profiles were generated by the 'Protein Production Core Facility' at the 'Centre of Structural Systems Biology Hamburg' using the Tycho NT.6 instrument. During the unfolding process of a protein with temperature changes, there are changes in the ratio of sample brightness measured at 350 nm to that measured at 330 nm. These changes result in a steep ascent of the curve, which are equivalent to the peaks of the first derivative curve. The temperatures at which these changes occur are known as inflection temperatures ( $T_i$ ) which are comparable to the melting points of antibodies.

In Figure 10A the first derivative views of the Tycho NT.6 data are depicted, with each peak corresponding to one  $T_i$ . GM2-AB1 IgG, GM2-AB2 IgG, and GM2-AB3 IgG as well as the anti-GD2 antibody ch14.18 IgG exhibited unfolding profiles with two inflection points where the  $T_{i2}$  value was above 70.4 °C and the  $T_{i3}$  was higher than 88.8 °C. In contrast, the curves of GM2-AB4 IgG and GM2-AB5 IgG had different shapes, with GM2-AB4 IgG showing only one  $T_i$  at a lower temperature of 61.7 °C, and GM2-AB5 IgG displaying three  $T_i$  at 65.1 °C, 74.0 °C, and 89.0 °C. Notably,  $T_{i2}$  and  $T_{i3}$  of GM2-AB5 IgG were in a similar range as the  $T_i$  values of the other antibodies, but  $T_{i1}$  of both, GM2-AB5 IgG and also GM2-AB4 IgG were at lower temperatures (Figure 10B). These observations indicate an unfolding at lower temperatures and differences in the thermostability of these two antibodies.

Additionally, the unfolding of GM2-AB3 IgG antibodies stored at different temperatures, including RT or -80 °C were further analyzed at various time points using the Tycho NT.6 device. For all storage conditions tested, the antibody showed almost identical unfolding profiles and the first derivative curves gave similar  $T_i$  values for each measuring time (Figure 10B). Throughout the entire observation period of 65 days, the differences between the initial and final signals of the absorbance at 350 nm/330 nm remained consistent for all storage conditions, and the mean  $T_i$  values were found to be at 74.5 °C and 89.2 °C. Also, the repeated freezing and thawing of the antibody did not affect the  $T_i$  values over time (data not shown), indicating a long-lasting stability independently from the storage temperature.

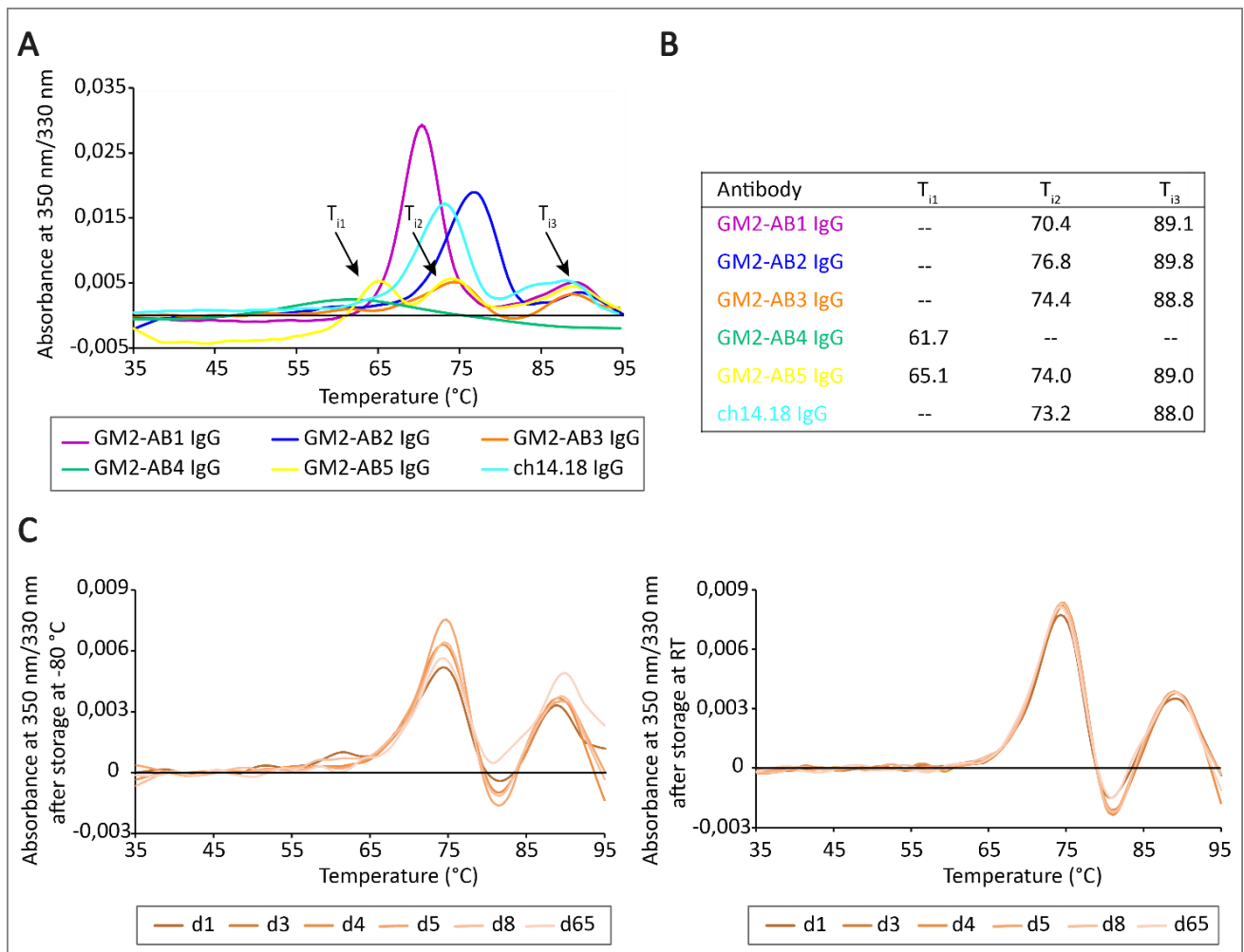


**Figure 10: Thermal unfolding profiles of tested anti-GM2 IgG antibody clones, revealed differences in their thermostability, but storage at different temperatures did not affect stability of anti-GM2-AB3 IgG over time.** First derivative curves of thermal unfolding for all anti-GM2 IgG antibodies tested and the anti-GD2 antibody ch14.18 IgG were obtained by measuring the absorbance at 350 nm/330 nm. The peaks observed in the first derivative curves represent the inflection temperatures ( $T_i$ ) as indicated by arrows (A). The detected  $T_i$  values from one representative experiment for each antibody are shown (B). The unfolding profiles of GM2-AB3 IgG antibody, stored at either RT or -80 °C, displayed very similar curves over the course of the entire 65-day measurement (C). d: day, RT: room temperature.

## 5.6 Binding of anti-GM2 antibodies to ganglioside test stripes and cell lines

After the successful production and assessment of stability of the anti-GM2 antibodies, their specific binding to gangliosides was evaluated using test stripes on which several gangliosides (GM1, GM2, GM3, GM4, GD1a, GD1b, GD2, GD3, GT1a, GT1b, and GQ1b) were coated.

As shown in Figure 11, among the five humanized anti-GM2 antibodies analyzed, three of them specifically recognized GM2 on the ganglioside test strips. While GM2-AB1 IgG and GM2-AB2 IgG did not show binding to any of the ganglioside, GM2-AB3 IgG, GM2-AB4 IgG, and GM2-AB5 IgG specifically recognized GM2 (Figure 11A). GM2-AB5 IgG showed a similar intense band as GM2-AB3 IgG, suggesting a similar binding strength to GM2. The intensity of 1  $\mu$ g GM2-AB3 IgG was more

pronounced than that of 1  $\mu\text{g}$  GM2-AB4 IgG, although these two antibodies have the same CDR. However, when using a higher amount (5  $\mu\text{g}$ ) of GM2-AB4 IgG a band for GM2 became visible. Also, different band intensities were observed when comparing 1  $\mu\text{g}$  of recombinant human GM2-AB5 IgG with 1  $\mu\text{g}$  of unpurified culture supernatant from the DMF10.167.4 IgG-secreting hamster hybridoma cell line. In comparison, the GD2 bands of both, ch14.18 IgG produced in HEK293T cells or the original Dinutuximab, were stronger with the same amount of antibody, when compared with the GM2 bands of GM2-AB3 IgG or GM2-AB5 IgG. Interestingly, the murine anti-GM2 antibody clone MK1-16 IgM, used for the analysis of ganglioside expression on NB cell lines (Figure 5A,C) did not show a band for GM2 or any other ganglioside on the test stripe. Negative controls (ctrls) included a human IgG1 Isotype antibody, referred to as the Isotype IgG, and Trastuzumab IgG produced using the same plasmid. Both did not show binding to any of the coated gangliosides.

Additionally, the binding specificity of the antibody isotypes IgG1 and IgM was compared. As depicted in Figure 11B, neither GM2-AB1 IgM nor GM2-AB2 IgM displayed any visible bands for GM2 or other gangliosides coated on the test stripes. The isotype switch from IgG to IgM did not affect the binding specificity of GM2-AB3, GM2-AB4 and GM2-AB5, as they continued to recognize exclusively GM2. In contrast, ch14.18 IgM, which specifically bound to GD2 in its IgG antibody format (Figure 11A), exhibited unspecific binding when switched to the IgM isotype. Ch14.18 IgM showed binding not only to GD2 but also to several other gangliosides, including GD1a, GD1b, GD3, GT1a, GT1b, and GQ1b, and sulfatides (Figure 11B).

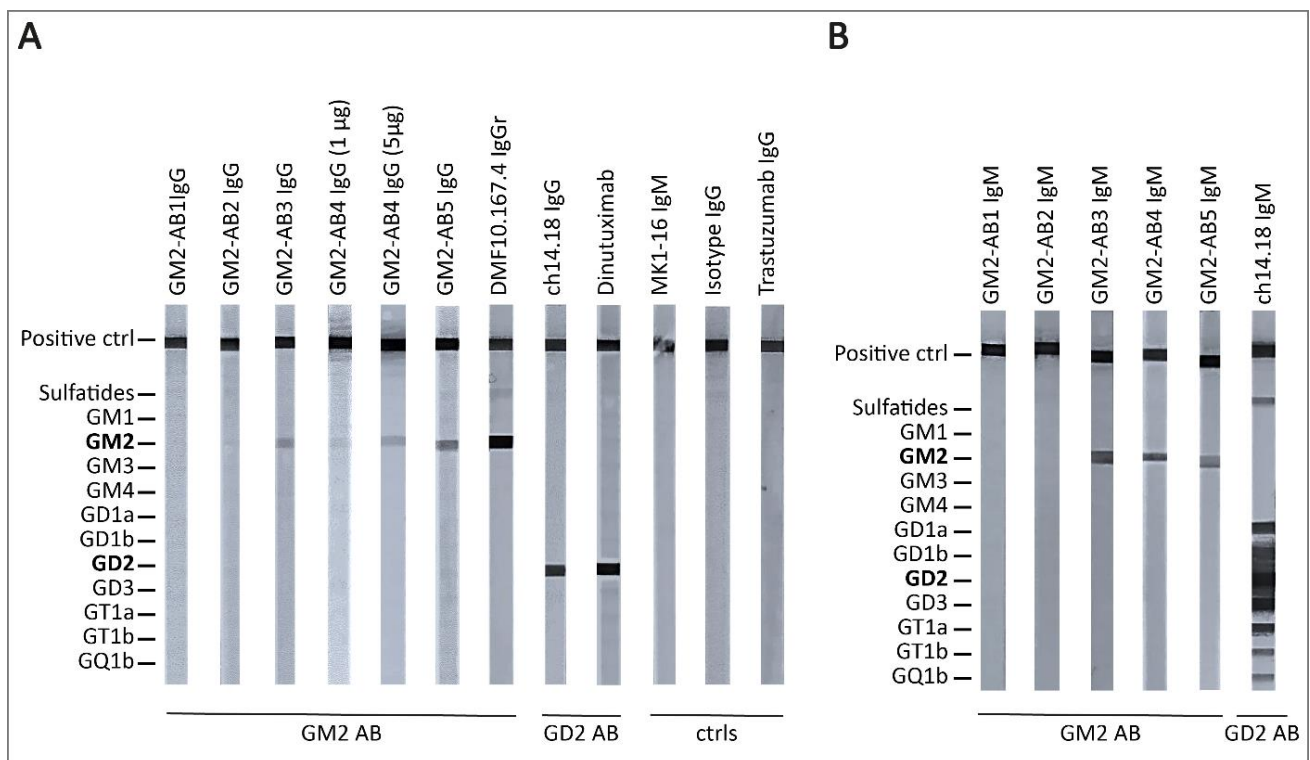


**Figure 11: Anti-GM2 IgG antibodies specifically recognized GM2 and maintained their specificity upon switching to IgM isotype.** 1  $\mu$ g (and 5  $\mu$ g) of the anti-GM2 IgG antibody clones (GM2-AB1, GM2-AB2, GM2-AB3, GM2-AB4 and GM2-AB5), the anti-GD2 antibody clones (ch14.18, Dinutuximab), and controls were tested on stripes coated with various gangliosides to determine their binding specificity (A). Unpurified cell culture supernatant containing anti-GM2, or anti-GD2 IgM antibodies was also tested (B). ctrl: control; AB: antibody.

Since GM2-AB3 IgG, GM2-AB4 IgG, and GM2-AB5 IgG, but not GM2-AB1 IgG and GM2-AB2 IgG were shown to specifically recognize GM2 on the test strips, the binding to NB cell lines was next evaluated. To assess the binding characteristics, flow cytometric analysis was performed using 1  $\mu$ g of each antibody and an APC-conjugated secondary anti-human IgG antibody for detection. As visualized in Figure 12, neither GM2-AB1 IgG nor GM2-AB2 IgG recognized SK-N-LO cells or any of the NB cell lines (Appendix A-2), which was consistent with their inability to bind to GM2 on the ganglioside stripes (Figure 11A). In contrast, GM2-AB3 IgG, GM2-AB4 IgG, and GM2-AB5 IgG showed binding to GM2<sup>+</sup> NB cell lines to varying degrees, with different percentages of APC<sup>+</sup> cells (Figure 12A). For instance, GM2-AB3 IgG recognized 95.2% of SK-N-LO cells, while GM2-AB4 IgG showed binding to 72.0% and GM2-AB5 IgG to 26.9% cells.

This differences in binding affinity of the anti-GM2 antibodies were also reflected in the average gMFI (Figure 12B). GM2-AB3 IgG demonstrated the highest binding to SK-N-LO and most other NB cell lines (Appendix A-2) compared to the other recombinant human anti-GM2 antibodies and the anti-GD2 antibody ch14.18 IgG. Specifically, GM2-AB3 IgG showed a mean gMFI of 29.6 when binding to SK-N-LO while GM2-AB4 IgG had an average gMFI of 15.7, and ch14.18 IgG had an average gMFI of 21.7 (Figure 12B). When comparing all NB cell lines tested, GM2-AB3 IgG exhibited the highest average gMFI for SK-N-BE(2) cells (85.2) and the lowest for SK-N-AS (1.9). Furthermore, the

average gMFI values for GM2-AB4 IgG, which has identical CDR to GM2-AB3 IgG, were generally lower for all NB cell lines tested (Appendix A-2).

The two antibodies with the variable sequence DMF10.167.4 showed significant differences in binding to SK-N-LO, with the humanized GM2-AB5 IgG having a 19.6-fold lower average gMFI (2.1) compared to the original hamster DMF10.167.4 IgG (41.2) (Figure 12B). Also, GM2-AB5 IgG showed poor recognition of other NB cell lines, with gMFI ranging from 0.0 (SK-N-AS) to 32.0 (SK-N-BE(2)), whereas the hamster antibody showed gMFI between 13.9 (SK-N-AS) to 91.3 (LS) at maximum (Appendix A-2). The mean gMFI values of DMF10.167.4 IgG were 1.4-fold higher than of GM2-AB3 IgG and interestingly, it was the only antibody that recognized the GM2<sup>low</sup> SK-N-AS cells. Both, GM2-AB3 IgG and DMF10.167.4 IgG showed a high variability among the individual data (Figure 12B).

The binding of the anti-GD2 antibody clone ch14.18 IgG expressed in HEK293T cells fell between GM2-AB3 IgG and GM2-AB4 IgG, and the gMFI values were more consistent compared to GM2-AB3 IgG and GM2-AB4 IgG. As a control Isotype IgG was tested which showed no binding to any NB cell line, confirming the previous results from the ganglioside test stripe.

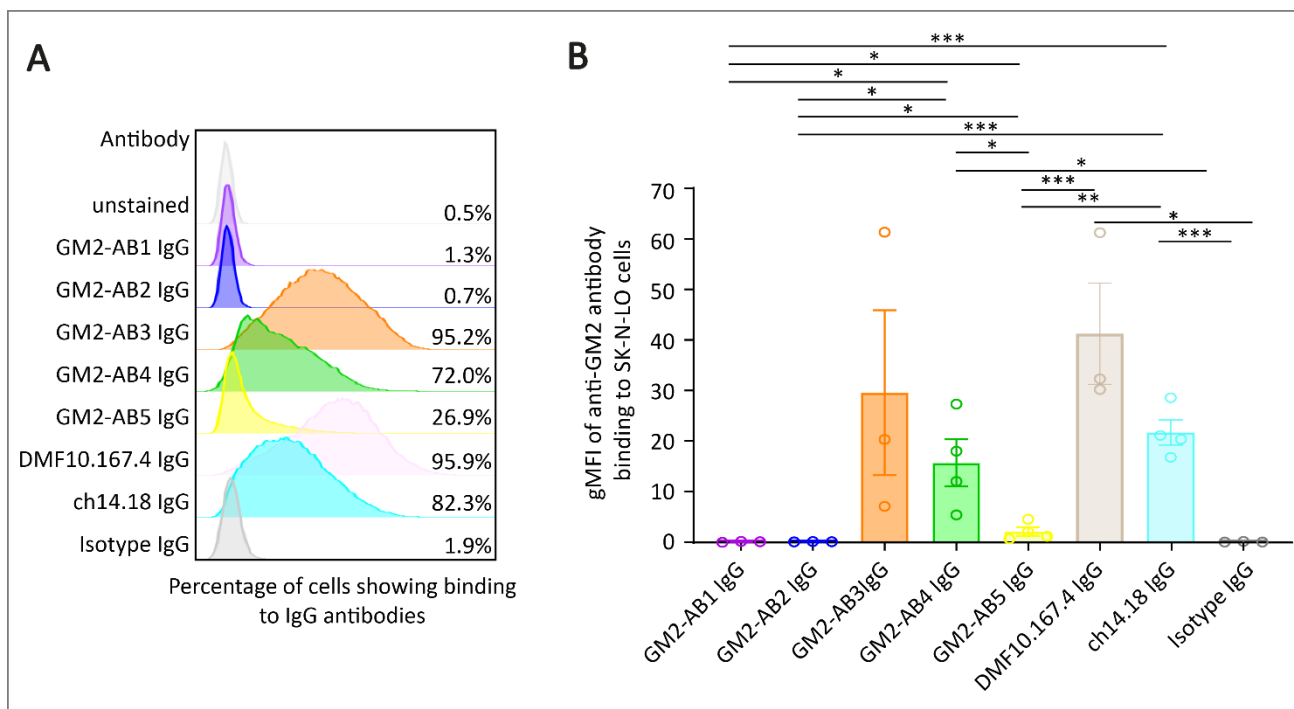


**Figure 12: Anti-GM2 antibodies demonstrated variable binding specificity to GM2<sup>+</sup> neuroblastoma cells.** Flow cytometric analysis was used to compare the binding of each anti-GM2 antibody (GM2-AB1 IgG, GM2-AB2 IgG, GM2-AB3 IgG, GM2-AB4 IgG, and GM2-AB5 IgG) and the anti-GD2 antibody ch14.18 IgG and Isotype IgG on the neuroblastoma cell line SK-N-LO. Depicted are exemplary histograms and percentages of cells that showed binding to each antibody (**A**) as well as the geometric mean fluorescent intensities of individual measurements, normalized to the secondary control (an APC-labeled anti-human IgG antibody) (**B**). At least  $n = 3$  independent representative experiments were performed, and the data show the mean gMFI and SEM. Statistical analysis was performed using Student's t-tests with multiple comparisons with \*\*\*  $P < 0.001$ , \*\*  $P < 0.01$ , \*  $P < 0.05$ . gMFI: geometric mean fluorescence intensity.

Furthermore, the binding of GM2-AB3 IgG to various other tumor cell lines was analyzed (Figure 13). GM2-AB3 IgG was able to recognize the GM2<sup>+</sup> cell lines C33A (cervix carcinoma), DAOY and SJMM4 (medulloblastoma), Saos-2 (osteosarcoma) and RH-30 (rhabdomyosarcoma). The average gMFI values ranged from 4.9 for Saos-2 to 36.8 for SJMM4 (Figure 12C). The binding patterns of GM2-AB3 IgG to these cell lines were in accordance with the GM2 expression levels measured using the murine anti-GM2 antibody clone MK1-16 IgM (Figure 13A). For example, SJMM4 cells, which were GM2<sup>high</sup>, exhibited the highest gMFI values when stained with GM2-AB3 IgG, while the gMFI were lowest for GM2<sup>low</sup> Saos-2 cells. In contrast, HeLa (cervix carcinoma), MCF7 and T47d (breast carcinoma), SK-MEL-2 and UACC62 (melanoma), HepG2 (hepatoblastoma) and U254 (glioblastoma) cells which did not express any GM2 were not recognized by GM2-AB3 IgG (Figure 13B).

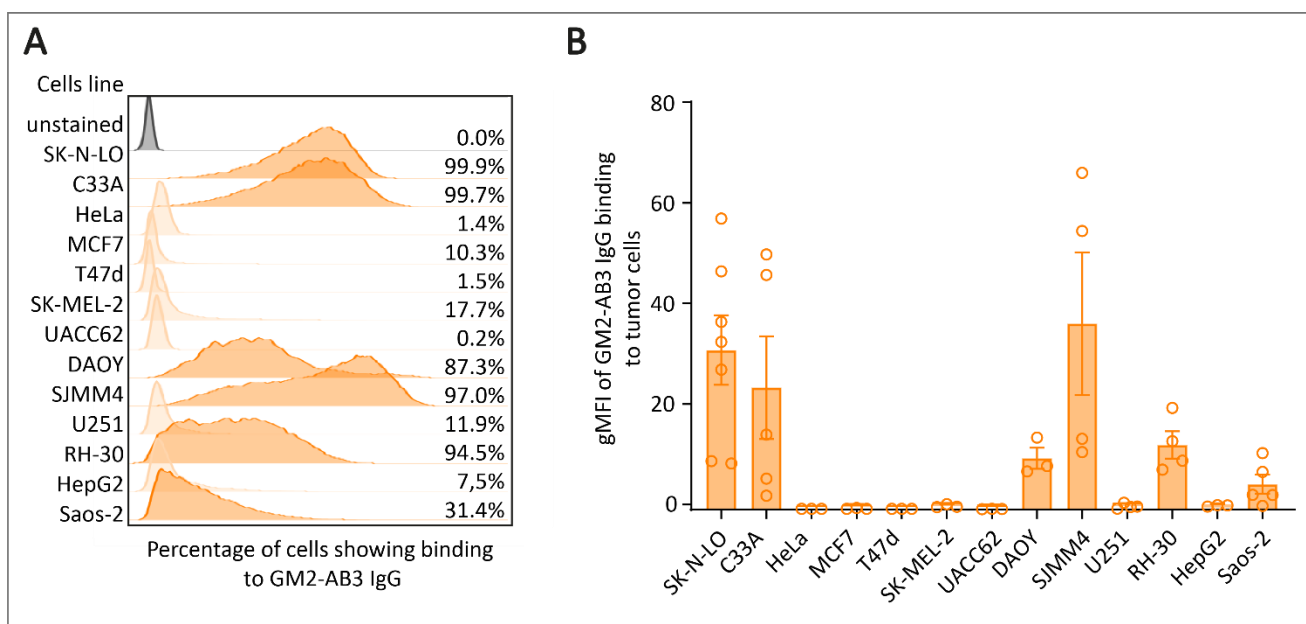


**Figure 13: GM2-AB3 IgG demonstrated variable binding specificity to different tumor types.** The binding of GM2-AB3 IgG to different tumor types including neuroblastoma (SK-N-LO), cervix carcinoma (C33A, HeLa), breast cancer (MCF7, T47d), melanoma (SK-MEL-2, UACC62), medulloblastoma (DAOY, SJMM4), glioblastoma (U251), rhabdomyosarcoma (RH-30), hepatoblastoma (HepG2), and osteosarcoma (Saos-2) was investigated. Histograms of one representative experiment (**A**) and the geometric mean fluorescent intensities (**B**) are exemplarily shown. At least  $n = 3$  independent representative experiments were performed, and the data show the mean gMFI and SEM. gMFI: geometric mean fluorescence intensity.

In summary, comparative analysis of the five anti-GM2 antibody clones tested, revealed that GM2-AB3 IgG showed superior binding to almost all NB cell lines, indicating highest affinity and specificity, which was not limited to NB cell lines, as other tumor types were also recognized by this antibody clone.

## 5.7 Evaluation of *in vitro* effector functions of anti-GM2 antibodies

As explained in chapter 3.2.2, complement-dependent cytotoxicity (CDC) is one mechanism of action of IgG antibodies, where the antibody triggers the activation of the classical complement pathway

upon binding to the antigen on the surface of the target cell. To assess the CDC potential of the anti-GM2 antibodies, NB cells were incubated with different concentrations of anti-GM2 antibodies along with serum from healthy human donors as a complement source using the IncuCyte Live Cell Imaging system.

Among the five anti-GM2 antibodies tested, only GM2-AB3 IgG and GM2-AB5 IgG exhibited cytotoxicity against SK-N-LO cells (Figure 14A) and other NB cell lines (Appendix A-3). Consistent with previous results, both GM2-AB1 IgG and GM2-AB2 IgG did not show any cytotoxic activity. Surprisingly, also GM2-AB4 IgG did not cause any lysis of SK-N-LO, although previous experiments showed that the antibody bound to SK-N-LO cells (Figure 12B). However, GM2-AB4 IgG exhibited lysis of 14% of Kelly cells when using a higher concentration of 8  $\mu\text{g/ml}$  antibody (Appendix A-3A). Moreover, GM2-AB5 IgG demonstrated a relative lysis of 5.7% and 19.5% of SK-N-LO cells, when using 4  $\mu\text{g/ml}$  or 8  $\mu\text{g/ml}$  of the antibody, respectively (Figure 14A).

The highest relative lysis was achieved with the GM2-AB3 IgG and was significantly higher than with the other anti-GM2 antibodies. Also, CDC was observed for other NB cell lines, including 80.8% lysis of Kelly, 71.0% lysis of SK-N-LO, 67.0% lysis for LS, and 23.6% lysis of SH-SY5Y cells at 8  $\mu\text{g/ml}$  concentration (Figure 14B). Even at half of the concentration GM2-AB3 IgG showed considerable killing, with 66.2% for Kelly, 45.6% for SK-N-LO, 35.0% of LS, and 23.4% for SH-SY5Y being lysed (Appendix A-3). CDC of GM2-AB3 IgG and Dinutuximab was at comparable levels when using 4  $\mu\text{g/ml}$  of the antibodies (Appendix A-3), but at higher concentration of 8  $\mu\text{g/ml}$  CDC of GM2-AB3 IgG was higher than that of the Dinutuximab. For example, the relative lysis of SK-N-LO cells with 8  $\mu\text{g/ml}$  GM2-AB3 IgG (71.0%) was 1.2-fold higher than with 8  $\mu\text{g/ml}$  Dinutuximab (61.2%) (Figure 14B).

As negative controls, Trastuzumab IgG and Isotype IgG did not induce any lysis, confirming that the observed CDC was specifically mediated through the binding of the anti-GM2 antibodies to GM2 on the NB target cells.

Furthermore, CDC was evaluated using NB cell lines with a knockout of the *B4GALNT1* gene. Because the synthesis of all gangliosides except GM3, GD3, and GT3 was inhibited here, these cells did not express GM2 or GD2 on their cell surface. While GM2-AB3 IgG and Dinutuximab caused a killing of 71% and 61.2% of SK-N-LO WT cells, respectively, specific lysis of SK-N-LO KO cells completely disappeared upon *B4GALNT1* knockout and was below 0.5% (Figure 14C).

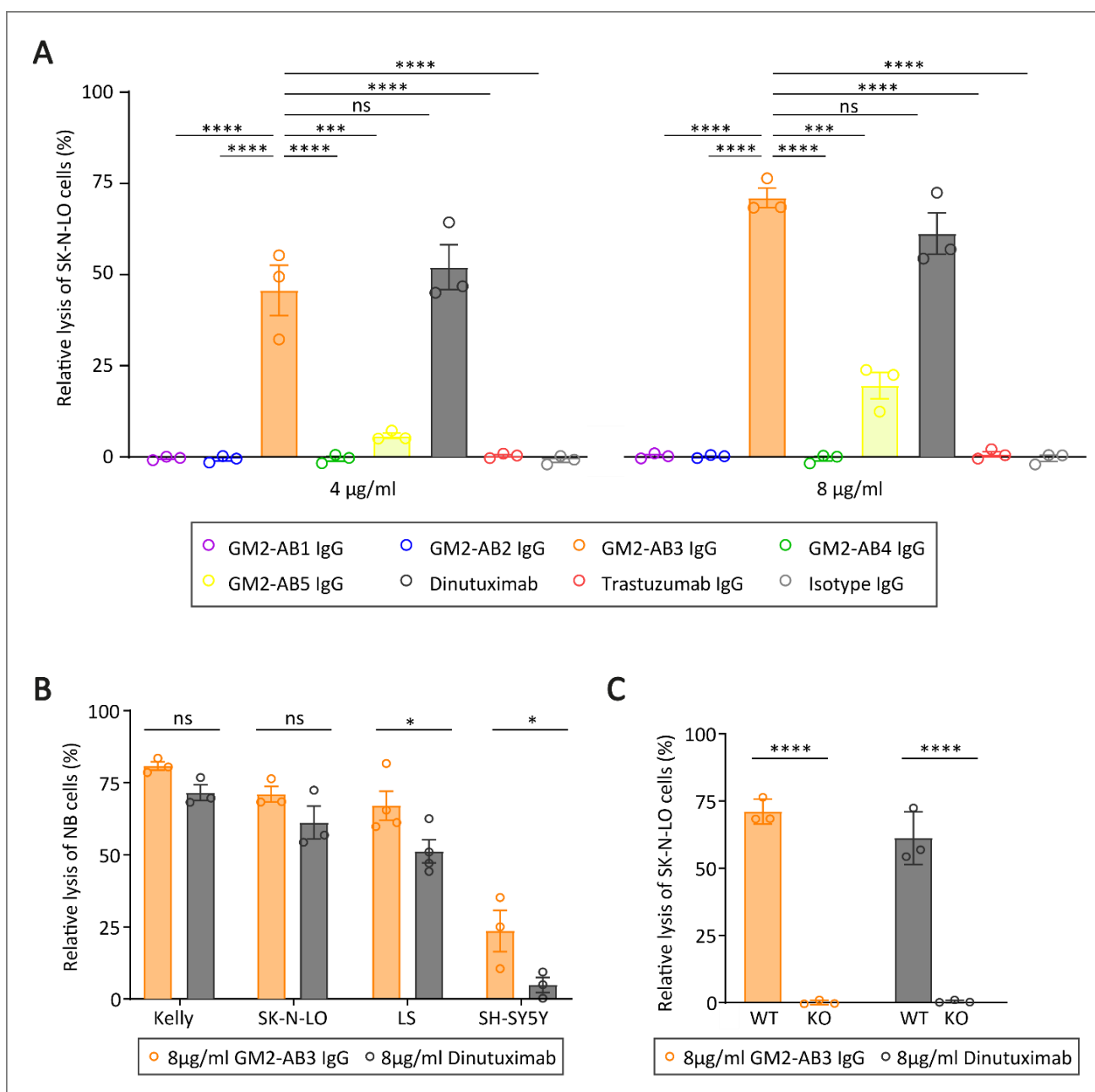


**Figure 14: Several anti-GM2 antibodies selectively induced complement-dependent cytotoxicity *in vitro* against GM2-expressing neuroblastoma cells, but not against *B4GALNT1* knockout cells, lacking GM2 and GD2.** The complement-dependent cytotoxic activity of GM2-AB1 IgG, GM2-AB2 IgG, GM2-AB3 IgG, GM2-AB4 IgG and GM2-AB5 IgG was assessed using the IncuCyte Live Cell Imaging system. SK-N-LO cells were incubated with 12.5% human serum and either 4 µg/ml or 8 µg/ml of the respective antibody for 2 h. Trastuzumab IgG and Isotype IgG were used as negative controls while the anti-GD2 antibody Dinutuximab was used as a positive control (**A**). The complement-dependent cytotoxicity of GM2-AB3 IgG was compared to Dinutuximab for the different neuroblastoma cell lines SK-N-LO, Kelly, LS, and SH-SY5Y (**B**). The specific lysis of SK-N-LO cells with a knockout of *B4GALNT1* was compared to wildtype cells (**C**). The columns represent the mean percentage of relative lysis of  $n = 3$  independent representative experiments and SEM. Statistics represent multiple unpaired t-tests with \*\*\*\*  $P < 0.0001$ , \*\*\*  $P < 0.001$ , \*\*  $P < 0.01$ , \*  $P < 0.05$ ; ns =  $P \geq 0.05$ . NB neuroblastoma; WT: wildtype; KO: knockout.

The GM2-AB3 IgG antibody, which showed superior binding and complement-dependent cytotoxicity against NB cells, was further investigated for its antibody-dependent cellular cytotoxicity (ADCC) activity. ADCC is another mechanism of action of IgG antibodies, where the antibody recruits immune

cells with the ability to kill the target cells. For the analysis of ADCC, NB cells were co-cultured with peripheral blood mononuclear cells (PBMC) at different effector to target (E:T) ratios, and 4  $\mu\text{g}/\text{ml}$  of the appropriate antibody was added for 4 h prior to flow cytometric measurement.

Figure 15 presents the results of the ADCC assay, depicting the relative lyses of Kelly (Figure 15A) and SK-N-LO (Figure 15B). At an E:T ratio of 5:1, GM2-AB3 IgG induced 20.4% lysis of Kelly cells and 16.1% lysis of SK-N-LO cells. The killing increased slightly when the E:T ratio was raised to 15:1. GM2-AB3 IgG induced higher ADCC against Kelly cells than the anti-GD2 antibody Dinutuximab, at both E:T ratios. For instance, at an E:T ratio of 15:1, the relative lysis with GM2-AB3 IgG was found to be twice as high as that of Dinutuximab (Figure 15A). On the other hand, GM2-AB3 IgG was also capable to induce ADCC in SK-N-LO cells. However, the cytotoxicity of Dinutuximab was higher in SK-N-LO cells, regardless of the PBMC amount used (Figure 15B). Additionally, some non-specific background lysis of up to 9.0% was observed with the Isotype IgG antibody.

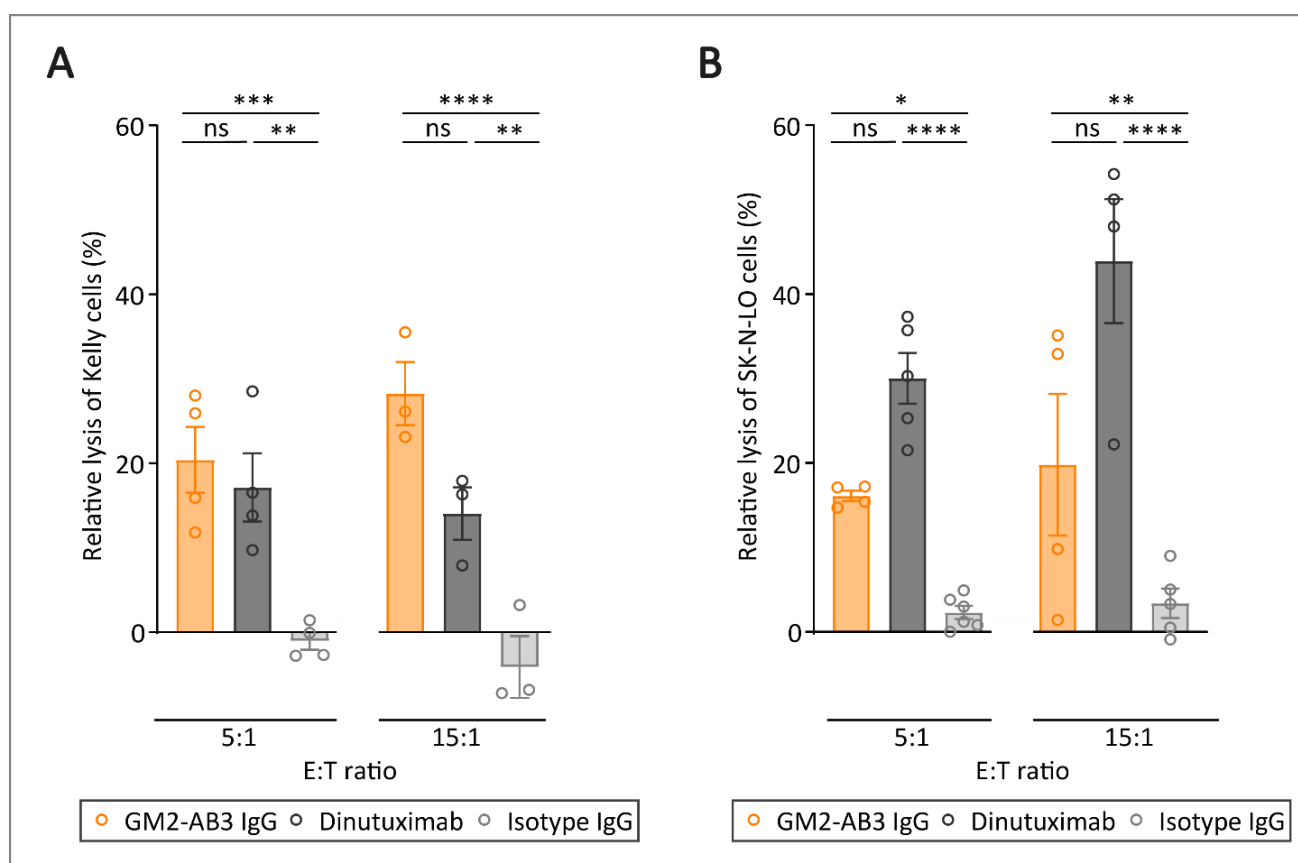


**Figure 15: GM2-AB3 IgG was able to induce antibody-dependent cellular cytotoxicity against neuroblastoma cells *in vitro*.** Antibody-dependent cellular cytotoxicity against Kelly (**A**) and SK-N-LO (**B**) was assessed in a flow cytometry-based killing assay using 4  $\mu\text{g}/\text{ml}$  GM2-AB3 IgG, Dinutuximab, or Isotype IgG with different amounts of peripheral blood mononuclear cells from healthy donors, serving as effector cells. The columns represent the mean percentage of relative lysis of at least  $n = 3$  biological replicates and SEM. Statistical analysis was conducted using multiple unpaired t-tests with \*\*\*\*  $P < 0.0001$ , \*\*\*  $P < 0.001$ , \*\*  $P < 0.01$ , \*  $P < 0.05$ ; ns =  $P \geq 0.05$ . E:T: effector to target.

When comparing the results of ADCC and CDC, it was observed that the relative lyses achieved with 4 µg/ml GM2-AB3 IgG were generally lower in ADCC, where the maximum lysis was found to be 28.2% in case of Kelly cells and 19.8% for SK-N-LO cells. In comparison, 66.2% of Kelly cells and 45.6% of SK-N-LO cells were killed with GM2-AB3 IgG in CDC (Figure 14A). Although the results from the CDC assay and the ADCC assay cannot be compared directly, a trend in the antibody's primary cytotoxic activity mechanism, which is complement-mediated cytotoxicity, can be assumed.

### 5.8 *In vivo* testing of GM2-AB3 IgG

Following the assessment of *in vitro* attributes of all anti-GM2 antibodies including the binding capacity and effector functions like CDC as well as ADCC, it was concluded that the anti-GM2 antibody variant GM2-AB3 IgG with the variable sequence of KM966 had the most favorable characteristics and was thus the most promising candidate. To further evaluate the potential of GM2-AB3 IgG, it was compared to the Isotype IgG in a mouse model. The experimental procedure for this is illustrated in Figure 16A.

In this study, immunodeficient triple transgenic NOD.Cg-*Prkdc*<sup>scid</sup>Il2rg<sup>tm1Wjl</sup>Tg(CMV-IL3,CSF2,KITLG)1Eav/MloySzJ (NSG-SGM3) mice expressing human IL-3, GM-CSF (CSF2) and SCF (KITLG) were humanized by irradiation, followed by intravenously (i.v.) injection of human hematopoietic stem cells (hHSC). The humanization process was monitored by flow cytometric analysis of the blood as described in chapter 9.7.2. An initial increase of hCD45<sup>+</sup> cells to an average of 25.5% was detected six weeks after the humanization. However, the percentage of hCD45<sup>+</sup> cells subsequently declined to an average of 10.3% after 11 weeks and 9.4% after 14 weeks (Figure 16B). In some mice, the percentage of CD45<sup>+</sup> cells showed an upward trend again between week 11 and week 14, but all but one mouse remained below 20%. Although the percentage of hCD45<sup>+</sup> cells fell below the recommended threshold of 25%, the mice were treated with either 140 µg of GM2-AB3 IgG or Control IgG per injection. Mice showing the highest engraftment of hHSC were selected for the treatment with GM2-AB3 IgG antibody. The tumors were palpable approximately after seven to 14 days after the inoculation of SK-N-LO cells. No differences in tumor growth or mouse survival were observed between the two treatment groups (Figure 16C,D).

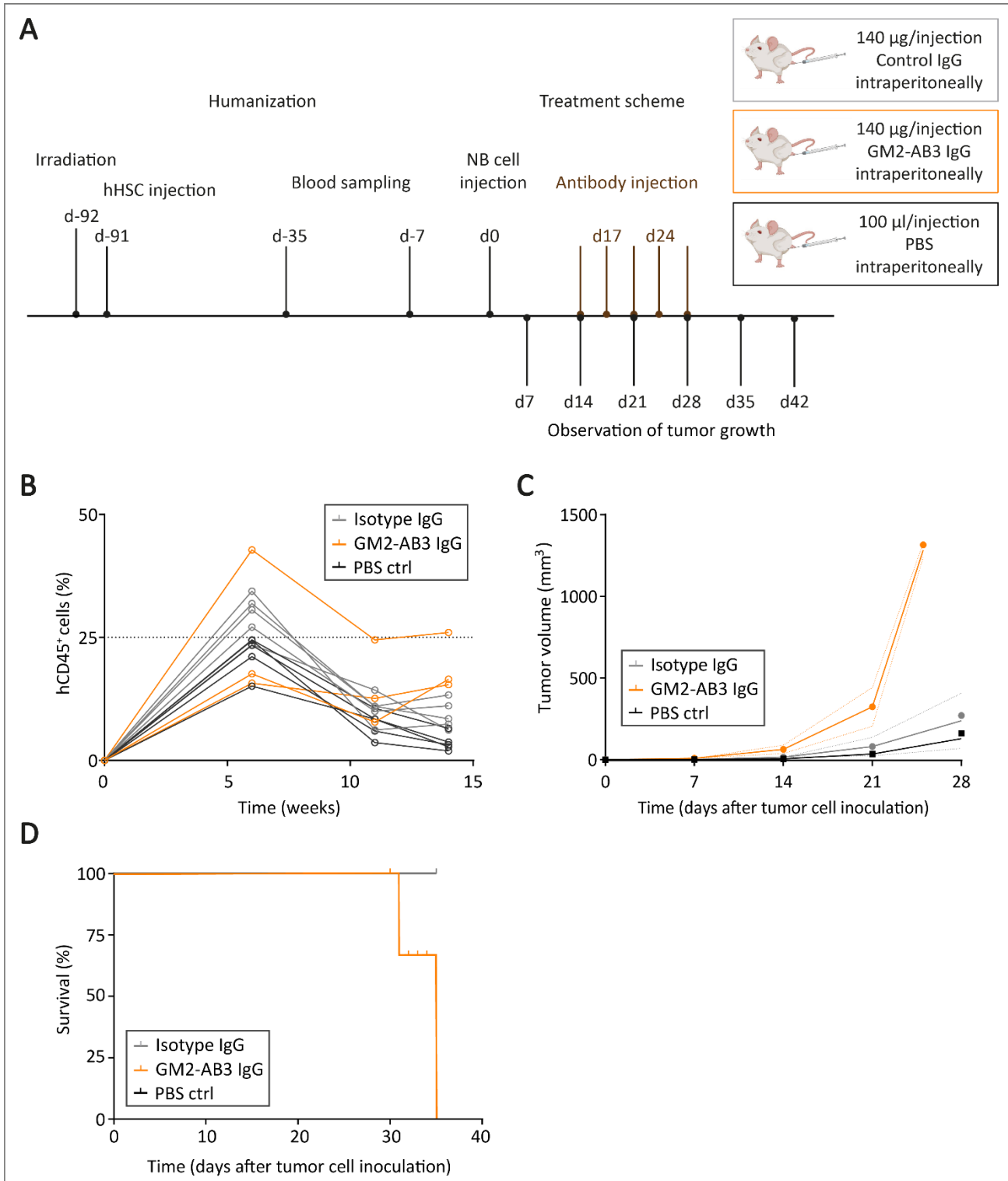


**Figure 16: Treatment of poorly humanized mice with GM2-AB3 IgG did not show any effects on tumor growth.** The experimental setup involved testing GM2-AB3 IgG in comparison to the Isotype IgG or PBS in humanized NSG-SGM3 mice bearing subcutaneously injected SK-N-LO tumor cells (A). The humanization process was monitored by measuring the percentage of human CD45<sup>+</sup> cells at different time points prior to the injection of SK-N-LO tumor cells (B). Tumor volumes were measured either through tumor palpation or with a caliper once a week (C). Kaplan-Meier curves depict the survival of mice from both treatment groups until the experiment was ended (D). The experimental endpoints were defined as tumors reaching a volume of >1,500 mm<sup>3</sup> or a weight loss of >20% from the baseline weight over a 24-hour period. hHSC: human hematopoietic stem cells, NB: neuroblastoma, d: day.

In another *in vivo* experiment, the percentages of hCD45<sup>+</sup> cells were stable from week six to ten, with an average percentage of 33.5% (Figure 17A). Notably, in some mice, there was even an increase in the percentage of hCD45<sup>+</sup> cells, for example, from 22.4% to 30.3%, indicating successful engraftment of human hematopoietic cells. Although some mice showed a slight decrease in hCD45<sup>+</sup> cells, all values remained above the cut-off of 25% hCD45<sup>+</sup> cells. The body weights of the mice remained stable throughout the entire experiment, although in some mice, a slight decrease in body weight was observed in the first days after injection of hHSCs. This decrease was temporary, and the mice regained their normal body weight within a few days (Figure 17B). Upon treatment the mice showed similar linear tumor burden between d14 and d21. Starting from d21, tumor growth became exponential in three out of four mice in the control group, while in all five mice treated with GM2-AB3 IgG, the tumor growth remained linear resulting in smaller tumors (Figure 17C). At d28, the tumors in the control mice showed greater size variance compared to the GM2-AB3 IgG-treated group, and the tumors of two mice in the control group reached a size greater than 1,500 mm<sup>3</sup>, leading to their sacrifice (Figure 17D).

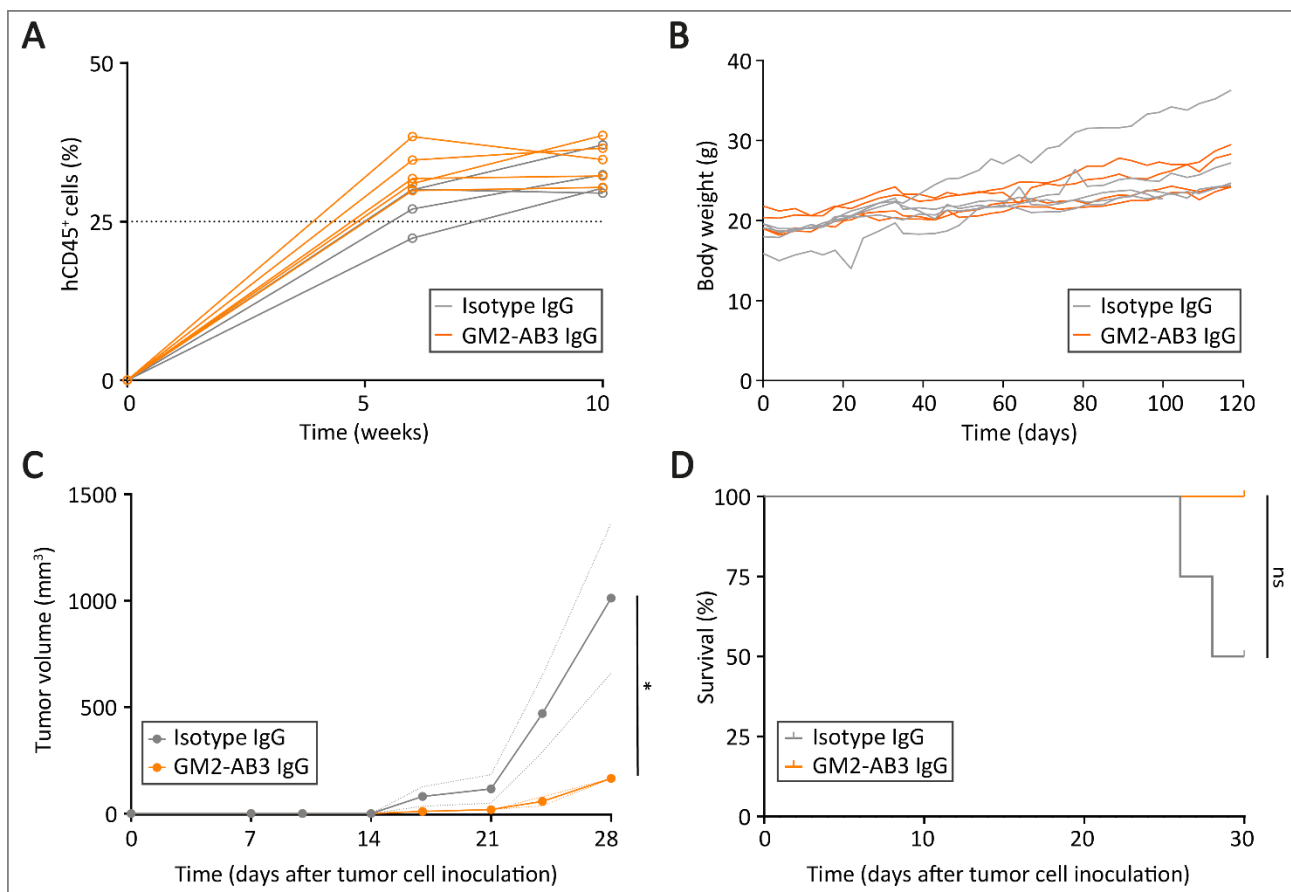


**Figure 17: Multiple treatments with GM2-AB3 IgG slowed down tumor growth *in vivo*.** The humanization process was monitored by measuring the percentage of human CD45<sup>+</sup> cells at two time points after intravenous injection of human hematopoietic stem cells (A). The body weight of the mice was also tracked throughout the experiment (B). Tumor volumes were measured regularly after the inoculation of SK-N-LO cells either by tumor palpation or with a caliper (C). Kaplan-Meier survival curves were generated for both treatment groups, until all mice were sacrificed on day 30 after tumor cell inoculation (D). The endpoints were met when tumors reached a volume of >1500 mm<sup>3</sup> or a weight loss of >20% from the baseline weight over 24h occurred. Statistical analysis was conducted using either Two-way RM-ANOVA (C) or Mantel-cox test (D) with \*\*\*\*  $P < 0.0001$ , \*\*\*  $P < 0.001$ , \*\*  $P < 0.01$ , \*  $P < 0.05$ ; ns =  $P \geq 0.05$ .

## 6 Discussion

### 6.1 Analysis of GD2 and GM2 expression on tumor cell lines *in vitro*

Gangliosides have been extensively studied for their involvement in various cancer types where they modulate signal transduction by interacting with signaling receptors on the cell surface [72,76]. These interactions can affect cell proliferation, differentiation, migration, and survival, contributing to the development and progression of cancer [123]. In the context of NB, ganglioside GD2 was found to be highly overexpressed on tumor cells, and it has been extensively studied as an immunotherapeutic target [81,124], eventually leading to the development of the chimeric human/murine antibody Dinutuximab [31,125]. After having discovered the ganglioside GM2 as the target of naturally occurring and NB lysing antibodies, we concentrated on validating the presence of GM2 on NB and other tumor cell lines in comparison to GD2. This validation was accomplished by examining the cell surface expression on both wildtype and knockout cell lines using flow cytometric staining.

#### 6.1.1 Variability of ganglioside expression on neuroblastoma cell lines

The expression of gangliosides, specifically GD2 and GM2, was found to be highly variable among different NB cell lines and even within the same cell line. This variability was evident in the widely dispersed gMFI of GM2 expression on SK-N-LO cells, for example. While there is limited data available for the ganglioside expression pattern on SK-N-LO [126,127], existing literature demonstrated distinct findings for the GD2 expression on SH-SY5Y cells. Prior research conducted by our working group, along with studies by Mabe *et al.*, proofed the presence of GD2 on SH-SY5Y cells, although GD2 was not detected on these cells in this work [128,129]. In another study, it was shown that GD2, accounted for 18% of the total ganglioside composition on SH-SY5Y cells, equivalent to 8 nmol/10<sup>8</sup> cells, which was the lowest GD2 content among all analyzed cell lines there [92]. In contrast, Ruan *et al.* did not detect GD2 or its precursor GD3, as well as no mRNA levels or activity of the GD3 synthase in SH-SY5Y cells [101]. These findings suggest that ganglioside expression patterns on cell lines are generally variable and may depend on several factors.

Data obtained from the 'Human Protein Atlas' corroborated very low *ST8SIA1* mRNA expression below 0.3 nTPM for SK-N-AS, SH-SY5Y and SK-N-SH. These findings correlated with the diminished GD2 expression detected, potentially originating from reduced levels of its precursor GD3, which is synthesized by the encoded GD3 synthase. On the other hand, Kelly cells, for example, had higher *ST8SIA1* mRNA levels of 2.0 nTPM which probably contributes to higher surface levels of GD2 [130,131]. In comparison, mRNA expression data for *B4GALNT1*, the gene encoding GM2/GD2 synthase, were higher and in the range of 6.7 nTPM for SK-N-AS, 11.6 nTPM for SH-SY5Y, and 28.2 nTPM for IMR32, confirming that the synthesis of GM2 and GD2 is potentially possible in

these cell lines [130,131]. Additionally, research by Hettmer *et al.* analyzed GM2 content in NB cell lines LAN-1, IMR-32, SK-N-SH, and SH-SY5Y, demonstrating the presence of GM2 in all four cell lines, consistent with the findings of this work [92]. Although there is no definitive correlation between the expression levels of glycosyltransferases and the presence of specific gangliosides on the cell surface, it provides an indication of whether a cell line is capable to synthesize those gangliosides. But ganglioside synthesis is much more an interplay of different enzymes including glycosyltransferases and sialidases as described in chapter 3.3.1.

Diverse expression of gangliosides in tumor cells was described in various publications where this phenomenon was attributed to cell density. For instance, density-dependent changes in ganglioside composition were observed in murine cholinergic NB cells, where pre-confluent cells predominantly expressed GM3 and post-confluent cells highly expressed GD1a. The highest GM2 expression was observed in confluent cultures of cholinergic NB cells, while noradrenergic cells displayed the lowest GM2 expression at confluency, indicating that the cell subtype also plays a role in the ganglioside composition [132]. Furthermore, it has been reported that the *de novo* synthesis of GD2 can occur independently from changes in synthase expression levels which was observed in osteosarcoma cell lines, where an upregulation of GD2 expression was detected as cell confluency increased. In all but one cell line tested, the levels of GD3 synthase and GM2/GD2 synthase remained unchanged [133]. This suggests that the expression of gangliosides might be susceptible to environmental factors such as nutrient availability or oxygen levels which are associated with cell density [134–137].

It is important to be cautious when interpreting these results, as the analysis was performed on cell lines in a two-dimensional (2D) culture, representing an artificial *in vitro* environment that may not fully reflect the presence and significance of GM2 in NB patients. For instance, in the context of pancreatic ductal adenocarcinoma GM2 expression was found to be higher in 3D spheres [123]. Therefore, it would be beneficial to analyze the GM2 and GD2 content on NB cell lines using more complex and multifactorial models, such as 3D tumor models, to gain a better understanding of their presence and role under conditions that more closely resemble the situation *in vivo*. Another limitation to consider is the used murine antibody clone, MK1-16 IgM, as it specifically recognizes only the Neu5Ac isoform of GM2 [138]. In culture conditions using FBS the presence of other isoforms such as the Neu5Gc-GM2 were shown to be higher than in the presence of human serum [139,140]. This may result in a bias in favor of one GM2 isoform, leading to incorrect assumptions about the total GM2 content.

Despite the limitations of the *in vitro* 2D-culture conditions and the high variability in the expression levels of GM2, the ganglioside was found to be present on the cell surface of each NB cell line tested, as well as some other tumor types. In contrast, GD2 was absent in three out of ten NB cell lines and in all other tumor types. GM2 expression was found on breast cancer, medulloblastoma, hepatoblastoma, and rhabdomyosarcoma cell lines, which was consistent with the findings of Lee *et*

*al.*, who also observed the absence of GD2 expression in several tumor types while GM2 was present in all tested tumor cell lines [141]. GM2 expression has further been reported in melanoma [142,143], Ewing sarcoma [144] osteosarcoma [133], pancreatic ductal adenocarcinoma [123] and small cell lung cancer [145]. These findings indicate that an immunotherapeutic approach targeting GM2 is not restricted to NB but may also be a potential therapeutic approach for other tumor types.

### **6.1.2 Changes in ganglioside composition on neuroblastoma cells following *B4GALNT1* knockout**

Given that gangliosides themselves cannot be stably modified through genetic knockout, focusing on enzymes responsible for their synthesis, holds greater promise in regulating their expression. Using the CRISPR/Cas9 technology, a successful knockout of the *B4GALNT1* gene, was achieved in various NB cell lines. The quantification of genome editing revealed a consistent non-homologous end-joining repair mechanism across different cell lines. Consequently, the reading frame shift caused by 1 bp insertion led to an aberrant amino acid sequence with a premature stop codon and thus to an unfunctional protein. By employing a GM2/GD2 synthase KO, we successfully generated stable control cell lines that completely lacked GM2 and GD2 which has not been previously investigated in the context of NB. This KO cell line served as a valuable reference for our studies and allowed for the determination of the specific effects and contributions of GM2 and GD2 on NB cells and its relevance to immunotherapeutic treatments with our antibodies.

Furthermore, attempts to knock out the *ST8SIA1* gene, encoding GD3 synthase are ongoing. The function of GD3 synthase has previously been explored within the context of triple negative breast cancer and glioma and proved the complete absence of GD2 expression upon *ST8SIA1* KO [146,147]. Therefore, this *ST8SIA1* KO cell lines would be a valuable tool to verify the specificity of the tested antibodies to ensure that there is no cross-reactivity with other b- or c-series gangliosides. Additionally, altering the balance between GD3 and GM2 synthesis from their common precursor GM3 could potentially increase GM2 expression levels on the cell surface and minimize the variability in expression due to fewer synthesis pathway options in the ganglioside pathway.

In conclusion, the expression of gangliosides, such as GD2 and GM2, exhibited heterogeneity among NB cell lines, influenced by both the regulation of the enzymes involved in synthesis and environmental factors. However, GM2 showed widespread expression on NB cell lines and other tumor types, making it a potential target for immunotherapeutic approaches. KO cell lines can further serve as valuable models to investigate the balance in ganglioside expression and the verification of antibody specificities. Additionally, these models can aid in generating antibodies against other gangliosides.

## 6.2 Relevance of *in vivo* GM2 expression for the treatment of neuroblastoma

In the scope of this work, it was shown that GD2 was consistently expressed at a high level in samples from NB patients. However, the expression of GM2 was very heterogenous and not detectable by flow cytometric analysis in all analyzed specimens. These findings are in line with the results reported by Paret *et al.*, who investigated the expression of gangliosides on 14 NB samples by thin layer chromatography. Their study revealed a high, yet variable expression of GD2 and more complex gangliosides such as GT1b in the majority of samples. In contrast, GM2 was detected in six out of 14 samples and at a lower level [148]. Remarkably, specimens derived from individuals with high-risk NB exhibited minimal GM2 expression, whereas the sample from a stage 4S patient displayed the highest levels of GM2 expression. However, the exact ganglioside expression in stage 4S NB and its correlation to other stages would require a more comprehensive analysis.

### 6.2.1 Different isoforms of GM2 complicate the detection by antibodies with different specificities

While the murine antibody clone MK1-16 IgM did not recognize GM2 on any of the specimens, the binding of GM2-AB3 IgG showed variable results among the analyzed samples. The lack of GM2 detection in the human samples by MK1-16 IgM, might be attributed to its specificity for Neu5Ac-GM2 [138]. Although, the most common form of sialic acid in human tissues is Neu5Ac, there is evidence that the Neu5Gc isoform can be acquired through dietary sources. This could potentially lead to Neu5Gc-GM2 becoming the predominant isoform in tumors, consequently hindering the recognition by MK1-16 IgM [83,84,149]. Additionally, it has been demonstrated that under hypoxic conditions, Neu5Gc-GM2 expression is upregulated in colon cancer cells. This upregulation occurred independently from an altered expression of glycosyltransferases and was attributed to an increase in the expression of the sialic acid transporter [134]. It is important to note that the incorporation of Neu5Gc, alters the structure of GM2, rendering the antibody clone MK1-16 IgM ineffective in properly detecting the antigen.

In comparison, the antibody clone KM966 is known to recognize both isoforms of GM2, and thus has a higher probability of recognizing the target on NB cells [115]. In this work, the mean gMFI of GM2-AB3 IgG binding, containing the variable amino acid sequence of KM966, were higher for all NB cell lines compared to MK1-16 IgM. This provides additional evidence for the differential recognition of GM2 by these two antibodies. However, the extent to which each GM2 form is incorporated into tumors has not been analyzed yet, but it could be an interesting aspect to consider in the development of clinically relevant antibodies. Furthermore, an interesting approach would be to investigate the murine antibody sequence MK2-34, which was generated from the same mouse immunization as

MK1-16, and specifically recognizes Neu5Gc-GM2 [115]. Testing this clone could provide insights into the detection and characterization of Neu5Gc-GM2 in the analyzed samples.

### 6.2.2 The ganglioside composition is influenced by extrinsic and intrinsic factors

The comparison of patient material from different origins, such as fresh specimens and explanted tumor cells is challenging because it is well known that the cultivation conditions can influence the expression of gangliosides. Recently, Thirant *et al.* demonstrated that extrinsic factors such as EGF or TNF $\alpha$  in cell culture media induced a phenotype switch of NB cells through an epigenetic reprogramming. Furthermore, single-cell transcriptomic analysis showed that NB cells exclusively expressed a noradrenergic phenotype *in vivo* while xenograft cell lines derived from these patients exhibited a mesenchymal character *in vitro* [150,151]. This suggests that the cultivated cells from patient-derived explanted tumors may have an altered ganglioside expression pattern and may not accurately reflect the *in vivo* situation. Therefore, it would be beneficial to assess the GD2 and GM2 expression at the time of sample acquisition and compare it to the expression status after several weeks of cultivation. This comparison would provide a more comprehensive understanding of the changes that occur over time and help to obtain a clearer picture of GM2 and GD2 expression dynamics *in vivo* and *in vitro* as well as the correlation between the different NB cell identities.

So far, further evidence of the changes in ganglioside expression was provided in the context of the TH-MYCN transgenic mouse model. McNerney *et al.* showed that GD2 was highly expressed in tumors *in vivo*, however the GD2 expression decreased after several weeks of cultivation of tumor-derived cells. This was accompanied by a transition of NB cells, shifting from a noradrenergic GD2<sup>+</sup> phenotype *in vivo* to a mesenchymal GD2<sup>-</sup> phenotype *in vitro*. This transition was associated with the downregulation of GM2/GD2 synthase expression, which is responsible for the synthesis of both gangliosides [152]. However, GD2, but not GM2 was consistently expressed in all tumor samples in this study regardless of the sample type. This suggests that a downregulation of GM2/GD2 synthase, as described by McNerney *et al.* was unlikely to be the sole reason for the absence of GM2. In contrast, GM2, but not GD2, was present on all NB cell lines screened showing the opposite picture compared to the staining of the samples. Nevertheless, it is important to consider that the expression of gangliosides, in general, is highly variable and can be easily influenced by various extrinsic and intrinsic factors resulting in an epigenetic reprogramming and thus aberrant regulation of ganglioside synthetases.

Changes in ganglioside composition are known to occur under pathological conditions and are associated with modifications of transferase expression, as shown for the GD3 synthase which was overexpressed in several cancers such as lung and breast cancer [75]. For this, it is logical to consider the expression levels of all key galactosyl and sialyl transferases involved in ganglioside synthesis in

regard of variable ganglioside expression levels. Liang *et al.* for example showed a 5-fold upregulation of *B4GALNT1* gene expression and a 90.6-fold upregulation of *ST8SIA1* gene expression on RNA level in breast cancer stem cells compared to human mammary cell lines which was associated with increased expression of both GD2 and GM2 [153]. Recently, Sorokin *et al.* conducted RNA sequencing analysis using NB data from various databases. Contradictorily, their findings revealed that the gene expression of *B4GALNT1* was higher compared to *ST8SIA1* [33]. These observations indicate that the expression levels of the synthases alone are not the cause of the imbalance observed between GM2 and GD2 expression in NB samples. Interestingly, three different isoforms of *B4GALNT1* that may exhibit differential expression and functional characteristics exist [154]. This observation aligns with the findings of Ruan *et al.*, who observed varying mRNA levels of *B4GALNT1*, indicating the potential for differences in their activity and substrate specificities that could contribute to diverse ganglioside profiles [101].

Another aspect to consider is the enzymatic velocity which is different for both synthases. Some years ago, the enzymatic activities of these enzymes were investigated showing that LAN-5 cells, for example, exhibited an enzymatic activity of 1.416 pmol/h × mg protein for the GM2/GD2 synthase while the measured activity of the GD3 synthase was lower with 572 pmol/h × mg protein. That suggest that activity alone is not responsible for the differential expression of GD2 and GM2. It is important to note that these findings were obtained from cell lines, which may not accurately represent the synthase activity observed in patient samples and provide an artificial picture of synthase activity [155].

It is likely, that the ganglioside composition of cells is also influenced by the bioavailability of substrates such as GalNAc and sialic acids which are necessary for the synthesis of GM2 and GD2 or GD3, respectively. The relative abundance of substrates like GalNAc and sialic acids can vary depending on the specific tissue, cell type, developmental stage, disease state or physiological conditions. Published data has demonstrated that the GD3 synthase is strongly dependent on the presence of sialic acids, as evidenced by its downregulation in embryonic stem cells lacking sialic acids [156]. The regulation of transferases involved in ganglioside synthesis is not yet fully understood. Consequently, it remains unclear why the tumor samples analyzed in the scope of this work consistently expressed GD2, whereas the GM2 expression was highly variable, although both gangliosides are synthesized by the same enzyme.

When identifying a new cell surface molecule as a potential target for immunotherapeutic treatment, it is crucial to evaluate its expression in patient samples on the one hand but also in healthy tissues on the other hand, in order to avoid undesirable side effects. An example illustrating this challenge is the anti-GD2 antibody Dinutuximab, which exhibits on-target off-tumor cytotoxicity by binding to peripheral nerve cells, leading to severe neuropathic pain during treatment [30,157]. In contrast, the

naturally occurring anti-GM2 antibodies do not show any side effects in individuals who possess these antibodies, indicating that the application of anti-GM2 antibodies is generally safe and less side effects are expected. Although the expression of GM2 is primarily associated with malignant diseases, it is generally known that complex gangliosides are expressed in developing tissue and are typically present in the nervous system of healthy adults while simple gangliosides can be found in normal extraneural human tissue [75]. A study conducted by Tai *et al.* in 1983 reported that GM2 accounted for 13.4% of total sialic acids in the fetal brain, and only 3.6% in the adult brain [158]. Though these findings suggest a substantial decrease in GM2 levels during brain maturation, it persists to a lesser extent. Anyway, the expression of GM2 in other normal tissue remains unclear, highlighting the importance of expression analysis, particularly for determining potential on-target off-tumor cytotoxicity of antibodies.

### 6.2.3 Limitations in the detection of gangliosides in human samples

The interpretation of the results from patient sample staining has some limitations such as the small number of specimens analyzed thus far, as well as the difficulty in obtaining material from children. Furthermore, the incidence of neuroblastoma is low, with 120 children newly diagnosed with NB in Germany each year [159]. To enhance the quality and reliability of the findings, it is essential to evaluate a larger number of patient samples and establish a standardized operating procedure for handling this valuable material. The analysis of gangliosides is generally constrained due to the necessity for specific methodologies for their detection. For instance, immunohistochemistry on formalin-fixed, paraffin-embedded (FFPE) samples, is a controversial method for the detection of ganglioside expression. This controversy arises from the extraction of tissue lipids caused by solvents, such as ethanol, used in the process [160,161]. Consequently, the use of methodology is limited to techniques like mass spectrometry, immunohistochemistry on fresh frozen sections or flow cytometric analysis. Only the latter method was utilized in this work due to the limited available material.

This analysis is subject to another limitation, namely the differences in sample types ranging from bone marrow to tumor biopsies and patient-derived (PD) explanted tumor cells which required individual staining protocols. For instance, in bone marrow specimens an advantage was the analysis without enzymatic tissue digestion but the predominant cell population detectable was comprised of hematopoietic progenitor cells [162]. This may have interfered with the analysis of tumor cells that are present at a much lower frequency. Although the quantity of tumor cells is higher in biopsy specimens, other cell types such as immune cells or stromal cells also contribute to the tumor microenvironment [163]. Due to the distinct compositions of these samples, it is not feasible to apply a uniform analysis panel, thus making comparisons difficult.

In conclusion, further investigation is required to fully understand the GM2 expression and its relevance for therapeutically applicable treatments for NB patients. It is necessary to eliminate methodological difficulties to ensure a reliable analysis of GM2 expression. Although the expression of GM2 in NB samples was inconsistent within the analyzed sample population, nevertheless it might be a promising target for immunotherapy for patients who respond poorly to anti-GD2 immunotherapy. Approximately 50% of patients treated with anti-GD2 antibodies still relapse [164]. Modulation of the expression of GM2 through strategies involving the use of inhibitors or enhancers could increase its expression on the cell surface. For instance, it has been demonstrated that the expression of GD2 can be upregulated by pharmacologically inhibiting the histone methyltransferase enhancer zeste homolog 2, thereby leading to increased expression of GD3 and GM2/GD2 synthase [165]. Similar approaches could be explored to manipulate the expression of GM2 by targeting specific regulatory factors or pathways associated with its synthesis. A prerequisite for implementing such a strategy would be its specificity to tumor-associated elevation of GM2, while sparing healthy tissues. Further, it is important to note, that clinically targetable antigens, suitable for treatment of NB, are rare and it remains a challenge to identify those [166,167].

### 6.3 Performance analysis of different anti-GM2 antibodies

The aim of this work was to evaluate all described anti-GM2 antibodies (GM2-AB1 – GM2-AB5) for their potential application in treatment of high-risk NB patients. To assess their characteristics and effectiveness in targeting GM2, several key features of the antibodies were analyzed such as expression quantity, stability, specificity, binding capacity, and ability to mediate the lysis of NB cell *in vitro* and *in vivo*. The five antibodies tested originated from different sources (chapter 5.4) and showed different properties.

#### 6.3.1 Differential expression and stability of anti-GM2 antibodies and isotypes

Initially, differences in antibody expression levels were noticed, which manifested in different yields and ratios of heavy and light chains. Successful expression and high-yield production of antibodies generally depend on several factors, including vector design, host cell line, and culture conditions.

In the scope of this work, the pVITRO expression system was used, which has the advantage of encoding both heavy and light chains under the control of two individual promoters in a single plasmid [168]. Handling a single plasmid is also less time consuming and cost-effective for tasks like DNA preparations, transfection and antibiotic selection. Additional restriction sites were inserted to the backbone to have more variability in the exchange of individual VH and VL fragments for the testing of further anti-GM2 antibodies. In previous work by Yang *et al.*, long-term, and large-scale production of adalimumab, an IgG antibody targeting TNF- $\alpha$ , was demonstrated using a dual promoter

expression plasmid. Their results showed that the dual expression system outperformed monocistronic and bicistronic vectors by achieving 4.4- and 9.4-fold higher yields, respectively, after a two-day expression period in Chinese hamster ovary (CHO) cells [169].

Furthermore, the intracellular availability of heavy and light chains significantly affects proper antibody assembly, folding, and glycosylation patterns, thereby influencing the expression levels. These factors can be influenced by different vector designs [170,171]. A study on different expression vectors for an anti-HER2 antibody demonstrated that an excess of light chain fragments resulted in higher levels of antibody and prevented fragment aggregation as well as aberrant glycosylation [172]. In this work, lower and varying amounts of light chains were detected for each antibody, and the ratio between heavy and light chains also differed within the antibody pool. Consequently, it would be advantageous to test various expression formats, such as a monocistronic system, which enables the adjustment of different molar ratios and allows for precise control of the amount of light chain in each construct. Another vector design option is a bicistronic vector that contains a single open reading frame, with antibody chains separated by internal ribosomal entry sites (IRES) [170,173–175] or a self-splicing internal protein (intein) [176,177]. Although the pVITRO plasmid contains two elongation factor-1-alpha (EF-1 $\alpha$ ) promoters which are widely used in different mammalian cell types due to their consistent strength, it is conceivable to use a combination of different promoters to affect the expression ratio of heavy and light chain [178,179].

Another important aspect to consider is the choice of host cell line for antibody expression and the optimization of culture conditions during the expression process. Various cell types are suitable for antibody production, including prokaryotic hosts such as gram-negative or gram-positive bacteria as well as eukaryotic hosts like yeast or insect cells [180]. Therapeutic antibodies are produced predominantly in mammalian cells as for instance HEK and CHO cells to minimize the risk of immunogenicity or impaired effector functions that could occur due to altered glycosylation patterns as shown for antibodies produced in *E. coli* [181,182]. In this work, HEK cells were used for the antibody production because they are known to yield higher amounts of IgG antibodies during transient transfection compared to CHO cell lines. For instance, HEK293T and CHO-K1 cells yielded up to 14 mg/ml and 3 mg/ml antibody, respectively, following transient transfection [170,180]. Similarly, Backliwal *et al.* achieved antibody amounts of 100 mg/ml and 30 mg/ml in HEK293E and CHO-DG44 cells, respectively [183]. However, for IgM antibodies, the productivity has been shown to be lower in HEK293 cells compared to CHO-DG44 [184], which could explain the observed low yields of GM2-AB3 IgM after transient transfection in this work. This was also consistent with previously reported results, according to which the productivity of IgG-secreting cells was approximately 3.5 times higher than that of IgM-secreting cells [185]. This can be explained by the more complex pentameric structure of IgM antibodies. Consequently, GM2-AB3 IgM could not be tested in further

experiments due to low amounts. For this, the establishment of a stable, long-term antibody expressing cell line would be advantageous and could further help avoiding fluctuations due to transient transfections. Most commonly, CHO cells are used for stable antibody expression, employing antibiotic selection methods [180]. Since the pVITRO plasmid contains a hygromycin resistance cassette, this strategy could be tested for expression of IgM antibodies in future experiments.

Additionally, it was demonstrated that culture conditions, such as a temperature shift from 37 °C to 33 °C or the utilization of a fed-batch culture strategy improved the yield of adalimumab expressed by CHO cells [169]. Metabolite profiling was also used to identify key nutrients such as specific combinations of glucose, amino acid mixtures, and pyruvate, as well as an optimized feeding regimen that allowed for higher antibody yields [186]. The application of these strategies could also be useful for optimizing the expression of IgM antibodies.

In the context of antibody stability, the unfolding profiles of three out of the five anti-GM2 antibodies tested (GM2-AB1 IgG, GM2-AB2 IgG and GM2-AB3 IgG) and the anti-GD2 antibody clone ch14.18 IgG exhibited similar characteristics with two distinct inflection points during thermal unfolding. These inflection temperatures ( $T_i$ ) were consistent with those reported in literature for IgG1 antibodies, indicating that a pretransition at 71 °C and a main transition at 85 °C occurred as two independent unfolding events for the  $F_{ab}$  and  $F_c$  fragments. The pretransition involving 220 amino acids is proposed to correspond to the unfolding of the  $C_{H2}$  domain of the  $F_c$  fragment, while the main transition involving 850 amino acids is responsible for the unfolding of the  $F_{ab}$  fragment and the  $C_{H3}$  domain of the  $F_c$  fragment [187,188]. When examining the stability of GM2-AB3 IgG under various storage conditions, no effect on long-term stability was observed. The  $T_i$  remained consistent throughout the 65-day observation period, suggesting that the storage conditions did not significantly impact the antibody's stability. Some studies have also reported the presence of three inflection points at 73 °C, 78 °C, and 84 °C for intact IgG antibodies, corresponding to the unfolding of the  $C_{H2}$ -domain,  $C_{H3}$ -domain, and  $F_{ab}$  fragment, respectively [189]. However, the unfolding profiles of GM2-AB4 IgG and GM2-AB5 IgG differed from the other antibodies, indicating lower thermostability. This could also be attributed to the formation of aggregates of  $F_{ab}$  fragments during thermal unfolding. For instance, it was shown that increasing pH influenced the stability of antibodies and caused a shift in the first  $T_i$  of an IgG1 antibody to lower temperatures [188]. This might be an explanation for the additional peak observed at lower temperatures for GM2-AB5 IgG.

On the other hand, glycosylation plays an important role in antibody stability. Studies showed that the complete absence of glycosylation lead to decreased stability in the  $C_{H2}$  domain and a lower unfolding temperature, while the stability of the  $F_{ab}$  fragment and  $C_{H3}$  domain remained unaffected by glycosylation patterns [188,190,191]. In addition, Kayser *et al.* demonstrated that aglycosylated

antibodies were more prone to form aggregates than their glycosylated counterparts [192]. However, since all antibodies were produced in the same host cells, this glycosylation-dependent explanation seems unlikely. Notably, significant differences in antibody stability were observed between GM2-AB3 IgG and GM2-AB4 IgG, despite their identical CDR and high similarity within the framework of the variable region. According to Ito *et al.*, pH stability might be an issue here, because at higher pH values, the unfolding transition of the C<sub>H</sub>2 domain overlapped with that of the F<sub>ab</sub> fragment, leading to the emergence of a single peak [189]. Apart from the influence of the F<sub>c</sub> fragment on thermostability, the variable antibody domains seemingly impact stability [188]. This suggests that other factors within the variable domains contribute to the observed differences in stability. Interestingly, it has been demonstrated that IgG1 antibodies are more susceptible to fragmentation through non-enzymatic proteolysis, while IgG2 antibodies for example are more prone to aggregation under low pH conditions [189]. Thus, exploring different antibody backbones could be an intriguing approach to address the stability issues observed with GM2-AB4 IgG and GM2-AB5 IgG.

It should be noted that the spectroscopic detection method employed in this work, does not provide information regarding the amplitude of the peaks. But further information about the thermal behavior of the antibodies could be obtained from techniques like differential scanning calorimetry and provide more detailed insights, for example into the melting enthalpy [188].

### 6.3.2 The recognition of GM2 varied between the different anti-GM2 antibodies

In order to evaluate the specificity of the anti-GM2 antibodies, a comparison was conducted among the different antibodies based on their binding properties to GM2 on ganglioside test stripes and GM2-expressing NB cell lines.

Initially, the antibodies were evaluated for their specific binding using test strips coated with several gangliosides. Three out of the five antibodies tested (GM2-AB3 IgG, GM2-AB4 IgG, GM2-AB5 IgG) showed specific recognition of only GM2. Interestingly, even though 1 µg of purified antibody was used for detection, the intensities of GM2 binding varied, indicating differences in antibody binding capabilities. This difference in binding intensities became more pronounced when testing the same amounts of antibodies on different NB cell lines. Here, GM2-AB3 IgG was the most competent antibody in recognizing GM2 on the cell surface and displayed a higher binding affinity. The reason for the superior binding of GM2-AB3 IgG could be due to higher specificity or better accessibility of the epitope or to its ability to recognize two different forms of GM2, the NeuAc and NeuGc forms [115]. The differences in binding could also potentially be attributed to the inherent flexible arrangement of gangliosides on the cell surface, where they tend to organize in lipid rafts, which can dynamically change their size and composition. This inconsistency on the cell surface then could result in a limited accessibility to GM2 and antibody epitopes [193,194]. Further, it was demonstrated within this work

that GM2-AB3 IgG recognized GM2<sup>+</sup> cells of different tumor types to comparable extents as NB cell lines. So, we have presented here an antibody that can be used as therapeutic option not exclusively for NB but also in the context of other GM2-expressing tumors.

GM2-AB4 IgG with the variable sequence US2011, which is closely related to KM966, was expected to exhibit similar binding to GM2 on test strips and NB cell lines but this could not be confirmed. The inferior performance of GM2-AB4 IgG might be attributed to impaired antibody stability, as discussed previously. It is possible that the F<sub>ab</sub> fragment fails to make correct conformational changes and side chain rearrangements upon binding, resulting in a disrupted induced-fit mechanism in the antibody-antigen interaction [163,164]. This could lead to impaired target recognition and affinity. On the other hand, an unstable F<sub>c</sub> fragment may not be recognized by the secondary labeled antibody used for fluorescence detection resulting in a reduced signal upon detection. However, with an increased amount of antibody, the recognition of GM2 by GM2-AB4 IgG on the test strips became comparable to GM2-AB3 IgG, but further testing on NB cell lines with higher amounts was not performed.

GM2-AB5 IgG also showed weaker binding to GM2 on the ganglioside test stripes and cell lines compared to the original DMF10.167.4 IgG hamster antibody. The binding of both antibodies to NB cell lines exhibited high variability, as evidenced by the broad range of gMFI. This differential binding could possibly be explained by the use of unpurified supernatant from cell culture for hamster DMF10.167.4 IgG, where other proteins and factors may have interfered and influenced binding. Also, the differences in antibody scaffolds and glycosylation affected binding [195,196].

Interestingly, the antibodies GM2-AB3 IgG, GM2-AB4 IgG, and GM2-AB5 IgG showed specific binding exclusively to GM2, regardless of their antibody format IgG1 or IgM. In comparison, the anti-GD2 antibody clone ch14.18 IgM displayed binding to a broader range of gangliosides on the test stripes. Those included all gangliosides of the b-series and more complex gangliosides of the a-series and indicated a loss of specificity. The cloning strategy for ch14.18 into both expression plasmid was identical, with no gaps for in-frame expression being present. Because a different plasmid system was used for the expression of anti-GM2 antibodies, it would be helpful to compare the expression in both systems to rule out the possibility that the loss of specificity was due to the backbone. For anti-GM2 antibodies, both isotypes showed specific binding to GM2 exclusively. This discovery presents an opportunity to compare the advantageous features of IgG1 and IgM antibodies and will help to determine the optimal antibody format for potential immunotherapeutic applications both *in vitro* and *in vivo* studies.

Compared with the above-mentioned antibodies, GM2-AB1 IgG and GM2-AB2 IgG did not show any detectable binding to GM2 on test strips or in flow cytometric analysis, although they were successfully produced and had similar unfolding profiles as GM2-AB3 IgG. This indicates that these antibodies

were unable to specifically recognize and bind to the GM2 antigen in the experimental setups used. As described previously, the HuCAL sequence was generated by phage display which is a widely used approach for the generation of antibodies and was rewarded with the 'Nobel Prize in Chemistry' in 2018 [197]. There are several antibodies already in clinical trials or approved for treatment such as adalimumab, an anti-TNF $\alpha$  antibody [198]. Compared to antibodies generated through animal immunization or hybridoma technology, phage display offers the advantage of reduced immunogenicity and additional antibody engineering can be bypassed. This is because phage display allows antibodies to be produced using human antibody libraries, thus eliminating the need for additional modifications, such as humanization, to make them suitable for human applications.

However, GM2-AB1 IgG did not show any binding, suggesting that the use of phage display is also associated with certain disadvantages, one of which is the limited antibody diversity. Although the method utilizes a library that includes a vast repertoire of human antibody sequences with  $10^9$  specificities [112], the natural antibody diversity is much higher with an estimated theoretical range of  $10^{15}$ - $10^{18}$  unique sequences [199,200]. The synthetic nature of phage display-derived antibody sequences means that they may have different structural and functional properties compared to antibodies generated through natural immune responses. This can potentially affect their binding affinity, specificity, and other characteristics that are crucial for their intended applications. An aspect to consider when using a bacterial system for antibody production is the difference in post-translational modifications, particularly glycosylation. *E. coli*, the most commonly used bacterial systems for phage display, lacks the machinery to perform complex glycosylation common to antibodies produced in mammalian cells [201]. Additionally, the presentation of antigens during the phage display process may not guarantee the correct conformational arrangement of the antigen [202]. This can limit the accessibility of certain epitopes and result in the generation of antibodies that may not fully recognize or bind to the native form of the target antigen. The original antibody sequence generated by the HuCAL technology contained a  $\lambda_3$  light chain, while in the pVITRO plasmids, the C<sub>L</sub> region was a  $\kappa$  light chain. Although  $\lambda$  and  $\kappa$  constant chains have similar overall structures and molecular masses [203] several studies have indicated that the choice of light chain subtype can have a slight impact on the activity of antibodies by influencing the conformation of the heavy chain and thereby affecting antibody binding [204]. For example, a significant higher amount of beta structures was observed in CDR-L1 and CDR-L2 regions of  $\kappa$  light chains compared to  $\lambda$  light chains [205]. In another study in which the  $\kappa$  light chain of an antibody was replaced by a  $\lambda$  light chain, X-ray structures of the antigen binding site revealed changes in the stability and affinity of the antibody. However, this substitution did not significantly hinder antibody reactivity [206]. These findings highlight that the choice of light chain subtype, whether  $\lambda$  or  $\kappa$ , can have subtle effects on antibody activity and may also have impaired the binding of GM2-AB1 IgG.

In contrast to the other sequences, L55-81 (GM2-AB2 IgG) was the only originally human sequence derived from peripheral blood B lymphocytes of a melanoma patient and did not require engineering for the application in humans [113]. Although a precursor antibody, L55 IgM, showed reactivity with four out of eight GM2-expressing NB tissues [207], the original L55-81 IgM itself has not been specifically tested in the context of NB yet. Instead, it was primarily described in the context of melanoma, colon carcinoma, or breast cancer [113]. Changes in the amino acid sequences between L55 and L55-81 could significantly affect the binding specificity. Nishinaka *et al.* have shown that a deviation of 20 amino acids in the variable regions caused the related antibodies L55-81 and L612 to bind to different targets, namely GM2 and GM3 [208]. The methods employed to detect the binding of GM2-AB2 IgG to GM2 in this study differed from those used in previous publications which were thin-layer chromatography and immunohistochemical staining. In general, these methods should give the same results in terms of antibody binding, but it is worth noting that the latter method is considered controversial for ganglioside detection. Furthermore, the lack of binding to GM2 observed on the test stripes and in flow cytometric analysis could not solely be attributed to the shift from IgM to IgG, as testing the antibody in an IgM format revealed the same results. However, Nishinaka *et al.* also encountered curiosities in L55-81 IgM binding such as lower binding to cell lines containing higher GM2 content compared to those with lower GM2 content [113]. They explained this phenomenon by a cross-reactivity with molecules having a similar epitope or the presence of GM2 derivatives with varying carbohydrate moieties that potentially change conformational arrangement and interfere with binding [209]. Similar observations have been made for an anti-GM3 antibody, that exclusively recognized GM3 on melanoma cells but no other GM3-expressing tumor types, emphasizing the influence of carbohydrate chain length [210].

Surprisingly, murine MK1-16 IgM did not show any binding to ganglioside test stripes, even though the ability to detect GM2 on NB cell lines was shown. This discrepancy suggests that MK1-16 IgM might recognize an epitope that was not accessible or had a divergent conformation on the test stripes. Also, the lack of GM2 detection on the test stripes could be attributed to its inability to recognize Neu5Gc-GM2 [138]. As anticipated, Trastuzumab IgG did not demonstrate any binding to gangliosides, confirming that the backbone itself does not contribute to nonspecific effects. Also, Isotype IgG did not show any binding to test stripes or NB cell lines, verifying this antibody as a suitable negative control for further experiments conducted within this work.

### **6.3.3 GM2-AB3 IgG showed superior cytotoxic potential**

To determine the most effective anti-GM2 antibody, their functional attributes were assessed and compared. In terms of antibody effector functions, the ability to induce complement-dependent cytotoxicity (CDC) or antibody-dependent cell-mediated cytotoxicity (ADCC) can vary between

antibodies as seen within this work. Several factors contribute to differences in effector functions, including post-translational modifications and the antibody isotype or subclass.

Firstly, it was shown that GM2-AB3 IgG exhibited significantly higher levels of CDC compared to the other anti-GM2 antibodies tested, which is consistent with the observed binding capabilities. Lower cytotoxicity observed for GM2-AB4 IgG and GM2-AB5 IgG could be attributed to their instabilities. Notably, GM2-AB4 IgG showed a killing effect only at higher concentrations, suggesting that increasing the concentration could yield higher cytotoxicity, as evidenced by the increased binding to ganglioside test stripes at higher concentrations. Differences in cytotoxicity among the cell lines could be attributed to the varying recognition of GM2 on the cell surfaces. GM2-AB3 IgG showed the highest binding to GM2 on Kelly cells, followed by SK-N-LO and SH-SY5Y, which was consistent with CDC. Increasing the serum concentration, which was 12.5% in this assay, could further increase cytotoxicity [211]. CDC mediated by Dinutuximab was consistent with the results reported in the literature, showing lysis ranging from 50% to 90% depending on the cell line [212]. GM2-AB3 IgG demonstrated cytotoxicity to a comparable extent as Dinutuximab against Kelly and SK-N-LO cells.

Conversely, GM2-AB1 IgG and GM2-AB2 IgG exhibited no cytotoxic activity in the CDC assay, likely due to their inability to recognize GM2 or bind GM2-expressing NB cells. In contrast to previous findings where the original L55-81 IgM demonstrated CDC against a human melanoma cell line of up to 60% and 35% in the presence of human or rabbit complement, respectively [113], the lack of CDC observed for GM2-AB2 IgG having identical variable sequence like L55-81 might be attributed to the different human antibody scaffold. The absence of CDC in the case of GM2-AB4 IgG might be due to stability issues as observed in the unfolding profile measurement.

In comparison to CDC, GM2-AB3 IgG demonstrated lower ADCC activity spanning from 16% to 28% at an antibody concentration of 4 µg/ml. Nevertheless, this was consistent with other publications reporting around 25% cytotoxicity with chimeric GM2-AB3 IgG at an E:T ratio of 10:1 and an antibody concentration of 10 µg/ml [213]. Higher ADCC activity of 60-70% was observed when using higher E:T ratios of 40:1 or 50:1 [103,213]. The killing was similarly noted for Dinutuximab but could be explained by the fact that ADCC mediated by Dinutuximab is mainly driven by neutrophils, whereas in this assay setup, PBMC were used as effector cells, and granulocytes were excluded after cell isolation by Ficoll density gradient centrifugation [214]. Thus, lower ADCC could be due to the lack of the main effector cell population.

In general, specific post-translational modifications such as N-glycosylation, fucosylation, mannose residues and terminal galactose residues influence the CDC and ADCC activity of antibodies [215]. For example, modifications like high content of bisecting GlcNAc or degalactosylation were shown to impact the effector functions of the anti-CD20 antibody Rituximab, leading to increased ADCC or

reduced CDC, respectively [216]. Furthermore, the absence of core fucose significantly increased ADCC activity by enhancing the interaction with the human F<sub>c</sub>RIIIa receptor without affecting C1q binding [50,55,217]. A recent study by Zabczynska *et al.* demonstrated that the enzymatic removal of sialic acids from the F<sub>c</sub> region of IgG antibodies increased potency in inducing ADCC, but a reduction in CDC was observed [211]. This suggests that the presence or absence of sialic acids can influence the balance between ADCC and CDC activities of antibodies.

Apart from post-translational modifications, the antibody's isotype and subclass also play a significant role in mediating effector functions. IgG1 antibodies, for instance, exhibit the strongest ADCC, while IgM antibodies cannot mediate ADCC. In contrast, CDC is highest for IgG3 antibodies, despite all IgG antibodies having a high amino acid identity [218,219]. Isotype shuffling experiments have demonstrated that the swapping of C<sub>H</sub>1, hinge, and F<sub>c</sub> domains between IgG1 and IgG3 enhanced CDC activity without the need of artificial editing [51,220]. Lua *et al.* used the example of Trastuzumab to show that isotype swapping within the light and heavy chains is possible and that antibody binding and production was only impaired in a few mixed combinations [221].

Consequently, by modifying the expression plasmid or using modified host cell lines, it might be possible to increase ADCC activity. In particular, when antigens are expressed at low density, as is the case with SK-N-AS cells, antibody engineering could increase the sensitivity of the antibodies [220]. Furthermore, various studies showed that the addition of interleukins or cytokines enhanced ADCC effects in the case of Dinutuximab. For example, the addition of IL-2 resulted in a 2-fold increase in ADCC with melanoma cells [222]. Also, the presence of GM-CSF and G-CSF was found to enhance killing mediated by granulocytes [223,224]. In combination with IL-15 or IL-21, Dinutuximab increased the cytotoxic capacity of NK cells against IMR32 cells from 20% to 80% [225]. These findings suggest that the addition of interleukins or cytokines may also provide an opportunity to improve ADCC of GM2-AB3 IgG.

In conclusion, the GM2-AB3 IgG antibody showed several advantageous properties that made it a promising candidate for targeting GM2 in the treatment of NB. In this comparative study with five different anti-GM2 antibodies of different origins and species, GM2-AB3 IgG demonstrated specific recognition of the antigen and cytotoxic activity against GM2-expressing NB cell lines. In this regard, GM2-AB3 IgG outperformed all other anti-GM2 antibodies by showing superior binding ability and highest CDC against various NB cell lines. Moreover, GM2-AB3 IgG showed comparable recognition of GM2<sup>+</sup> cells across different tumor types, highlighting its application potential beyond NB. In addition to the cytotoxic mechanism mediated by complement, GM2-AB3 IgG was also capable of ADCC. In contrast to the anti-GD2 antibody sequence ch14.18, the KM966 sequence (GM2-AB3) retained its specificity for GM2 regardless of its format, which will allow comparison of the beneficial features of

both antibody isotypes. These findings highlight the favorable attributes of GM2-AB3 IgG and its potential as an immunotherapeutic agent for GM2-expressing NB.

### **6.3.4 Suppression of tumor growth through treatment with GM2-AB3 IgG in a humanized mice**

In an initial mouse experiment, where the engraftment of hHSC showed a decreasing trend over the long term, the anticipated effects of tumor reduction or extended survival through immunotherapeutic treatment with the GM2-AB3 IgG were not observed. This outcome could be attributed to the immune deficiency of the mice which lack mature lymphocytes and NK cells as well as complement components [226–228] which in turn is necessary for the engraftment of human tumor cells in mice. While most complement factors are synthesized by liver cells [229,230], immune cells like neutrophils, mast cells, or macrophages also contribute to the production and secretion of complement factors [231–233]. Therefore, both these factors play pivotal roles in the execution of antibody effector functions and the success of immune therapies. The extent of engraftment of transplanted hHSC varied among mice, which may be theoretically attributed to factors such as the age of the mice, the source and manipulation of the hHSC, and the mode of administration [234]., but was controlled and consistent in this experiment.

In another mouse experiment, where the engraftment of hHSC remained stable over time with a consistent percentage of hCD45<sup>+</sup> cells, the growth of tumors was notably suppressed, leading to prolonged survival among the mice when treated with GM2-AB3 IgG in comparison to mice treated with the Isotype IgG. This suggests that a specific proportion of human immune cells is imperative for the success of immunotherapeutic approaches. It is conceivable that with a higher proportion of effector cells and especially complement factors, complete eradication of tumor cells could potentially be achieved, as it was demonstrated that CDC primarily drove the mechanism of action of GM2-AB3 IgG. To evaluate this hypothesis, an alternative mouse strain like NSG-Hc1, characterized by an intact complement system capable of mediating CDC activity, could be considered for future experiments [235]. Alternatively, the additional injection of human mononuclear cells (MNC) might be an option. This was previously tested within the context of a GM2-expressing malignant pleural mesothelioma model with the non-fucosylated anti-GM2 antibody clone BIW-8962 which was closely related to the precursor antibody clone of KM966. The addition of MNC in this model resulted in heightened antitumor activity [236].

In summary, GM2-AB3 IgG has been demonstrated as the most promising antibody for therapeutic applications *in vitro*. Its high expression levels and feasibility for IgM expression enable a direct comparison between antibody isotypes, aiding in the determination of the optimal antibody format and characteristics. Unlike other anti-GM2 antibodies, GM2-AB3 IgG does not exhibit stability concerns

or binding issues. Additionally, it demonstrates high levels of cytotoxicity *in vitro* and *in vivo*, which could be further enhanced through antibody engineering. These favorable attributes position GM2-AB3 IgG as a highly viable candidate for therapeutic application. In contrast, other anti-GM2 antibodies, like BIW-8962 IgG for example, did not demonstrate any positive response in a phase I clinical trial involving patients with multiple myeloma [237].

### 6.4 Conclusion

Five distinct anti-GM2 antibody clones GM2-AB1 to GM2-AB5 with the respective variable sequences HuCAL, L55-81, KM966, US2011, DMF10.167.4 were successfully engineered, produced in HEK293 cells, and functionally tested. GM2-AB1 IgG and GM2-AB2 IgG failed to detect the antigen. However, GM2-AB3 IgG, GM2-AB4 IgG, and GM2-AB5 IgG demonstrated the ability to specifically bind to GM2, regardless of their IgG or IgM isotype. Antibody stability and cytotoxic efficacy were different for those three antibodies, with GM2-AB4 IgG and GM2-AB5 IgG exhibiting poor binding and lysis of NB cells. As a result, GM2-AB3 IgG emerged as the most promising candidate for the treatment of GM2-expressing NB tumor, displaying strong binding to GM2-expressing NB and other tumor cell lines, as well as exhibiting high CDC and the ability to mediate ADCC.

Although occasional poor humanization of mice in certain experiments presented a challenge in this study, nevertheless the capability of GM2-AB3 IgG to decelerate tumor growth *in vivo* was successfully demonstrated. Within this experimental context, the presence of a minimal proportion of human immune cells proved to be of importance for investigating the effects of human antibodies in mice. This is particularly relevant considering the severe neuropathic pain caused by the anti-GD2 antibody Dinutuximab due to its binding to GD2 on normal peripheral nerve fibers. Up to this point, there hasn't been any anti-GM2 antibody that has been tested in an animal model within the context of NB. Before proceeding to clinical studies, it is important to thoroughly investigate the antibody's characteristics in an animal model with a human-like immune system, as demonstrated in this research.

Interestingly, the GM2-AB3 IgG antibody recognized not only NB cell lines but also cell lines of other GM2-expressing tumor types, such as medulloblastoma and rhabdomyosarcoma. This finding suggests that GM2-AB3 IgG could potentially serve as an effective antibody for the treatment of various other tumor entities.

Taken together, in this research project five anti-GM2 antibody clones were successfully engineered and tested. Among these clones, the GM2-AB3 IgG variant with the variable sequence KM966 showed the most promising results for potential application in the treatment of GM2-expressing

NB tumors. Ultimately, the findings of this work are an important contribution to the preclinical testing of this antibody clone and pave the way for the antibody's path to future clinical application.

### 7 Outlook

Since GM2-AB3 IgG has been identified as the most promising antibody candidate for the treatment of NB, its functionality can be further improved by antibody engineering techniques. For example, genetic modification of the host cell line allows manipulation of the glycosylation pattern, thereby influencing antibody properties such as half-life or effector functions. Additionally, modification of the antibody backbone, particularly in the variable sequence, could further improve the stability and binding properties of the antibody by generating variants with structural differences and higher affinity, respectively.

With the successful generation of both antibody isotypes, namely IgG1 and IgM, comparative analysis could provide further valuable insights into the advantages of each isotype. This comparison could shed light on various aspects, including proper antibody folding, stability, target recognition and binding capacity, as well as cytotoxic mechanisms. The investigation of alternative treatment modalities like antibody drug conjugates (ADC), CAR-T or CAR-NK cells, and BiTE will broaden the potential application spectrum of the KM966 sequence in the future. This exploration will help to identify the treatment format that exhibits the most promising molecular characteristics, efficacy in patients, and minimal side effects.

Furthermore, prior to clinical application of the anti-GM2 antibody clone GM2-AB3 IgG in patients, it is essential to evaluate the expression of GM2 in tumor samples from patients rather than solely on cell lines, which represent a highly artificial system. So far, the level of GM2 expression in patient samples remains uncertain, but the analysis of a larger cohort could give a more comprehensive understanding. Additionally, it is important to consider the physiological expression of GM2. This consideration is essential to avoid adverse effects of the antibody on healthy tissue when the target antigen is also naturally found in such tissue. In addition to flow cytometric analysis, which was conducted here, other analytical techniques, such as thin layer chromatography or mass spectrometry, could be utilized to provide valuable insights into the ganglioside composition on tumor cells.

In summary, the generated antibody GM2-AB3 IgG, harboring the variable sequence KM966, represents a promising foundation for subsequent structural refinements and improvements. The research into the optimal treatment modality could further lead to significant advancements in its therapeutic potential.

## 8 Material

### 8.1 Instruments

Table 3 provides a list of essential instruments utilized for the execution and analysis of the experiments. All instruments were used following the manufacturers' instructions. Routine cleaning and maintenance were carried out regularly to ensure proper functioning.

**Table 3: Instruments used for analysis and experimental setup.**

Name	Company (city, country headquarter)
ÄKTA Pure Fluid Chromatograph	GE Healthcare Europe GmbH (Freiburg, Germany)
BD FACSCanto™ II Flow Cytometry System	Becton, Dickinson & Company (Franklin Lakes, USA)
BD LSRFortessa™ Cell Analyzer	Becton, Dickinson & Company (Franklin Lakes, USA)
BIOBEAM 2000	Gamma Service Medical GmbH (Leipzig, Germany)
Biometra Biodoc GelAnalyzer	Analytik Jena (Jena, Germany)
Chemostar PLUS ECL & Fluorescence Imager	Intas Science Imaging Instruments GmbH (Göttingen, Germany)
CO <sub>2</sub> resistant shaker	Thermo Fisher Scientific Inc. (Waltham, USA)
Countess 3 Automated Cell Counter	Thermo Fisher Scientific Inc. (Waltham, USA)
E-Box-VX2 Gel Detector	Vilber (Eberhardzell, Germany)
IncuCyte Live-Cell Analysis System	Sartorius AG (Göttingen, Germany)
MACSQuant® X Flow Cytometer	Miltenyi Biotec (Bergisch-Gladbach, Germany)
NanoDrop™ 2000/2000c Spectrophotometer	Thermo Fisher Scientific Inc. (Waltham, USA)
NanoDrop™ One/OneC Spectrophotometer	Thermo Fisher Scientific Inc. (Waltham, USA)
Nikon Eclipse Ts2R Microscope	Nikon Europe B.V. (Amstelveen, The Netherlands)
Structurix M ECO	GE Inspection Technologies (Boston, USA)
Varioskan™ LUX Multimode Microplate Reader	Thermo Fisher Scientific Inc. (Waltham, USA)
Xenogen IVIS-200 System	PerkinElmer Technologies GmbH & Co. KG (Waltham, USA)

### 8.2 Laboratory consumables

Laboratory consumables used for experimental procedures are listed in Table 4. Standard consumables including reaction tubes, pipettes or culture plates are not specially mentioned.

**Table 4: Consumables used for *in vitro* and *in vivo* experiments.**

Name	Provider (city, country headquarter)	Cat. No.
Amersham™ Protran® Western Blotting Membrane, Nitrocellulose	Merck Millipore (Darmstadt, Germany)	GE10600015
EDTA S-monovettes, sterile, 7,5 ml	Sarstedt AG & Co. KG (Nümbrecht, Germany)	11605011
Falcon™ round bottom polystyrene tubes	Thermo Fisher Scientific Inc. (Waltham, USA)	10186360
HiTrap Protein G HP, 1 x 5 ml	Cytiva (Marlborough, USA)	17040501
LS Columns	Miltenyi Biotec (Bergisch-Gladbach, Germany)	130-042-401
Microvette® 500 Lithium-Heparin, 500 µl	Sarstedt AG & Co. KG (Nümbrecht, Germany)	201345

## 8 Material

Microvette® 500 Serum, 500 µl	Sarstedt AG & Co. KG (Nümbrecht, Germany)	20. 1343
Nalgene™ Oak Ridge High-Speed Centrifuge Tubes	Thermo Fisher Scientific Inc. (Waltham, USA)	3139-0030
Nunc™ Transparent Immune Standard Modules MaxiSorp	Thermo Fisher Scientific Inc. (Waltham, USA)	469949
NuPAGE™ 4-12% Bis-Tris Protein Gels, 1.0 mm	Thermo Fisher Scientific Inc. (Waltham, USA)	NP0322BOX
Pierce™ Protein Concentrator PES, 100K MWCO, 20-100 mL	Thermo Fisher Scientific Inc. (Waltham, USA)	88537
Pierce™ Protein Concentrator PES, 30K MWCO, 5-20 mL	Thermo Fisher Scientific Inc. (Waltham, USA)	88529
Pre-Separation Filters, 30 µm	Miltenyi Biotec (Bergisch-Gladbach, Germany)	130-041-407
QuadroMACS Magnetic Cell Separator with MACS MultiStand	Miltenyi Biotec (Bergisch-Gladbach, Germany)	130-091-051
Safety Lancet	Sarstedt AG & Co. KG (Nümbrecht, Germany)	85.1018
Sterile Single-Bottom Disposable Erlenmeyer Flasks	Thermo Fisher Scientific Inc. (Waltham, USA)	4117-0500

### 8.3 Chemicals, reagents, and solutions

Chemicals, reagents, and solutions used for *in vitro* experimental procedures are listed in Table 5.

**Table 5: Chemicals, reagents and solutions used for *in vitro* experiments.**

Name	Provider (city, country headquarter)	Cat. No.
2.5 M Calcium chloride (CaCl <sub>2</sub> )	Carl Roth GmbH (Karlsruhe, Germany)	HN04.1
25 mM Chloroquine	Sigma-Aldrich (Munich, Germany)	C6628
Ampicillin	Carl Roth GmbH (Karlsruhe, Germany)	15140148
Biocoll® separating solution	Bio&SELL GmbH (Nürnberg, Germany)	BS.L6115
Blastizidin	Invivogen (San Diego, USA)	ant-bl-05
Bovine serum albumin (BSA)	Carl Roth GmbH (Karlsruhe, Germany)	8076.4
CellTox™ Green Cytotoxicity dye	Promega (Mannheim, Germany)	G8743
Collagenase from <i>Clostridium histolyticum</i>	Sigma-Aldrich (Munich, Germany)	C6885-25MG
Dimethyl sulfoxide (DMSO)	Carl Roth GmbH (Karlsruhe, Germany)	A994.2
Dithiothreitol (DTT)	Thermo Fisher Scientific Inc. (Waltham, USA)	R0861
dNTPs	Promega (Mannheim, Germany)	U1511
Dulbecco's Modified Eagle Medium (DMEM)	Gibco/Life Technologies (Carlsbad, USA)	41965120
Dulbecco's Phosphate Buffered Saline (DPBS)	Gibco/Life Technologies (Carlsbad, USA)	14190-094
eFluor670™ Proliferation dye	Thermo Fisher Scientific Inc. (Waltham, USA)	65-0840-85
Ethanol	Merck Millipore (Darmstadt, Germany)	107017
Ethidium bromide	Sigma-Aldrich (Munich, Germany)	E1510-10ML
Ethylene diamine tetra acetic acid (EDTA)	Th. Geyer GmbH (Renningen, Germany)	2281.1000
Fetal bovine serum (FBS)	Life Technologies (Carlsbad, USA)	10270-106
GeneRuler 100bp DNA ladder	Thermo Fisher Scientific Inc. (Waltham, USA)	SM0242
GeneRuler 1kb DNA ladder	Thermo Fisher Scientific Inc. (Waltham, USA)	SM0311
Hexadimethrine bromide (Polybrene)	Sigma-Aldrich (Munich, Germany)	H9268

Horse serum	Sigma-Aldrich (Munich, Germany)	H1270-500mL
Human TruStain FcX™	BioLegend (San Diego, USA)	422302
Hybridoma-SFM	Thermo Fisher Scientific Inc. (Waltham, USA)	12045076
Hygromycin	Gibco/Life Technologies (Carlsbad, USA)	10687010
Interleukin-2 (IL-2)	PeptoTech Inc. (Hamburg, Germany)	200-02-1MG
Isoflurane	Baxter (Unterschleißheim, Germany)	20E01A31
Isopropanol	Th. Geyer GmbH (Renningen, Germany)	1136.1000
jetOPTIMUS® DNA transfection reagent	Polyplus (Illkirch-Graffenstaden, France)	117-07
L-glutamine (200 mM)	Gibco/Life Technologies (Carlsbad, USA)	25030024
Lipofectamine3000™	Thermo Fisher Scientific Inc. (Waltham, USA)	L3000015
Luria-Bertani medium (LB Medium)	Carl Roth GmbH (Karlsruhe, Germany)	X968.1
Methanol	Carl Roth GmbH (Karlsruhe, Germany)	8388.6
Minimum Essential Medium Eagle (MEM)	Merck Millipore (Darmstadt, Germany)	M8042
NuPAGE™ MES SDS running buffer (20x)	Life Technologies (Carlsbad, USA)	NP000202
Opti-MEM	Gibco/Life Technologies (Carlsbad, USA)	31985070
PageRuler™ Plus prestained protein ladder	Thermo Fisher Scientific Inc. (Waltham, USA)	26619
Paraformaldehyde solution (37 %)	Carl Roth GmbH (Karlsruhe, Germany)	7398.1
Para-nitrophenylphosphate (pNPP)	Mabtech AB (Nacka Strand, Sweden)	3652-P10
Penicillin/Streptomycin (10,000 U/ml)	Gibco/Life Technologies (Carlsbad, USA)	15070063
Pierce™ ECL western blotting Substrate	Thermo Fisher Scientific Inc. (Waltham, USA)	32109
Pierce™ Protein A/G agarose	Thermo Fisher Scientific Inc. (Waltham, USA)	20421
Pierce™ Protein L agarose	Thermo Fisher Scientific Inc. (Waltham, USA)	20510
Propidium iodide solution	BioLegend (San Diego, USA)	421301
Red blood cell lysis buffer (10x)	BioLegend (San Diego, USA)	420301
ROTI®GelStain	Carl Roth GmbH (Karlsruhe, Germany)	3865.1
RPMI 1640 medium	Gibco/Life Technologies (Carlsbad, USA)	21875034
Skimmed milk powder	Spinnrad (Bad Segeberg, Germany)	2231018
Sodium pyruvate (100 mM)	Gibco/Life Technologies (Carlsbad, USA)	11360070
Tris acetate-EDTA (TAE) buffer (50x)	PanReac Applichem (Darmstadt, Germany)	A1691,1000
Tris(hydroxymethyl)aminomethane (Tris)	Th. Geyer GmbH (Renningen, Germany)	8085.1000
Triton X 100	Sigma-Aldrich (Munich, Germany)	T8787-250ML
TruStain FcX™ (anti-mouse CD16/32) antibody	BioLegend (San Diego, USA)	101320
Trypan blue solution (4 %)	Gibco/Life Technologies (Carlsbad, USA)	15250061
Trypsin / EDTA (0.05 %)	Gibco/Life Technologies (Carlsbad, USA)	25300054
Tween20	Th. Geyer GmbH (Renningen, Germany)	8022.0500
UltraPure™ agarose	Life Technologies (Carlsbad, USA)	16500100
Zeocin	Thermo Fisher Scientific Inc. (Waltham, USA)	R25001

#### 8.4 Cell culture media and buffer

The preparation of the cell culture media with its individual supplements as well as the composition of buffers used for all protocols is described in Table 6.

**Table 6: Different compositions of the growth media and buffers used for cell culture.**

No	Name	Composition
<b>Growth media with supplements</b>		
1	DMEM complete growth medium	DMEM (4,5 g/L glucose) + 10% h.i. FBS
2	Hybridoma medium	Hybridoma-SFM w/o supplements

## 8 Material

3	NK-92 complete growth medium	MEM + 12,5% h.i. FBS +12,5% h.i. horse serum + 2 mM L-glutamine + 100 U/ml Pen/Strep + 100 IU/ml IL-2
4	RPMI complete growth medium I	RPMI 1640 + 10% h.i. FBS + 1 mM sodium pyruvate
5	RPMI complete growth medium II	RPMI 1640 + 10% h.i. FBS
<b>Buffers</b>		
1	FACS buffer	PBS +2% h.i. FBS
2	Freezing medium	FBS + 20% DMSO
3	MACS buffer	PBS + 2 mM EDTA + 0.5% h.i. FBS

### 8.5 Cell lines

Table 7 gives an overview of cell lines used in this work, including various NB cell lines and cell lines from other tumor types. All cell lines were verified by short tandem repeat polymerase chain reaction (PCR).

**Table 7: Overview of cell lines used in this work and appropriate culture medium.**

Name	Characteristics (species; origin; growth; morphology; doubling time)*	Culture medium	Cat. No.
C33A	human; cervix carcinoma; adherent; epithelial; 32.6 h	1	ATCC: HTB-31
CHO-S	Chinese hamster; ovary; suspension; round; 17 h		
DAOY	human; medulloblastoma; adherent; polygonal; 32 h	1	ATCC: HTB-186
DMF10.167.4	Armenian hamster; secretion of monoclonal IgG antibodies	2	ATCC: pta-405
HEK293T	human; embryonal kidney; adherent; epithelial; 20 h	1	DSMZ: ACC 305
HeLa	human; cervical adenocarcinoma; adherent; epithelial; 23 h	1	ATCC: CCL-2
Hep-G2	human; hepatoblastoma; adherent; epithelial; 26 h	5	DMSZ: ACC 180
IMR32	human; neuroblastoma; adherent/suspension; fibroblast/neuroblast; 48 h	4	DSMZ: ACC 165
Kelly	human; neuroblastoma; adherent; epithelial; 30 h	4	DSMZ: ACC 355
LAN-1	human; neuroblastoma; adherent; epithelial; 100 h	4	DMSZ: ACC 655
LS	human; neuroblastoma; adherent; polymorph; 45 h	4	DSMZ: ACC 675
MCF7	human; breast adenocarcinoma; adherent; epithelial; 24 h	1	ATCC: HTB-22
NK-92	human; Non-Hodgkins Lymphoma; suspension; lymphoblast; 36 h	3	ATCC: CRL-2407
RH-30	human; rhabdomyosarcoma; adherent; epithelial; 37 h	5	DMSZ: ACC 489
Saos-2	human; osteosarcoma; adherent; epithelial; 48 h	5	DMSZ: ACC 243
SHEP	human; neuroblastoma; adherent; epithelial; unknown; carries GFP reporter + Luciferase gene	4	Not acquireable
SH-SY5Y	human; neuroblastoma; adherent; epithelial/neuronal; 55 h	4	ECACC: 94030304
SJMM4	human; medulloblastoma; adherent; unknown; unknown	1	Gift from AG Schüller
SK-MEL-2	human; melanoma; adherent; polygonal; 32 h	1	ATCC: HTB-68
SK-N-AS	human; neuroblastoma; adherent; epithelial; 39 h	4	ECACC: 94092302
SK-N-BE(2)	human; neuroblastoma; adherent; neuroblast; 27 h	4	ATCC: CRL-2271
SK-N-LO	human; neuroblastoma; adherent; epithelial; unknown; carries GFP reporter + Luciferase gene	4	CLS: 300400

## 8 Material

SK-N-SH	human; neuroblastoma; adherent; epithelial; 44 h	4	ECACC: 86012802
T47D	human; breast carcinoma; adherent; epithelial; 30-40 h	5	ATCC: CRL-2266
U251	human; glioblastoma (astrocytoma); adherent; epithelial; 23 h	1	ECACC: 09063001
UACC62	human; melanoma; adherent; epithelial; 31 h	1	Gift from AG Schüller

\*) Data about each cell line were researched from 'Cellosaurus-Cell line encyclopedia' [238].

### 8.6 Kits

Commercial kits listed in Table 8 were used for *in vitro* experiments. Unless otherwise stated, the kits were used in accordance with the manufacturer's instructions.

**Table 8: Utilized commercial kits.**

Name	Provider (city, country headquarter)	Cat. No.
Anti-Ganglioside Dot	GA Generic Assays GmbH (Dahlewitz, Germany)	5003
CD34 MicroBead Kit UltraPure	Miltenyi Biotec (Bergisch-Gladbach, Germany)	130-100-453
CloneJET PCR Cloning Kit	Thermo Fisher Scientific Inc. (Waltham, USA)	K1232
ExpiCHO™ Expression System	Thermo Fisher Scientific Inc. (Waltham, USA)	A29133
First Strand cDNA-Synthesis Kit	Thermo Fisher Scientific Inc. (Waltham, USA)	K1612
Hamster Armenian IgG ELISA Kit	Innovative Research Inc. (Novi, USA)	AHTIGGKT
Human C1q ELISA Kit	Hycult Biotech (Uden, The Netherlands)	HK356-01
Human IgG ELISA BASIC Kit (ALP)	Mabtech AB (Nacka Strand, Sweden)	3850-1AD-6
Human IgM ELISA BASIC Kit (ALP)	Mabtech AB (Nacka Strand, Sweden)	3880-1AD-6
NucleoBond® Xtra Midi Kit	Macherey-Nagel GmbH & Co. KG (Düren, Germany)	740410.100
NucleoSpin Gel and PCR Clean-up Mini Kit	Macherey-Nagel GmbH & Co. KG (Düren, Germany)	740609.50
NucleoSpin Plasmid EasyPure Mini Kit	Macherey-Nagel GmbH & Co. KG (Düren, Germany)	7405882.50
QIAGEN DNeasy Blood & Tissue Kit	QIAGEN (Hilden, Germany)	69504

### 8.7 Enzymes and buffers

For cloning procedures, the enzymes and buffers shown in Table 9 were used according to the manufacturer recommendations. Amplification of deoxyribonucleic acid (DNA) fragments was carried out using a polymerase with proofreading function such as Phusion or Q5 polymerase. To check the presence of inserted DNA fragments Taq polymerase was used.

**Table 9: Enzymes and buffers used for cloning.**

Name	Provider (city, country headquarter)	Cat. No.
50% PEG 4000 Solution	Thermo Fisher Scientific Inc. (Waltham, USA)	J61495.AK
BamHI	Thermo Fisher Scientific Inc. (Waltham, USA)	FD0055
BglII	Thermo Fisher Scientific Inc. (Waltham, USA)	FD0083

BsmBI	New England Biolabs Inc., (Ipswich, USA)	R0580S
Dream Taq Green DNA-Polymerase Mastermix (2x)	Thermo Fisher Scientific Inc. (Waltham, USA)	K1081
EcoRI	Thermo Fisher Scientific Inc. (Waltham, USA)	FD0274
EcoRV	Thermo Fisher Scientific Inc. (Waltham, USA)	FD0303
FastAP Thermosensitive Alkaline Phosphatase	Thermo Fisher Scientific Inc. (Waltham, USA)	EF0014
FastDigest Green Buffer (10x)	Thermo Fisher Scientific Inc. (Waltham, USA)	B72
Gibson Assembly Master Mix	New England Biolabs Inc., (Ipswich, USA)	E2611S
Kinase, Ligase, DpnI (KLD) Mastermix	New England Biolabs Inc., (Ipswich, USA)	M0554S
NcoI	Thermo Fisher Scientific Inc. (Waltham, USA)	FD0574
NheI	Thermo Fisher Scientific Inc. (Waltham, USA)	FD0973
Pfl23II	Thermo Fisher Scientific Inc. (Waltham, USA)	FD0854
Phusion High-Fidelity PCR Master Mix with HF Buffer	Thermo Fisher Scientific Inc. (Waltham, USA)	F531S
Q5 High-Fidelity DNA Polymerase	New England Biolabs Inc., (Ipswich, USA)	M0491L
Q5 Reaction Buffer (5x)	New England Biolabs Inc., (Ipswich, USA)	B9027S
T4 DNA Ligase	Thermo Fisher Scientific Inc. (Waltham, USA)	EL0012
T4 DNA Ligase Buffer (10x)	Thermo Fisher Scientific Inc. (Waltham, USA)	B69
T4 Polynucleotide Kinase (PNK)	Thermo Fisher Scientific Inc. (Waltham, USA)	EK0032
XbaI	Thermo Fisher Scientific Inc. (Waltham, USA)	FD0684
XhoI	Thermo Fisher Scientific Inc. (Waltham, USA)	FD0694

## 8.8 Oligonucleotides

HPLC-purified and dissolved oligonucleotides were purchased at a concentration of 100 mM from Metabion (Planegg, Germany). All used oligonucleotides and their specific applications are listed in Table 10.

**Table 10: Oligonucleotide sequences used for cloning of antibody expression plasmids or for CRISPR/Cas9 knockout plasmids.**

No	Name	Sequence (5' – 3')	Application
1	LR13	TGGTTTGTCCAAACTCATCAA TGT	Sequencing of CH region in pVITRO-IgG1/IgM
2	LR30_GM2_VL_Seq	GAGGCTAATTCTCAAGCCTC	Sequencing of VL chain in pVITRO-IgG1/IgM
3	GM2_VH_Seq_fw	GTTGTGAAAACCAACCGCTAA	Sequencing of VH chain in pVITRO-IgG1

4	LR31_GM2_VH_Seq	CGTACTTCCCGCCTCTCAGA	Sequencing of VH chain in pVITRO-IgM
5	pVITRO-BglIII-for	CCAGATGACAAGCTGGAGAT CAAACAGATCTCGTACGGTG GCGGCGCCATC	Insertion of BglIII restriction site to pVITRO IgG1/IgM
6	pVITRO-EcoRI-rev	GAGACGGTGACCACCAGCTG CACCTCGAATTCGGAGTGCG CGCCTGTGGC	Insertion of EcoRI restriction site to pVITRO IgG1/IgM
7	pVITRO-IgG-NcoI-for	AGCTGGTGGTCACCGTCTCC TCACCATGGGCTAGCACCAA GGGCCATCG	Insertion of NcoI restriction site to pVITRO IgG1/IgM
8	pVITRO-IgM-NcoI-for	GCTGGTGGTCACCGTCTCCT CACCATGGGGATCTGCATCC GCTCCAACCC	Insertion of NcoI restriction site to pVITRO IgG1/IgM
9	pVITRO-XhoI-rev	ATCTCCAGCTTGTCTATCTGGA TGTCCTCGAGACCGCGGCTA GCTGGAACC	Insertion of XhoI restriction site to pVITRO IgG1/IgM
10	Trast-VH-EcoRI-IgG-rev	CCGCCACAGGCGCGCACTCC GAATTCGAGGTGCAGCTGGT GGAGTC	Insertion of EcoRI restriction site to Trastuzumab VH
11	Trast-VH-NcoI-IgG-rev	GATGGGCCCTTGGTGCTAGC CCATGGTGAGGAGACGGTGA CAAGAG	Insertion of NcoI restriction site to Trastuzumab VH (for pVITRO-IgG1)
12	Trast-VH-NcoI-IgM-rev	GTTGGAGCGGATGCAGATCC CCATGGTGAGGAGACGGTGA CAAGAG	Insertion of NcoI restriction site to Trastuzumab VH (for pVITRO-IgM)
13	Trast-VL-XhoI-for	GGGTTCCAGCTAGCCGCGGT CTCGAGGACATCCAGATGAC CCAGTC	Insertion of XhoI restriction site to Trastuzumab VL
14	Trast_VL-BglIII-rev	CAGATGGCGCCGCCACCGTA CGAGATCTTTTGATCTCCAGC TTGGTACCTTG	Insertion of BglIII restriction site to Trastuzumab VL
15	HuCAL-VH-EcoRI-for	CCGCCACAGGCGCGCACTCC GAATTCAGGTGCAGCTGGT TCAGTC	Insertion of EcoRI restriction site to HuCAL VH
16	HuCAL-VH-NcoI-IgG-rev	GATGGGCCCTTGGTGCTAGC CCATGGACTAGACACTGTGA CCAGGG	Insertion of NcoI restriction site to HuCAL VH (for pVITRO-IgG1)
17	HuCAL-VL-XhoI-for	GGGTTCCAGCTAGCCGCGGT CTCGAGGACATCGAGCTGAC ACAGCC	Insertion of NcoI restriction site to HuCAL VH (for pVITRO-IgM)
18	HuCAL-VL-BglIII-rev	AGATGGCGCCGCCACCGTAC GAGATCTGTCCCAGCACT GTCAGC	Insertion of XhoI restriction site to HuCAL VL
19	HuCAL-VH-NcoI-IgM-rev	GTTGGAGCGGATGCAGATCC CCATGGACTAGACACTGTGA CCAGGG	Insertion of BglIII restriction site to HuCAL VL
20	E345K_Mutagenesis_fw	AAGGGCAGCCCCGAAAGCCA CAGGTGTACAC	E345K mutagenesis in pVITRO-IgG1
21	E345K_Mutagenesis_rv	TGGCTTTGGAGATGGTTTTCT CGATGG	E345K mutagenesis in pVITRO-IgG1

22	LR17	CACCGTTATCGGCAGCTGCT GAGCG	sgRNA for <i>B4GALNT1</i> knockout
23	LR18	AAACCGCTCAGCAGCTGCCG ATAAC	sgRNA for <i>B4GALNT1</i> knockout
24	B4GALNT1_TIDE_fw	GTGGGTGGACGACGACTTCG	Amplification <i>B4GALNT1</i> for TIDE
25	B4GALNT1_TIDE_rv	CCTCTCCTCCTAGGCTGCAG	Amplification <i>B4GALNT1</i> for TIDE
26	B4GALNT1_TIDE_Seq	GCCTTGAACAGGCTAAGGCC CGATACAAGGCTGTTAGAGA	Sequencing of <i>B4GALNT1</i> for TIDE
27	U6_Prom. F	GA	Sequencing of sgRNA

## 8.9 Plasmids

Table 11 lists the original plasmids used for cloning. In addition, all new plasmids generated in this work are listed with their features and purpose. The plasmid maps of constructs 10, 11, 18, 20, and 25 are exemplarily included in Appendix B-1 to Appendix B-5.

**Table 11: Original plasmids used for cloning and the new plasmids generated in this work with their properties and use.**

No	Name	Information (properties; use; provider)
<b>Original Plasmids</b>		
1	pL40C-CRISPR.EFS.dTomato NL SL	Cas9 and dTomato; for insertion of sgRNA (AG Müller; University Medical Center Hamburg-Eppendorf)
2	pVITRO1-Trastuzumab-IgG1/k	IgG1 CH and CL sequences / VH and VL of Trastuzumab; expression of anti-HER2 IgG1 (No. 61883; Addgene, Teddington, United Kingdom)
3	pVITRO1-Trastuzumab-IgM/k	IgM CH and CL sequences / VH and VL of Trastuzumab; expression of anti-HER2 IgM (No. 61881; Addgene, Teddington, United Kingdom)
4	pdHL7-ch14.18	IgG1 CH and CL sequences; expression of the chimeric ch14.18 IgG1 (AG Lode; University Medicine Greifswald)
5	pFUSEss-CLIg-hk	VL and CL sequence; ch14.18 κ light chain expression plasmid (Franziska Baatz based on pfuse2-hclk; InvivoGen, San Diego, USA)
6	pFUSEss-CHIg-hM	VH and CH sequence; ch14.18 μ heavy chain expression plasmid (Franziska Baatz based on pfuse2-hclk; InvivoGen, San Diego, USA)
7	pMDLg/pRRE	Gag/pol; production of lentiviral particles
8	pCMV-VSV-G	VSV-G; production of lentiviral particles
9	pRSV-REV	Rev; production of lentiviral particles
<b>Newly generated plasmids</b>		
10	pVITRO1-IgG1/k + restriction sites	IgG1 CH and CL sequences with additional restriction sites; IgG1 antibody expression
11	pVITRO1-IgM/k + restriction sites	IgM CH and CL sequences with additional restriction sites; IgM antibody expression
12	pVITRO-Trastuzumab-IgG	No 10 with VH and VL of Trastuzumab; expression of anti-HER2 IgG1
13	pVITRO-Trastuzumab-IgM	No 11 with VH and VL of Trastuzumab; expression of anti-HER2 IgM
14	pVITRO-HuCAL-IgG	No 10 with VH and VL of HuCAL; expression of anti-GM2 IgG1
15	pVITRO-HuCAL-IgM	No 11 with VH and VL of HuCAL; expression of anti-GM2 IgM

## 8 Material

16	pVITRO-L55-81-IgG	No 10 with VH and VL of L55-81; expression of anti-GM2 IgG1
17	pVITRO-L55-81-IgM	No 11 with VH and VL of L55-81; expression of anti-GM2 IgM
18	pVITRO-KM966-IgG	No 10 with VH and VL of KM966; expression of anti-GM2 IgG1
19	pVITRO-KM966-IgG (E345K)	No 10 with a point mutation in CH and with VH and VL of KM966; expression of anti-GM2 IgG1
20	pVITRO-KM966-IgM	No 11 with VH and VL of L55-81; expression of anti-GM2 IgM
21	pVITRO-US2011-IgG	No 10 with VH and VL of US2011; expression of anti-GM2 IgG1
22	pVITRO-US2011-IgM	No 11 with VH and VL of US2011; expression of anti-GM2 IgM
23	pVITRO-DMF10.167.4-IgG	No 10 with VH and VL of DMF10.167.4; expression of anti-GM2 IgG1
24	pVITRO-DMF10.167.4-IgM	No 11 with VH and VL of DMF10.167.4; expression of anti-GM2 IgM
25	pL40C-CRISPR.B4GALNT1.EFS.dTomato	Cas9 and dTomato; plasmid for knockout of <i>B4GALNT1</i> gene

### 8.10 Antibodies

The antibodies listed in Table 12 were used for western blot analysis and flow cytometric staining.

**Table 12: Antibodies used for flow cytometric or western blot analysis.**

Name	Dilution	Provider (city, country headquarter)	Cat. No.
<b>Flow Cytometry</b>			
Anti-human CD34, FITC	1:100	Miltenyi Biotec (Bergisch-Gladbach, Germany)	130-113-178
Anti-human CD45, APC/Fire750	1:50	BioLegend (San Diego, USA)	368518
Anti-human CD56, PE	1:50	Miltenyi Biotec (Bergisch-Gladbach, Germany)	130-113-312
Anti-human GD2, APC/Fire 750	1:20	BioLegend (San Diego, USA)	357322
Anti-human GD2, BV510	1:20	BioLegend (San Diego, USA)	357316
Anti-human GM2 (L55-81), AF647	1:100	Novus Biologicals (Wiesbaden, Germany)	NBP2-81278AF647
Anti-human GM2 (MK1-16)	1:50	TCI Deutschland GmbH (Eschborn, Germany)	A2575
Anti-human IgG, APC	1:50	Miltenyi Biotec (Bergisch-Gladbach, Germany)	130-119-772
Anti-human IgG, FITC	1:50	Miltenyi Biotec (Bergisch-Gladbach, Germany)	130-118-479
Anti-human IgG, unconjugated	1:1.250	Thermo Fisher Scientific Inc. (Waltham, USA)	31154
Anti-human IgM, APC	1:50	Miltenyi Biotec (Bergisch-Gladbach, Germany)	130-122-959
Anti-mouse CD45, Pacific Blue	1:200	BioLegend (San Diego, USA)	103126
Anti-mouse IgM, APC	1:20	BioLegend (San Diego, USA)	406509
Anti-mouse IgM, BV421	1:50	BioLegend (San Diego, USA)	406532
Anti-mouse IgM, FITC	1:50	BioLegend (San Diego, USA)	406506
Anti-mouse IgM, PE	1:100	BioLegend (San Diego, USA)	406507
Dinutuximab	1:500	Department of Pediatric Oncology and Hematology, University Medicine Greifswald	--
Human IgG1 REA Control (S), PE	1:50	Miltenyi Biotec (Bergisch-Gladbach, Germany)	130-113-438

## 8 Material

Mouse IgG1, $\kappa$ Isotype, APC/Fire750	1:50	BioLegend (San Diego, USA)	400196
Mouse IgG2a, $\kappa$ Isotype, APC/Fire 750	1:20	BioLegend (San Diego, USA)	400284
Mouse IgG2a, $\kappa$ Isotype, BV510	1:20	BioLegend (San Diego, USA)	400267
Rabbit IgG Isotype (PbNP15), AF647	1:100	Thermo Fisher Scientific Inc. (Waltham, USA)	51-4616-82
Rat IgG2b, $\kappa$ Isotype, Pacific Blue	1:200	BioLegend (San Diego, USA)	400627
<b>Western Blot</b>			
Anti-hamster (Armenian) IgG (H+L), HRP	1:5.000	Novus Biologicals (Wiesbaden, Germany)	NB100-2066
Anti-human IgG (H+L), HRP	1:10,000	Thermo Fisher Scientific Inc. (Waltham, USA)	31420
Anti-human IgM Antibody, HRP	1:10,000	Novus Biologicals (Wiesbaden, Germany)	NB7439
Anti-human Kappa, HRP	1:5,000	Southern Biotech (Birmingham, USA)	2060-05
Anti-mouse IgG + IgM (H+L), HRP	1:10.000	Jackson ImmunoResearch Laboratories Ltd. (West Grove, USA)	115-035-068
Anti-mouse IgG/IgA/IgM, HRP	1:1.000	Dako Agilent (Santa Clara, USA)	447

### 8.11 Software and tools

To design single guide (sg) ribonucleic acid (RNA) for generating NB cell lines with knockouts, the online tool 'CCTop CRISPR.cos' from the University of Heidelberg was utilized. Subsequently, the knockout efficiency was evaluated using the 'TIDE online tool' (version 3.3.0) from the Netherlands Cancer Institute. For the analysis of data generated during this work, the software listed in Table 13 were utilized.

**Table 13: Software used for analysis of data.**

<b>Software/Online tool</b>	<b>Provider (city, country headquarter)</b>
Adobe Illustrator 27.4	Adobe Inc. (San José, USA)
Biometra BioDocAnalyze 2.2	Analytik Jena (Jena, Germany)
Clustal Omega	EMBL-EBI (Cambridgeshire, UK)
Fiji ImageJ	U. S. National Institutes of Health (Bethesda, USA)
Flow Jo version 10.6.1	Tree Star Inc. (Ashland, USA)
GraphPad PRISM version 8.3.0	GraphPad Software Inc. (La Jolla, USA)
IncuCyte 2021A Software	Sartorius AG (Göttingen, Germany)
NanoDrop 2000/2000c	Thermo Fisher Scientific Inc. (Waltham, USA)
SnapGene® 4.3.11	GSL Biotech LLC (San Diego, USA)

### 9 Methods

#### 9.1 Cell culture

Cell lines described in Table 7 were cultivated under sterile conditions at 37 °C and 5% carbon dioxide (CO<sub>2</sub>). The cells were subcultured two to three times a week when reaching 90-95% confluency. Adherent cells were washed with PBS and detached using Trypsin/EDTA solution at 37 °C for 5 min. The reaction was stopped by addition of three volumes of complete growth medium. For suspension cells, the appropriate volume of the cell suspension was discarded, and fresh complete growth medium was added. Cell splitting ratios ranged from 1:2 to 1:20, depending on the doubling time. Regularly, the cells were checked for mycoplasma contamination.

For cryopreservation, detached cells were transferred into a 15 mL falcon tube and centrifuged at 300 × g for 5 min and room temperature (RT). The old medium was discarded and the cells were resuspended in fresh complete growth medium. The cell suspension was mixed with an equal volume of cryopreservation medium consisting of 20% dimethyl sulfoxide (DMSO) in FBS. 1 mL of the mixed suspension was transferred into freezing tubes which were immediately frozen in a cryopreservation box at -80 °C. For long-term storage the cells were transferred to liquid nitrogen at -150 °C a few days later.

To thaw cells, tubes were gently warmed at 37 °C in a water bath. The cell suspension was immediately transferred into a 15 mL falcon tube with prewarmed complete growth medium. The cells were centrifuged at 300 × g and RT for 5 min. After centrifugation, the medium was discarded, and the cells were suspended in fresh prewarmed complete growth medium and transferred into culture flasks.

For cell counting during experimental procedures, a Neubauer chamber was used. 15 µL of the cell suspension was diluted 1:1 with 15 µl trypan blue dye. This dye can pass the cell membrane of dead cells to distinguish between live and dead cells. 10 µl of the mixed cell suspension was pipetted to the Neubauer chamber and inserted into the Countess 3 Automated Cell Counter.

#### 9.2 Cloning

The subsequent chapters describe the cloning procedures to create the IgG1 and IgM antibody expression plasmids (chapter 9.2.1) as well as the process of generating the plasmid containing single guide (sg) sgRNA and Cas9 protein for the knockout of enzymes involved in the ganglioside synthesis (chapter 9.2.2).

### 9.2.1 Generation of plasmids for the expression of anti-GM2 IgG and IgM antibodies

pVITRO1-Trastuzumab-IgG1/ $\kappa$  and pVITRO1-Trastuzumab-IgM/ $\kappa$  were obtained from Addgene where they were provided by Dodev et al [168] and used for the expression of human antibodies of the IgG1 or IgM isotype. Each plasmid encodes the kappa ( $\kappa$ ) constant light ( $C_L$ ) region and either the constant heavy ( $C_H$ ) chain of IgG1 or IgM. Furthermore, the plasmids encode for the variable heavy ( $V_H$ ) and variable light ( $V_L$ ) sequences of the anti-HER2 antibody Trastuzumab. To introduce restriction sites flanking the  $V_H$  and  $V_L$  sequences of Trastuzumab, site-directed mutagenesis was conducted (Figure 18A,B). Specifically, the  $V_H$  sequence was flanked with the EcoRI restriction site at the 5'-end and the NcoI restriction site at the 3'-end. For the  $V_L$  sequence the restriction site for BglII was inserted at the 5'-end and for XhoI at the 3'-end. The site-directed mutagenesis was performed, using PCR with the Phusion High-Fidelity PCR master mix as described in the user guide with primers 5-9 and an annealing temperature of 65 °C.

PCR products were analyzed on a 1% agarose gel. For this, the PCR products were loaded onto the gel containing 1% ROTI® GelStain. The gel was then run within an electric field in a Tris(hydroxymethyl)aminomethane (Tris) acetate-EDTA (TAE) buffer-filled chamber at 120 V for 30 min. Subsequently, the DNA was visualized under ultraviolet (UV) light, and the corresponding bands were excised blindly from the gel using a disposable scalpel. DNA was purified using the NucleoSpin Gel and PCR Clean-up Mini Kit according to the manufacturer's instructions. The elution was performed in 20  $\mu$ l H<sub>2</sub>O instead of the provided elution buffer.

The gel-purified PCR products were joined by Gibson Assembly. For this, two fragments, each containing the inserted restriction sites for either the IgG1 or IgM expression plasmid, were combined in a 1:1 molar ratio with 10  $\mu$ l 2 $\times$  Gibson Assembly Master Mix in a final volume of 20  $\mu$ l. The mixture was then incubated at 50 °C for 30 min. Next, 2  $\mu$ l of the assembled DNA were transformed into chilled chemically competent *E. coli* JM109 Mix&Go bacteria and placed on ice for 30 min, followed by a heat shock at 42 °C for 30 s. Then the bacteria were immediately transferred to ice for 2 min. 950  $\mu$ l super optimal broth with catabolite repression (SOC) medium was added and the bacteria were incubated at 37 °C for 60 min while shaking at 250 rpm. After the incubation period, the bacteria were plated on Luria-Bertani (LB) agar plates containing 100  $\mu$ g/ml Hygromycin B antibiotic. The plates were incubated overnight at 37 °C.

The following day, bacterial colonies were picked from the plates using a pipette tip and transferred into pre-warmed LB medium with Hygromycin B antibiotic. The bacteria were incubated overnight at 37 °C while shaking. To isolate the plasmid DNA from the bacterial colonies the NucleoSpin Plasmid EasyPure Mini Kit was used. Following the manual with the modification that the DNA was eluted in 20  $\mu$ l H<sub>2</sub>O instead of elution buffer. For sequencing, 800 ng of the purified plasmid was diluted in 12  $\mu$ l

H<sub>2</sub>O and 3 µl of the appropriate primer was added. The sequencing procedure was outsourced to Microsynth Seqlab.

The V<sub>H</sub> and V<sub>L</sub> sequences from published anti-GM2 antibodies (chapter 5.4) with appropriate restriction sites were synthesized using Invitrogen GeneArt Gene Synthesis Service. 2 µg of each plasmid containing either the V<sub>H</sub> or V<sub>L</sub> antibody sequences was mixed with 2 µl of 10× FD Green Buffer and 1 µl of each restriction enzymes. EcoRI and NcoI were used for the restriction of the V<sub>H</sub> sequence and BglII and XhoI for the V<sub>L</sub> sequence. The sample was filled with water to a volume of 20 µl and incubated at 37 °C for 30 min. After the restriction digest, the antibody fragments were separated with the help of an agarose gel electrophoresis. The products were excised from the 1% agarose gel and purified with the NucleoSpin Gel and PCR Clean-up Mini Kit as described previously. For the ligation reaction, the restricted pVITRO-IgG or pVITRO-IgM vector was used in a 1:3 molar ratio with the restricted V<sub>H</sub> and V<sub>L</sub> inserts. The ligation reaction was carried out as mentioned before, leading to the generation of the final IgG1 and IgM antibody expression plasmids. As an example, the cloning procedure is shown for the plasmid pVITRO-KM966-IgG in Figure 18.

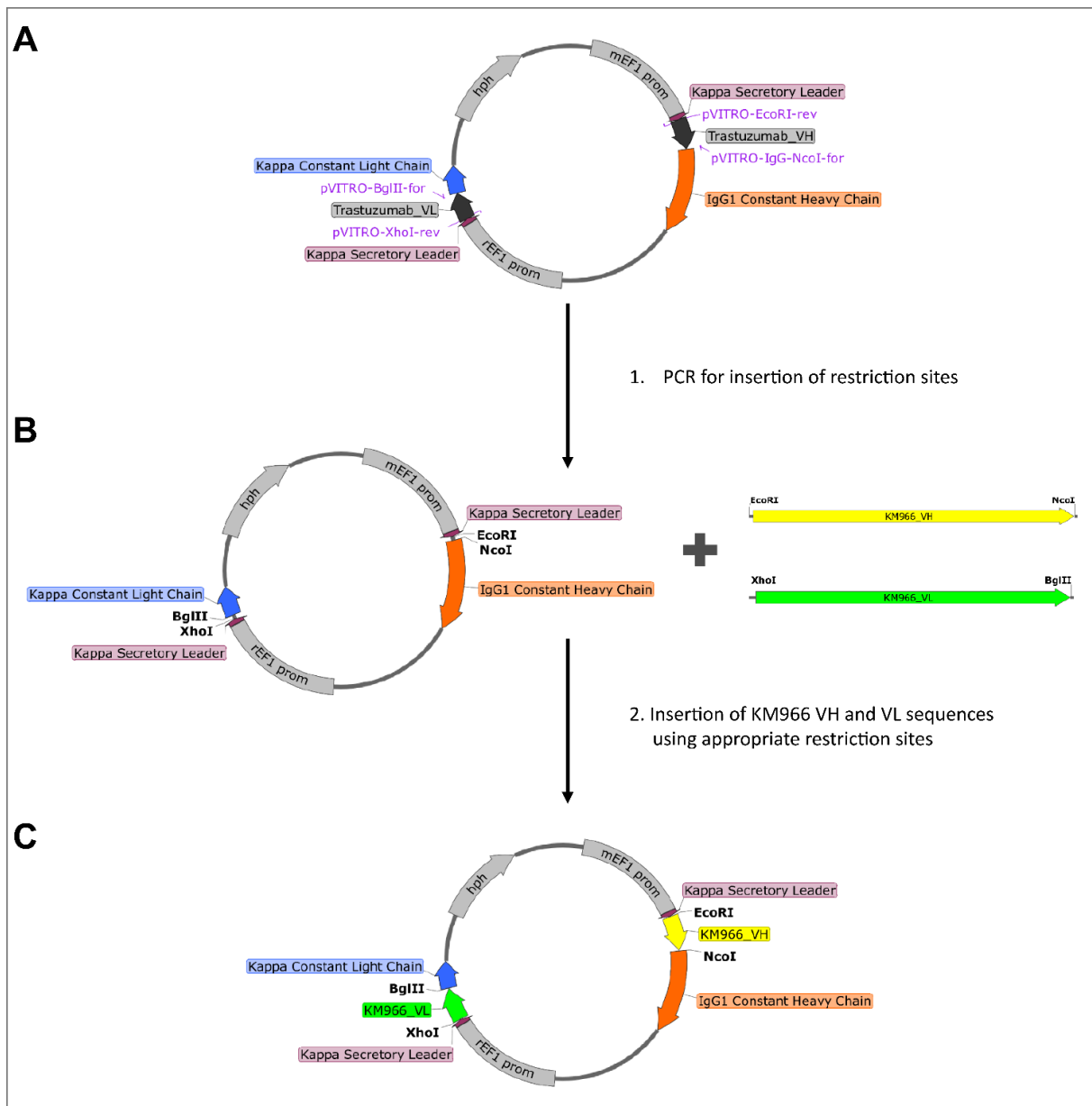


**Figure 18: Cloning strategy for insertion of KM966 variable sequences into the pVITRO-IgG1/k expression plasmid.** 1. The restriction sites EcoRI, NcoI, XhoI and BglII were inserted into the original plasmid pVITRO-Trastuzumab-IgG1/k (**A**) using appropriate primers (purple). 2. The resulting plasmid pVITRO-IgG1/k and KM966 variable heavy and light sequences (**B**) were sequentially cut and ligated at the corresponding restriction sites, resulting in the plasmid pVITRO-KM966-IgG1/k (**C**). VH: variable heavy; VL: variable light; PCR: polymerase chain reaction.

### 9.2.2 Plasmid construction for CRISPR/Cas9-based knockout strategy

To investigate the specificity of the generated antibodies, several NB cell lines with a knockout of the *B4GALNT1* gene were generated. For this, a CRISPR/Cas9-based approach, utilizing a plasmid with sgRNA targeting the *B4GALNT1* gene, was employed. For cloning, the plasmid pL40C-CRISPR.EFS.dTomato NL SL which encodes CRISPR-associated (spCas9) under the control of an elongation factor 1-alpha 1 (EF1a) promoter connected to a mNeon fluorescent protein via a P2A

sequence was kindly provided by Dirk Heckl [239] (Appendix B-5). The plasmid features two BsmBI restriction sites for the insertion of the sgRNA.

The sgRNA was designed using the online tool CRISPR/Cas9 target online predictor (CCTop) [240,241]. In the first step, the 25 base pair (bp) long complementary oligonucleotides were annealed and phosphorylated. For this, 1  $\mu$ l of each oligonucleotide (100  $\mu$ M), 1  $\mu$ l 10 $\times$  T4 DNA ligase buffer and 0.5  $\mu$ l T4 Polynucleotide Kinase (PNK) were mixed with H<sub>2</sub>O in a total volume of 10  $\mu$ l. The mixture was incubated in the thermocycler at 37 °C for 45 min, followed by an incubation at 95 °C for 2.5 min. Finally, the mixture was cooled to 22 °C with a decrease of 0.1 °C/s. The pL40C-CRISPR.EFS.dTomato NL SL plasmid was restricted with 1  $\mu$ l BsmBI enzyme in the presence of 3  $\mu$ l restriction buffer and filled with H<sub>2</sub>O to 30  $\mu$ l. After incubating at 37 °C for 30 min, 1  $\mu$ l alkaline phosphatase (ALP) was added, followed by another 15 min of incubation at 37 °C. The restricted plasmid was excised from the 1% agarose gel and purified with the NucleoSpin Gel and PCR Clean-up Mini Kit as described before. For ligation, the annealed and phosphorylated oligonucleotides were diluted 1:500 in H<sub>2</sub>O. 1  $\mu$ l was mixed with 50 ng of the restricted CRISPR/Cas9 plasmid, 0.5  $\mu$ l T4 DNA ligase buffer and 0.5  $\mu$ l T4 DNA ligase in a final volume of 5  $\mu$ l H<sub>2</sub>O. The mixture was then incubated at RT for 15-30 min, transformed into competent *E. coli* bacteria and subsequently plated on LB agar plates with 100 mg/ml Ampicillin.

### 9.3 Production of lentiviral particles and transduction

Lentiviral particles were produced following the protocol published by Weber *et al.* with some modifications [242]. HEK293T cells were used as the producer cell line and seeded at a density of  $3 \times 10^6$  cells per 10 cm cell culture dish. To enable adhesion, the cells were incubated at 37 °C for at least 6 h. The required amounts of plasmids (10  $\mu$ g of pL40C-B4GALNT1.EFS.dTomato; 10  $\mu$ g of pMDLg/pRRE; 5  $\mu$ g of pRSV-Rev, and 2  $\mu$ g of phCMV-VSV-G) were diluted to a total volume of 450  $\mu$ l in H<sub>2</sub>O, and 50  $\mu$ l of 2.5 M Calcium chloride (CaCl<sub>2</sub>) was added. This solution was then added drop by drop to a 15 ml falcon tube where 500  $\mu$ l 2 $\times$  HBS were prepared beforehand. While incubating the mixture at RT for 15 min the old medium was removed from the cells and replaced by fresh medium supplemented with 25  $\mu$ M Chloroquine. Subsequently, the mixture containing the plasmids was added to the cells drop by drop while swirling the dish gently. The cells were then incubated at 37 °C overnight. The next day, the medium was exchanged for chloroquine-free medium. Another 24 h later, the supernatant was harvested with a syringe and filtered through 0.45  $\mu$ m filters into Nalgene™ Oak Ridge High-Speed centrifuge tubes. To concentrate the viral particles centrifugation was performed at 20,000  $\times$  g and 4 °C for 4 h. The supernatant was discarded, and the pelleted viral particles were dissolved in 300-500  $\mu$ l medium, aliquoted, and stored at -80 °C until further use.

For titer calculation 50,000 HEK293T cells per well were seeded in a 24-well plate in medium supplemented with 8 µg/ml polybrene. Different volumes (0.1 µl, 1 µl, 10 µl) of supernatant containing the viral particles were added to the wells after adhesion of the cells. The measurements were performed in duplicates. The transduced cells were then incubated at 37 °C for 72 h. After the incubation period, the cells were harvested into Falcon™ round bottom polystyrene tubes and fixed with 1% paraformaldehyde (PFA). Transduction efficiencies were measured using the MACSQuant X Flow Cytometer and titers were calculated using a sample ideally showing between 5% to 20% transduced cells. Transduction rates above 20% could lead to multiple integrations per cell and thus to an underestimation of the titer [243]. The titer was calculated with the help of the following equation:

$$\text{Titer (IU)/mL} = \frac{\% \text{ transduced cells } P \times \text{plated cells } N}{\text{volume } V \text{ [mL]}}$$

where  $P$  is the proportion of transduced cells,  $N$  is the number of plated cells and  $V$  is the volume of supernatant containing the viral particles.

For lentiviral transduction, various NB cell lines such as SH-SY5Y or SK-N-LO were used. 50,000 cells per well were seeded in a 24-well plate in medium supplemented with 8 µg/ml polybrene. After allowing the cells to adhere for 4-6 h, different volumes of lentiviral particles were tested. The Multiplicity of infection (MOI) ranged from 1 to 10. The required volumes of lentiviral particles were calculated with the help of the previously calculated titer using the subsequent equation:

$$\text{Volume } V \text{ [mL]} = \frac{\text{MOI} \times \text{plated cells } N}{\text{titer} \left[ \frac{\text{IU}}{\text{mL}} \right]}$$

### 9.4 Isolation of human CD34<sup>+</sup> stem cells from bone marrow blood

The isolation of human CD34<sup>+</sup> stem cells was performed from leukapheresis material using the CD34 MicroBead Kit UltraPure according to the manufacturer's instructions. First, the cells were washed with MACS buffer, which is composed of PBS supplemented with 2 mM EDTA and 0.5% FBS. To lyse the erythrocytes, 10 ml of 1× red blood cell lysis buffer was added to 1 ml sample and incubated at RT for 10 min. After another washing step, the cells were counted and resuspended to 1×10<sup>8</sup> cells in 300 µl MACS buffer. 100 µl FcR blocking reagent and 100 µl CD34 MicroBead UltraPure were added for up to 1×10<sup>8</sup> cells. After an incubation time of 30 min at 4°C, the cells were washed again and resuspended to 1×10<sup>8</sup> cells in 500 µl buffer. The magnetic separation of CD34<sup>+</sup> cells was performed using pre-separation filters and LS columns. Following a rinsing step with 3 ml buffer, the labeled cell suspension was applied to the filter on the column. The column was washed three times with 3 ml buffer. Then, the column was removed from the magnetic field and placed on a new collection tube. The human CD34<sup>+</sup> cells were eluted with 5 ml buffer, counted, and frozen for later use.

### 9.5 Antibody production and purification

Large amounts of antibodies were produced and purified at the 'Centre for Structural Systems Biology'. Antibodies were stored at -80 °C before use. Small amounts of antibodies were produced in-house either using the ExpiCHO™ Expression System from Thermo Fisher Scientific according to the manufacturer's instructions, or by transient transfection of HEK293T cells.

For the ExpiCHO™ Expression System, ExpiCHO-S cells were expanded to the required quantity. One day prior to transfection, the cells were counted and seeded at a concentration of  $4 \times 10^6$  cells/ml. The next day, cells were counted and diluted in fresh and pre-warmed expression medium to a concentration of  $6 \times 10^6$  cells/ml. All transfection reagents were directly taken from the fridge and used coldly. For 100 ml culture volume, 80 µg plasmid DNA was mixed with 4 ml OptiPro SFM in a 15 ml falcon tube. In another 15 ml falcon tube, 320 µl ExpiFectamine CHO reagent was mixed with 3.7 ml OptiPro SFM. Both tubes were mixed by gentle inversion. In the next step, the diluted ExpiFectamine CHO reagent was added to the diluted DNA and mixed gently. The mixed sample was incubated at RT for 2 min and slowly added to the cell suspension while swirling gently. The transfected cells were incubated at 37 °C in an incubator with a humidified atmosphere of 8% CO<sub>2</sub> in air. The cells were shaking gently on an orbital shaker platform. The following day, 600 µl of ExpiCHO enhancer and 24 ml of ExpiCHO feed were added to the culture flask while swirling the flask gently. For the standard protocol, the cells were incubated at 37 °C with 8% CO<sub>2</sub> and harvested 8 to 10 days post-transfection. Following harvest, the supernatant was centrifuged at 4 °C and at  $4,000 \times g$  for 30 min. The supernatant was filtered through a 0.22 µm filter and stored at 4 °C.

Transient transfection of HEK293T cells was performed following the protocol of the 'European Monoclonal Antibodies Network' [244] and jetOPTIMUS® transfection guidelines. Here,  $2 \times 10^6$  cells were seeded into a T75 culture flask in complete growth medium. The following day, when the cells reached about 70-80% confluence, the medium was removed, the cells were washed once with PBS, and 8 ml pre-warmed OptiMEM medium was added. In one reaction tube 40 µl plasmid DNA was diluted in 200 µl jetOPTIMUS buffer. The mixture was vortexed for 1 s and centrifuged shortly. Then, 30 µl jetOPTIMUS Transfection Reagent was added, vortexed for 1 s and spun down shortly. The mixture was incubated at RT for 10 min. Finally, 1 ml of the mixture was added to the cells dropwise. The cells were incubated at 37 °C at least for 6 h prior to the addition of 8 ml complete growth medium. The supernatant was harvested about 6 days later, when nearly all HEK293T cells were detached from the flask. The supernatant was centrifuged at 4 °C and  $4,000 \times g$  for 30 min, filtered through a 0.22 µm filter and stored at 4 °C.

In-house produced antibodies were purified by affinity chromatography using the ÄKTA pure fluid chromatograph. A 1 ml HiTrap® Protein G high performance column was used for the purification of

IgG antibodies. All buffers were sterile filtered through a 0.45 µm filter before use. The supernatant containing the antibodies was diluted in a 1:1 ratio in PBS, which served as binding buffer. The sample was then applied to the ÄKTA pure via a sample pump. 15 ml falcon tubes were prepared with 200 µl of 1M Tris-HCl (pH 9.0) neutralization buffer and placed into the fraction collector. The column was first washed with 10 column volumes of binding buffer at a flow rate of 1 ml/min. The sample was automatically applied at a flow rate of 2 ml/min. Following this, the column was washed with 10 columns of binding buffer prior to elution with 0.1 M glycine-HCl (pH 2.7) elution buffer in 1 ml fractions. Elution was carried out with a total of 25 column volumes. All elution fractions were collected into the prepared 15 ml falcon tubes. After use, the column was cleaned and stored in 20% ethanol at 4 °C. The antibody-containing elution fractions were pooled and stored at 4 °C for further use.

### 9.6 Antibody validation *in vitro*

Various methods were employed for the validation of antibodies *in vitro*. These methods are described in detail in the following chapters 9.6.1 to 9.6.7.

#### 9.6.1 Western Blot

Antibody production was confirmed and visualized through Western Blot analysis. Purified antibodies (2 µg) were prepared with 10 mM Dithiothreitol (DTT) and 1× loading dye, then heated to 70 °C for 10 min. The samples were loaded to the sodium dodecyl sulfate (SDS) polyacrylamide gel electrophoresis (PAGE) under reducing conditions. The gel was run at 150 V for 60-75 min. Proteins were blotted to a nitrocellulose membrane using the wet/tank blot technique, with transfer conditions set to 400 mA and 4°C for 2-3 h. The membrane was blocked overnight with 5% skimmed milk powder in Tris-buffered saline with 0.1% Tween20 (TBS-T) while shaking. The following day, the appropriate secondary HRP-labeled detection antibody diluted in blocking buffer was added and incubated at RT for 2 h while shaking. Washing steps with TBS-T were repeated thrice for 10 min. Finally, for detection ECL solution was used.

#### 9.6.2 Enzyme-linked immunosorbent assay (ELISA)

For the concentration determination of in-house produced antibodies, the human IgG (or IgM) ELISA BASIC Kit from Mabtech was used. The kit was applied following the manufacturer's instructions. In brief, Nunc transparent immune standard modules MaxiSorp stripes were coated with 100 µl of the capture antibody diluted to a final concentration of 2 µg/ml in PBS and incubated overnight at 4 °C. The following day, the plate was emptied and 200 µl of incubation buffer (PBS supplemented with 0.05% Tween20 and 0.1% bovine serum albumin (BSA)) was added to block unspecific binding sites. The plate was incubated at RT for 1 h. Meanwhile, an IgG (or IgM) standard was serially diluted, and

the samples were prepared in incubation buffer at 1:1,000 dilution. The plate was washed five times with 300  $\mu$ l PBS supplemented with 0.05% Tween20. Then, 100  $\mu$ l of the standards or diluted samples were added to the plate in duplicates and incubated at RT for 2 h. The plate was washed as described before and 100  $\mu$ l of the detection antibody diluted 1:1,000 in incubation buffer were added to the wells. The plate was incubated at RT for another 1 h. After washing five times, 100  $\mu$ l of the para-nitrophenylphosphate (pNPP) substrate was added to the wells and incubated at RT for 10 min. The absorbance was measured at 405 nm with the Varioskan LUX Multimode microplate reader.

### 9.6.3 Tycho stability measurement

To assess the antibody stability, a measurement with the Tycho NT.6 device was conducted at the 'Centre for Structural Systems Biology'. Purified antibody was mixed with 20 mM sodium phosphate buffer (pH 7.4) containing 150 mM NaCl in a 1:1 ratio, resulting in a final volume of 11  $\mu$ l. Each sample was soaked into individual capillaries, and Tycho NT.6 measurement was initiated.

### 9.6.4 Flow cytometry

To determine the expression of gangliosides GM2 and GD2 on the cell surface and evaluate the binding specificity of the newly generated anti-GM2 antibodies, NB cell lines were subjected to flow cytometric analysis. For the analysis, cells were harvested, washed twice with PBS supplemented with 2% FBS (FACS buffer) and counted. A total of  $3 \times 10^5$  cells in 100  $\mu$ l were used for staining. To prevent nonspecific binding of antibodies via their  $F_c$  receptor, cells were incubated with 2  $\mu$ l Human TruStain FcX™ blocking solution at 4 °C for 15 min. Two different types of staining were carried out in this work: (i) direct staining with an antibody directly labeled with a fluorophore, and (ii) indirect staining with an unlabeled antibody using a secondary fluorescence-labeled antibody. Direct staining was performed at 4 °C for 20 min. Indirect staining was performed in two steps at 4 °C for 30 min with each antibody. After each staining step, cells were washed twice with FACS buffer, involving a centrifugation step at  $300 \times g$  for 5 min. All washing steps include a centrifugation step at  $300 \times g$  for 5 min. The measurement of fluorescence was performed using the MACSQuant X flow cytometer. Cells were gated according to their size in the forward and sideward scatter (SSC-A/FSC-A) and doublets were excluded with FSC-H/FSC-A gating before assessing the antigen expression. Data analysis was conducted using the FlowJo software.

### 9.6.5 Ganglioside test stripes

To determine the binding specificity of the newly generated antibodies, test strips on which different gangliosides are spotted were used for the analysis. The assay kit was used following the manufacturer's instructions. Briefly, the test stripes were incubated in 1 ml buffer solution with 1  $\mu$ g of the antibody at 4 °C for 2 h while shaking gently. After washing with 1 ml of the buffer solution, 50  $\mu$ l

of the conjugate was added to the incubation tray along with 1 ml buffer solution and incubated at 4 °C for 1 h. Next, 500 µl of the substrate was added and incubated at RT for 10 min. Finally, the tray was washed with 1 ml of buffer solution and with 1 ml H<sub>2</sub>O, each for 2 min.

### 9.6.6 Complement-dependent cytotoxicity assay

For the complement-dependent cytotoxicity (CDC) assay, a total of  $1.5 \times 10^4$  cells were plated in triplicates in 96-well flat-bottom plates in complete growth medium and incubated overnight. The next day, medium was replaced by 50 µl RPMI medium containing 2× CellTox Green dye. A zero-point measurement was taken after 30 min following the insertion of the plate into the incubator. This measurement served as the initial baseline prior to the addition of the test components and allows for the assessment of any background signal. Next, the test components containing pooled serum from healthy human donors as the complement source and the antibodies at different concentrations were added to the wells, resulting in a final volume of 100 µl and a final concentration of 12.5% serum. The plates were imaged in 30-minute intervals for 3 h using the IncuCyte Live-Cell Analysis System. Two images per well were taken with the 10× objective at each time point. The analysis of the results was performed using the IncuCyte 2021A Software.

### 9.6.7 Antibody-dependent cellular cytotoxicity assay

The first step was the isolation of peripheral blood mononuclear cells (PBMC) from blood obtained from healthy human donors. For this, blood was collected in ethylene diamine tetra acetic acid (EDTA) tubes and mixed with PBS in a 1:1 ratio. 5 ml Ficoll solution in a 15 ml falcon tube was carefully overlaid with a maximum of 10 ml of the blood:PBS mixture. The tubes were centrifuged at  $900 \times g$  for 20 min, with the acceleration set to level 3 and the deceleration to level 2. Following centrifugation, the interphase containing the PBMC was carefully transferred into a new falcon tube. The tube was filled with PBS supplemented with 2 mM EDTA and centrifuged at  $300 \times g$  for 5 min. The supernatant was transferred into a new falcon tube and the centrifugation was repeated. The cell pellet was washed two more times with PBS supplemented with 2 mM EDTA and finally resuspended in RPMI medium. The cells were counted and immediately used for the assay.

Next, NB target cells were harvested and washed with PBS once. Target cells that did not express a fluorescent reporter were labeled with eFluor670 dye prior to seeding. For this, the cells were pelleted by centrifugation at  $300 \times g$  for 5 min and resuspended in PBS to a final concentration of  $5 \times 10^5$  cells/ml. The eFluor670 dye was diluted 1:2,000 in the cell suspension, and the cells were incubated at 37 °C for 10 min. To stop the staining reaction, 2.5 volumes of a stopping solution composed of 25% FBS in RPMI were added. The cells were incubated at 4 °C for 5 min and after another centrifugation step the medium was removed. The cells were then resuspended to a final

concentration of  $1 \times 10^6$  cells/ml in RPMI medium, and 100  $\mu$ l per well were seeded into a 96-well plate.

In the next step, the plate was centrifuged, and the medium was removed. 50  $\mu$ l of the diluted antibody was added to the wells to achieve a final concentration of 4  $\mu$ g/ml. Finally, 50  $\mu$ l of the isolated PBMC was added at different effector to target (E:T) ratios. All conditions were tested in triplicates. The cells were incubated at 37 °C for 4h. After the incubation time, the plate was centrifuged, the medium was removed, and the cells were resuspended in 100  $\mu$ l FACS buffer with 1  $\mu$ l of propidium iodide (PI) for the detection of dead cells.

The detection of PI<sup>+</sup> cells was performed with the MACSQuant X Flow Cytometer. Cells were gated according to their size in the forward and sideward scatter (SSC-A/FSC-A), and doublets were excluded with FSC-H/FSC-A gating. NB cells were differentiated from PBMC due to their green fluorescent protein (GFP) reporter expression or eFluor670 labeling. The assessment of cytotoxicity was performed by detecting PI<sup>+</sup> cells. Data analysis was performed using the FlowJo software.

### 9.7 Mouse experiments

After evaluating the *in vitro* characteristics of the anti-GM2 antibodies, an *in vivo* mouse model was employed. All experimental procedures were approved by the Government of Hamburg, Germany (Approval No: N074/2020). The experiments were carried out in accordance with national regulations governing the ethical treatment of animals.

#### 9.7.1 Animal maintenance, husbandry, and care

NOD.Cg-*Prkdc*<sup>scid</sup>112rg<sup>tm1Wjl</sup>Tg(CMV-IL3,CSF2,KITLG)1Eav/MloySzJ (NSG-SGM3) mice were bred in the animal facility of the University Medical Center Hamburg-Eppendorf and were kept in groups of up to six males or females in individually ventilated cages under controlled specific pathogen-free conditions. The mice were maintained on a 12-hour light and 12-hour dark cycle, with access to autoclaved food and water *ad libitum*. Experimental procedures were exclusively undertaken with female animals to minimize biological variables. After the onset of the experiment, the mice were monitored and scored daily, and the body weight was determined at least twice a week. At the end of the experiment, the mice were anesthetized by floating the cage with CO<sub>2</sub> and sacrificed by cervical dislocation.

#### 9.7.2 Treatment with the monoclonal anti-GM2 antibody

To generate mice with a humanized immune system, female NSG-SGM3 mice aged six to eight weeks were irradiated with 240 cGy. After 16 h,  $3 \times 10^5$  CD34<sup>+</sup> human hematopoietic stem cells (hHSC),

which were freshly thawed and analyzed for viability as well as CD34 positivity by flow cytometry, were injected intravenously (i.v.) in 100  $\mu$ l PBS. Starting from week six after stem cell transplantation, peripheral blood samples were collected every four weeks via submandibular bleeding. The blood was collected using a lancet and EDTA microvettes. After lysis of the red blood cells with 1 $\times$  red blood cell lysis buffer and an incubation at RT for 10 min, staining was performed to analyze the percentage of hCD45<sup>+</sup> cells by flow cytometry. If the percentage of hCD45<sup>+</sup> cells exceeded 20% after 12 weeks post-injection, the humanization was evaluated as successful and  $3.5 \times 10^6$  NB cells were injected subcutaneously (s.c.) for a local tumor model. Fourteen days after the tumor inoculation, the antibody treatment was initiated. The mice were assigned to groups of at least five mice to allow for statistical analysis. Either 140  $\mu$ g of the anti-GM2 IgG or the Isotype IgG antibodies diluted in 100  $\mu$ l PBS were injected intraperitoneally (i.p.). The treatment period was five weeks, during which the mice received antibody injections twice a week and a total of five injections. The tumor volumes were measured by palpitation or with a caliper once a week beginning from the tumor cell inoculation. The mice were sacrificed as soon as tumor volumes reached 1.5 cm<sup>3</sup> or when a weight loss of 20% from the initial weight occurred.

### 9.8 Statistical analysis

Statistical analysis was performed using GraphPad Prism Software (version 8.3.0). Graphs represent group mean values and standard error of the mean (SEM) as indicated in the figure legends. *P* values <0.05 were considered statistically significant and are denoted with asterisks, \*\*\*\* = *P* < 0.0001, \*\*\* = *P* < 0.001, \*\* = *P* < 0.01, \* = *P* < 0.05, ns = *P* > 0.05. Number of repeats performed, and other statistical tests used are described in the relevant figure legends.

### 10 References

1. Rudolf Virchow (1863) *Hyperplasie der Zirbel und der Nebennieren*. (Erste Edition). Die Krankhaften Geschwulste Vol. 2 1864-65, Hirschwald, Berlin.
2. Park JR, Eggert A, Caron H (2010) Neuroblastoma: biology, prognosis, and treatment. *Hematol Oncol Clin North Am* 24: 65–86. <http://www.ncbi.nlm.nih.gov/pubmed/20113896>
3. Berthold F, Spix C, Kaatsch P, Lampert F (2017) Incidence, Survival, and Treatment of Localized and Metastatic Neuroblastoma in Germany 1979-2015. *Paediatr Drugs* 19: 577–593. <http://www.ncbi.nlm.nih.gov/pubmed/28786082>
4. Maris JM, Weiss MJ, Mosse Y, Hii G, Guo C, et al. (2002) Evidence for a hereditary neuroblastoma predisposition locus at chromosome 16p12-13. *Cancer Res* 62: 6651–6658. <http://www.ncbi.nlm.nih.gov/pubmed/12438263>
5. Cohn SL, Pearson ADJ, London WB, Monclair T, Ambros PF, et al. (2009) The International Neuroblastoma Risk Group (INRG) classification system: an INRG Task Force report. *Journal of clinical oncology : official journal of the American Society of Clinical Oncology* 27: 289–297. <http://www.ncbi.nlm.nih.gov/pubmed/19047291>
6. Maris JM, Hogarty MD, Bagatell R, Cohn SL (2007) Neuroblastoma. *Lancet* 369: 2106–2120. <http://www.ncbi.nlm.nih.gov/pubmed/17586306>
7. Monclair T, Brodeur GM, Ambros PF, Brisse HJ, Cecchetto G, et al. (2009) The International Neuroblastoma Risk Group (INRG) staging system: an INRG Task Force report. *Journal of clinical oncology : official journal of the American Society of Clinical Oncology* 27: 298–303. <http://www.ncbi.nlm.nih.gov/pubmed/19047290>
8. Brodeur GM, Pritchard J, Berthold F, Carlsen NL, Castel V, et al. (1993) Revisions of the international criteria for neuroblastoma diagnosis, staging, and response to treatment. *Journal of clinical oncology : official journal of the American Society of Clinical Oncology* 11. <http://www.ncbi.nlm.nih.gov/pubmed/8336186>
9. Tas ML, Reedijk AMJ, Karim-Kos HE, Kremer LCM, van de Ven CP, et al. (2020) Neuroblastoma between 1990 and 2014 in the Netherlands: Increased incidence and improved survival of high-risk neuroblastoma. *Eur J Cancer* 124: 47–55. <http://www.ncbi.nlm.nih.gov/pubmed/31726247>
10. Shimada H, Ambros IM, Dehner LP, Hata J-i, Joshi VV, et al. (1999) Terminology and morphologic criteria of neuroblastic tumors. *Cancer* 86: 349–363. [https://doi.org/10.1002/\(SICI\)1097-0142\(19990715\)86:2<349:AID-CNCR20>3.0.CO;2-Y](https://doi.org/10.1002/(SICI)1097-0142(19990715)86:2<349:AID-CNCR20>3.0.CO;2-Y)
11. Shimada H, Umehara S, Monobe Y, Hachitanda Y, Nakagawa A, et al. (2001) International neuroblastoma pathology classification for prognostic evaluation of patients with peripheral neuroblastic tumors. *Cancer* 92: 2451–2461. [https://doi.org/10.1002/1097-0142\(20011101\)92:9<2451:aid-cncr1595>3.0.co;2-s](https://doi.org/10.1002/1097-0142(20011101)92:9<2451:aid-cncr1595>3.0.co;2-s)
12. Schleiermacher G, Janoueix-Lerosey I, Delattre O (2014) Recent insights into the biology of neuroblastoma. *Int J Cancer* 135: 2249–2261. <http://www.ncbi.nlm.nih.gov/pubmed/25124476>
13. Andrew M. Davidoff Neuroblastoma. In: *Clinical Gate*, Chapter 66.
14. American Cancer Society (28th 2021) Signs and Symptoms of Neuroblastoma. <https://www.cancer.org/cancer/types/neuroblastoma/detection-diagnosis-staging/signs-and-symptoms.html> Accessed 12th June 2023.
15. Anderson J, Majzner RG, Sondel PM (2022) Immunotherapy of Neuroblastoma: Facts and Hopes. *Clin Cancer Res* 28: 3196–3206. <http://www.ncbi.nlm.nih.gov/pubmed/35435953>

## 10 References

---

16. Thompson D, Vo KT, London WB, Fischer M, Ambros PF, et al. (2016) Identification of patient subgroups with markedly disparate rates of MYCN amplification in neuroblastoma: A report from the International Neuroblastoma Risk Group project. *Cancer* 122: 935–945.  
<http://www.ncbi.nlm.nih.gov/pubmed/26709890>
17. Iolascon A, Giordani L, Borriello A, Carbone R, Izzo A, et al. (2000) Reduced expression of transforming growth factor-beta receptor type III in high stage neuroblastomas. *Br J Cancer* 82: 1171–1176.  
<http://www.ncbi.nlm.nih.gov/pubmed/10735501>
18. Raffaghello L, Prigione I, Bocca P, Morandi F, Camoriano M, et al. (2005) Multiple defects of the antigen-processing machinery components in human neuroblastoma: immunotherapeutic implications. *Oncogene* 24: 4634–4644. <http://www.ncbi.nlm.nih.gov/pubmed/15897905>
19. Ando K, Ohira M, Ozaki T, Nakagawa A, Akazawa K, et al. (2008) Expression of TSLC1, a candidate tumor suppressor gene mapped to chromosome 11q23, is downregulated in unfavorable neuroblastoma without promoter hypermethylation. *Int J Cancer* 123: 2087–2094.  
<http://www.ncbi.nlm.nih.gov/pubmed/18726896>
20. Nakagawara A, Arima M, Azar CG, Scavarda NJ, Brodeur GM (1992) Inverse relationship between trk expression and N-myc amplification in human neuroblastomas. *Cancer Res* 52: 1364–1368.  
<http://www.ncbi.nlm.nih.gov/pubmed/1737399>
21. Nakagawara A, Azar CG, Scavarda NJ, Brodeur GM (1994) Expression and function of TRK-B and BDNF in human neuroblastomas. *Mol Cell Biol* 14: 759–767. <http://www.ncbi.nlm.nih.gov/pubmed/8264643>
22. Mossé YP, Laudenslager M, Longo L, Cole KA, Wood A, et al. (2008) Identification of ALK as a major familial neuroblastoma predisposition gene. *Nature* 455: 930–935.  
<http://www.ncbi.nlm.nih.gov/pubmed/18724359>
23. Bresler SC, Weiser DA, Huwe PJ, Park JH, Krytska K, et al. (2014) ALK mutations confer differential oncogenic activation and sensitivity to ALK inhibition therapy in neuroblastoma. *Cancer Cell* 26: 682–694. <http://www.ncbi.nlm.nih.gov/pubmed/25517749>
24. Trochet D, Bourdeaut F, Janoueix-Lerosey I, Deville A, Pontual L de, et al. (2004) Germline mutations of the paired-like homeobox 2B (PHOX2B) gene in neuroblastoma. *Am J Hum Genet* 74: 761–764.  
<http://www.ncbi.nlm.nih.gov/pubmed/15024693>
25. Wu ZL, Schwartz E, Seeger R, Ladisch S (1986) Expression of GD2 ganglioside by untreated primary human neuroblastomas. *Cancer Res* 46: 440–443. <http://www.ncbi.nlm.nih.gov/pubmed/3940209>
26. Mastrangelo S, Rivetti S, Triarico S, Romano A, Attinà G, et al. (2021) Mechanisms, Characteristics, and Treatment of Neuropathic Pain and Peripheral Neuropathy Associated with Dinutuximab in Neuroblastoma Patients. *Int J Mol Sci* 22. <http://www.ncbi.nlm.nih.gov/pubmed/34884452>
27. Woo SR, Oh YT, An JY, Kang BG, Nam D-H, et al. (2015) Glioblastoma specific antigens, GD2 and CD90, are not involved in cancer stemness. *Anat Cell Biol* 48: 44–53.  
<http://www.ncbi.nlm.nih.gov/pubmed/25806121>
28. Yanagisawa M, Yoshimura S, Yu RK (2011) Expression of GD2 and GD3 gangliosides in human embryonic neural stem cells. *ASN Neuro* 3. <http://www.ncbi.nlm.nih.gov/pubmed/21395555>
29. National Cancer Institute (US) (2002) PDQ Cancer Information Summaries: Neuroblastoma Treatment (PDQ®): Patient Version, Bethesda (MD).
30. Yu AL, Gilman AL, Ozkaynak MF, London WB, Kreissman SG, et al. (2010) Anti-GD2 antibody with GM-CSF, interleukin-2, and isotretinoin for neuroblastoma. *N Engl J Med* 363: 1324–1334.  
<http://www.ncbi.nlm.nih.gov/pubmed/20879881>
31. Committee for Medicinal Products for Human Use (23th 2017) Assessment report: Dinutuximab beta Apeiron.

32. Ladenstein R, Pötschger U, Valteau-Couanet D, Luksch R, Castel V, et al. (2018) Interleukin 2 with anti-GD2 antibody ch14.18/CHO (dinutuximab beta) in patients with high-risk neuroblastoma (HR-NBL1/SIOPEN): a multicentre, randomised, phase 3 trial. *Lancet Oncol* 19: 1617–1629. <http://www.ncbi.nlm.nih.gov/pubmed/30442501>
33. Sorkin LS, Otto M, Baldwin WM, Vail E, Gillies SD, et al. (2010) Anti-GD(2) with an FC point mutation reduces complement fixation and decreases antibody-induced allodynia. *Pain* 149: 135–142. <http://www.ncbi.nlm.nih.gov/pubmed/20171010>
34. Schumacher-Kuckelkorn R, Volland R, Gradehandt A, Hero B, Simon T, et al. (2017) Lack of immunocytological GD2 expression on neuroblastoma cells in bone marrow at diagnosis, during treatment, and at recurrence. *Pediatric blood & cancer* 64. <http://www.ncbi.nlm.nih.gov/pubmed/27654028>
35. Alberts B, Johnson A, Lewis J, et al. (ed) (2002) *Molecular Biology of the Cell: The Adaptive Immune System*. Chapter 24. (4th edition), Garland Science, New York.
36. Cushley W, Coupar BE, Mickelson CA, Williamson AR (1982) A common mechanism for the synthesis of membrane and secreted immunoglobulin alpha, gamma and mu chains. *Nature* 298: 77–79. <http://www.ncbi.nlm.nih.gov/pubmed/6806665>
37. Schroeder HW, Cavacini L (2010) Structure and function of immunoglobulins. *J Allergy Clin Immunol* 125: S41–52. <http://www.ncbi.nlm.nih.gov/pubmed/20176268>
38. Janeway CA Jr, Travers P, Walport M, et al. (ed) (2001) *Immunobiology: The structure of a typical antibody molecule*. (5th edition), Garland Science, New York.
39. Arnold JN, Wormald MR, Sim RB, Rudd PM, Dwek RA (2007) The impact of glycosylation on the biological function and structure of human immunoglobulins. *Annu Rev Immunol* 25: 21–50. <http://www.ncbi.nlm.nih.gov/pubmed/17029568>
40. Smith KA, Nelson PN, Warren P, Astley SJ, Murray PG, et al. (2004) Demystified...recombinant antibodies. *J Clin Pathol* 57: 912–917. <http://www.ncbi.nlm.nih.gov/pubmed/15333649>
41. Duarte JH (2016) Functional switching. *Nat Immunol* 17: S12–S12. <https://doi.org/10.1038/ni.3607>
42. Dorrington KJ, Bennich HH (1978) Structure-function relationships in human immunoglobulin E. *Immunol Rev* 41: 3–25. <http://www.ncbi.nlm.nih.gov/pubmed/100912>
43. Baudino L, Nimmerjahn F, Shinohara Y, Furukawa J-I, Petry F, et al. (2008) Impact of a three amino acid deletion in the CH2 domain of murine IgG1 on Fc-associated effector functions. *J Immunol* 181: 4107–4112. <http://www.ncbi.nlm.nih.gov/pubmed/18768867>
44. Jefferis R, Lund J (2002) Interaction sites on human IgG-Fc for FcγR: current models. *Immunol Lett* 82: 57–65. <http://www.ncbi.nlm.nih.gov/pubmed/12008035>
45. Mimura Y, Sondermann P, Ghirlando R, Lund J, Young SP, et al. (2001) Role of oligosaccharide residues of IgG1-Fc in FcγRIIb binding. *J Biol Chem* 276: 45539–45547. <http://www.ncbi.nlm.nih.gov/pubmed/11567028>
46. Deng X, Liu X, Zhang Y, Ke D, Yan R, et al. (2023) Changes of serum IgG glycosylation patterns in rheumatoid arthritis. *Clin Proteomics* 20: 7. <http://www.ncbi.nlm.nih.gov/pubmed/36810000>
47. Forthall DN (2014) Functions of Antibodies. *Microbiol Spectr* 2: 1–17. <http://www.ncbi.nlm.nih.gov/pubmed/25215264>
48. Janeway CA Jr, Travers P, Walport M, et al. (2001) *Immunobiology: The immune system in health and disease*. (5th edition), Garland Science, New York.
49. Horton RE, Vidarsson G (2013) Antibodies and their receptors: different potential roles in mucosal defense. *Front Immunol* 4: 200. <http://www.ncbi.nlm.nih.gov/pubmed/23882268>

## 10 References

---

50. Shields RL, Lai J, Keck R, O'Connell LY, Hong K, et al. (2002) Lack of fucose on human IgG1 N-linked oligosaccharide improves binding to human FcγRIII and antibody-dependent cellular toxicity. *J Biol Chem* 277: 26733–26740. <http://www.ncbi.nlm.nih.gov/pubmed/11986321>
51. Natsume A, In M, Takamura H, Nakagawa T, Shimizu Y, et al. (2008) Engineered antibodies of IgG1/IgG3 mixed isotype with enhanced cytotoxic activities. *Cancer Res* 68: 3863–3872. <http://www.ncbi.nlm.nih.gov/pubmed/18483271>
52. Shields RL, Namenuk AK, Hong K, Meng YG, Rae J, et al. (2001) High resolution mapping of the binding site on human IgG1 for FcγRI, FcγRII, FcγRIII, and FcRn and design of IgG1 variants with improved binding to the FcγR. *J Biol Chem* 276: 6591–6604. <http://www.ncbi.nlm.nih.gov/pubmed/11096108>
53. Jong RN de, Beurskens FJ, Verploegen S, Strumane K, van Kampen MD, et al. (2016) A Novel Platform for the Potentiation of Therapeutic Antibodies Based on Antigen-Dependent Formation of IgG Hexamers at the Cell Surface. *PLoS Biol* 14: e1002344. <http://www.ncbi.nlm.nih.gov/pubmed/26736041>
54. Peipp M, van Lammerts Bueren JJ, Schneider-Merck T, Bleeker WWK, Dechant M, et al. (2008) Antibody fucosylation differentially impacts cytotoxicity mediated by NK and PMN effector cells. *Blood* 112: 2390–2399. <http://www.ncbi.nlm.nih.gov/pubmed/18566325>
55. Okazaki A, Shoji-Hosaka E, Nakamura K, Wakitani M, Uchida K, et al. (2004) Fucose depletion from human IgG1 oligosaccharide enhances binding enthalpy and association rate between IgG1 and FcγRIIIa. *J Mol Biol* 336: 1239–1249. <http://www.ncbi.nlm.nih.gov/pubmed/15037082>
56. Gagez A-L, Cartron G (2014) Obinutuzumab: a new class of anti-CD20 monoclonal antibody. *Curr Opin Oncol* 26: 484–491. <http://www.ncbi.nlm.nih.gov/pubmed/25014645>
57. Marcus R, Davies A, Ando K, Klapper W, Opat S, et al. (2017) Obinutuzumab for the First-Line Treatment of Follicular Lymphoma. *N Engl J Med* 377: 1331–1344. <http://www.ncbi.nlm.nih.gov/pubmed/28976863>
58. Tao MH, Morrison SL (1989) Studies of aglycosylated chimeric mouse-human IgG. Role of carbohydrate in the structure and effector functions mediated by the human IgG constant region. *J Immunol* 143: 2595–2601. <http://www.ncbi.nlm.nih.gov/pubmed/2507634>
59. Geisberger R, Lamers M, Achatz G (2006) The riddle of the dual expression of IgM and IgD. *Immunology* 118: 429–437. <http://www.ncbi.nlm.nih.gov/pubmed/16895553>
60. Chen K, Xu W, Wilson M, He B, Miller NW, et al. (2009) Immunoglobulin D enhances immune surveillance by activating antimicrobial, proinflammatory and B cell-stimulating programs in basophils. *Nat Immunol* 10: 889–898. <http://www.ncbi.nlm.nih.gov/pubmed/19561614>
61. Boes M (2000) Role of natural and immune IgM antibodies in immune responses. *Mol Immunol* 37: 1141–1149. <http://www.ncbi.nlm.nih.gov/pubmed/11451419>
62. Vidarsson G, Dekkers G, Rispens T (2014) IgG subclasses and allotypes: from structure to effector functions. *Front Immunol* 5: 520. <http://www.ncbi.nlm.nih.gov/pubmed/25368619>
63. Delacroix DL, Dive C, Rambaud JC, Vaerman JP (1982) IgA subclasses in various secretions and in serum. *Immunology* 47: 383–385. <http://www.ncbi.nlm.nih.gov/pubmed/7118169>
64. Underdown BJ, Schiff JM (1986) Immunoglobulin A: strategic defense initiative at the mucosal surface. *Annu Rev Immunol* 4: 389–417. <http://www.ncbi.nlm.nih.gov/pubmed/3518747>
65. Sutton BJ, Davies AM, Bax HJ, Karagiannis SN (2019) IgE Antibodies: From Structure to Function and Clinical Translation. *Antibodies (Basel)* 8. <http://www.ncbi.nlm.nih.gov/pubmed/31544825>
66. Esfahani K, Roudaia L, Buhlaiga N, Del Rincon SV, Papneja N, et al. (2020) A review of cancer immunotherapy: from the past, to the present, to the future. *Curr Oncol* 27: S87-S97. <http://www.ncbi.nlm.nih.gov/pubmed/32368178>

## 10 References

---

67. The Royal Swedish Academy of Sciences (2018) The Nobel Prize in Physiology or Medicine 2018 was awarded jointly to James P. Allison and Tasuku Honjo "for their discovery of cancer The Nobel Prize in Physiology or Medicine 2018 was awarded jointly to James P. Allison and Tasuku Honjo "for their discovery of cancer therapy by inhibition of negative immune regulation": The Nobel Prize in Physiology or Medicine 2018. <https://www.nobelprize.org/prizes/medicine/2018/summary/> Accessed 29th August 2023.
68. Seidel JA, Otsuka A, Kabashima K (2018) Anti-PD-1 and Anti-CTLA-4 Therapies in Cancer: Mechanisms of Action, Efficacy, and Limitations. *Front Oncol* 8: 86. <http://www.ncbi.nlm.nih.gov/pubmed/29644214>
69. Giogen Idec Inc. (18th 2006) Chimeric anti-CD20 antibody, rituxan, for use in the treatment of chronic lymphocytic leukemia, San Diego.
70. Viani GA, Afonso SL, Stefano EJ, Fendi LI de, Soares FV (2007) Adjuvant trastuzumab in the treatment of her-2-positive early breast cancer: a meta-analysis of published randomized trials. *BMC Cancer* 7: 153. <http://www.ncbi.nlm.nih.gov/pubmed/17686164>
71. Syn NL, Teng MWL, Mok TSK, Soo RA (2017) De-novo and acquired resistance to immune checkpoint targeting. *Lancet Oncol* 18: e731-e741. <http://www.ncbi.nlm.nih.gov/pubmed/29208439>
72. Daniotti JL, Vilcaes AA, Torres Demichelis V, Ruggiero FM, Rodriguez-Walker M (2013) Glycosylation of glycolipids in cancer: basis for development of novel therapeutic approaches. *Front Oncol* 3: 306. <http://www.ncbi.nlm.nih.gov/pubmed/24392350>
73. Sipione S, Monyror J, Galleguillos D, Steinberg N, Kadam V (2020) Gangliosides in the Brain: Physiology, Pathophysiology and Therapeutic Applications. *Front Neurosci* 14: 572965. <http://www.ncbi.nlm.nih.gov/pubmed/33117120>
74. Fleurence J, Fougeray S, Bahri M, Cochonneau D, Clémenceau B, et al. (2017) Targeting O-Acetyl-GD2 Ganglioside for Cancer Immunotherapy. *J Immunol Res* 2017: 5604891. <http://www.ncbi.nlm.nih.gov/pubmed/28154831>
75. Groux-Degroote S, Guérardel Y, Delannoy P (2017) Gangliosides: Structures, Biosynthesis, Analysis, and Roles in Cancer. *Chembiochem* 18: 1146–1154. <http://www.ncbi.nlm.nih.gov/pubmed/28295942>
76. Groux-Degroote S, Rodríguez-Walker M, Dewald JH, Daniotti JL, Delannoy P (2018) Gangliosides in Cancer Cell Signaling. *Prog Mol Biol Transl Sci* 156: 197–227. <http://www.ncbi.nlm.nih.gov/pubmed/29747814>
77. Yamashita T, Wada R, Sasaki T, Deng C, Bierfreund U, et al. (1999) A vital role for glycosphingolipid synthesis during development and differentiation. *Proc Natl Acad Sci U S A* 96: 9142–9147. <http://www.ncbi.nlm.nih.gov/pubmed/10430909>
78. Svennerholm L (1980) Gangliosides and synaptic transmission. *Adv Exp Med Biol* 125: 533–544. <http://www.ncbi.nlm.nih.gov/pubmed/6244726>
79. Kracun I, Rosner H, Drnovsek V, Vukelic Z, Cosovic C, et al. (1992) Gangliosides in the human brain development and aging. *Neurochem Int* 20: 421–431. <http://www.ncbi.nlm.nih.gov/pubmed/1304337>
80. Sorice M, Parolini I, Sansolini T, Garofalo T, Dolo V, et al. (1997) Evidence for the existence of ganglioside-enriched plasma membrane domains in human peripheral lymphocytes. *J Lipid Res* 38: 969–980. <http://www.ncbi.nlm.nih.gov/pubmed/9186914>
81. Nazha B, Inal C, Owonikoko TK (2020) Disialoganglioside GD2 Expression in Solid Tumors and Role as a Target for Cancer Therapy. *Front Oncol* 10: 1000. <http://www.ncbi.nlm.nih.gov/pubmed/32733795>
82. Svennerholm L (1980) Ganglioside designation. *Adv Exp Med Biol* 125: 11. <http://www.ncbi.nlm.nih.gov/pubmed/7361610>

## 10 References

---

83. Suzuki A (2006) Genetic basis for the lack of N-glycolylneuraminic acid expression in human tissues and its implication to human evolution. *Proc Jpn Acad Ser B Phys Biol Sci* 82: 93–103. <http://www.ncbi.nlm.nih.gov/pubmed/25873750>
84. Varki A (1992) Diversity in the sialic acids. *Glycobiology* 2: 25–40. <http://www.ncbi.nlm.nih.gov/pubmed/1550987>
85. Bardor M, Nguyen DH, Diaz S, Varki A (2005) Mechanism of uptake and incorporation of the non-human sialic acid N-glycolylneuraminic acid into human cells. *J Biol Chem* 280: 4228–4237. <http://www.ncbi.nlm.nih.gov/pubmed/15557321>
86. Inokuchi J-I, Inamori K-I, Kabayama K, Nagafuku M, Uemura S, et al. (2018) Biology of GM3 Ganglioside. *Prog Mol Biol Transl Sci* 156: 151–195. <http://www.ncbi.nlm.nih.gov/pubmed/29747813>
87. Aureli M, Samarani M, Murdica V, Mauri L, Loberto N, et al. (2014) Gangliosides and cell surface ganglioside glycohydrolases in the nervous system. *Adv Neurobiol* 9: 223–244. <http://www.ncbi.nlm.nih.gov/pubmed/25151381>
88. William W. Christie (2009) Gangliosides: Structure, Occurrence, Biology and Analysis. <https://web.archive.org/web/20091217095434/http://lipidlibrary.aocs.org/Lipids/gang/index.htm> Accessed 15th July, 2023.
89. Krengel U, Bousquet PA (2014) Molecular recognition of gangliosides and their potential for cancer immunotherapies. *Front Immunol* 5: 325. <http://www.ncbi.nlm.nih.gov/pubmed/25101077>
90. Schulz G, Cheresch DA, Varki NM, Yu A, Staffileno LK, et al. (1984) Detection of ganglioside GD2 in tumor tissues and sera of neuroblastoma patients. *Cancer Res* 44: 5914–5920. <http://www.ncbi.nlm.nih.gov/pubmed/6498849>
91. Furukawa K, Hamamura K, Aixinjueluo W, Furukawa K (2006) Biosignals modulated by tumor-associated carbohydrate antigens: novel targets for cancer therapy. *Ann N Y Acad Sci* 1086: 185–198. <http://www.ncbi.nlm.nih.gov/pubmed/17185516>
92. Hettmer S, Ladisch S, Kaucic K (2005) Low complex ganglioside expression characterizes human neuroblastoma cell lines. *Cancer Lett* 225: 141–149. <http://www.ncbi.nlm.nih.gov/pubmed/15922866>
93. Valentino L, Moss T, Olson E, Wang HJ, Elashoff R, et al. (1990) Shed tumor gangliosides and progression of human neuroblastoma. *Blood* 75: 1564–1567. <http://www.ncbi.nlm.nih.gov/pubmed/2317562>
94. Labrada M, Dorvignit D, Hevia G, Rodríguez-Zhurbenko N, Hernández AM, et al. (2018) GM3(Neu5Gc) ganglioside: an evolution fixed neoantigen for cancer immunotherapy. *Semin Oncol* 45: 41–51. <http://www.ncbi.nlm.nih.gov/pubmed/30318083>
95. Blanco R, Quintana Y, Blanco D, Cedeño M, Rengifo CE, et al. (2013) Tissue Reactivity of the 14F7 Mab Raised against N-Glycolyl GM3 Ganglioside in Tumors of Neuroectodermal, Mesodermal, and Epithelial Origin. *J Biomark* 2013: 602417. <http://www.ncbi.nlm.nih.gov/pubmed/26317019>
96. Zhang X, Kiechle FL (2004) Review: Glycosphingolipids in health and disease. *Ann Clin Lab Sci* 34: 3–13. <http://www.ncbi.nlm.nih.gov/pubmed/15038664>
97. Fernández-Pérez EJ, Sepúlveda FJ, Peoples R, Aguayo LG (2017) Role of membrane GM1 on early neuronal membrane actions of A $\beta$  during onset of Alzheimer's disease. *Biochim Biophys Acta Mol Basis Dis* 1863: 3105–3116. <http://www.ncbi.nlm.nih.gov/pubmed/28844949>
98. Ollert MW, David K, Schmitt C, Hauenschild A, Bredehorst R, et al. (1996) Normal human serum contains a natural IgM antibody cytotoxic for human neuroblastoma cells. *Proc Natl Acad Sci U S A* 93: 4498–4503. <http://www.ncbi.nlm.nih.gov/pubmed/8633097>
99. Erttmann R, Schmitt C, Ollert MW, David K, Bredehorst R, et al. (1996) Naturally occurring humoral cytotoxicity against neuroblastoma (NB) cells in healthy persons and NB patients. *Pediatr Hematol Oncol* 13: 545–548. <http://www.ncbi.nlm.nih.gov/pubmed/8940738>

## 10 References

---

100. Jones PC, Irie RF (2016) Therapeutic Strategies for Human IgM Antibodies Directed at Tumor-Associated Ganglioside Antigens: Discoveries Made During the Morton Era and Future Directions. *Crit Rev Oncog* 21: 75–81. <http://www.ncbi.nlm.nih.gov/pubmed/27481004>
101. Ruan S, Raj BK, Lloyd KO (1999) Relationship of glycosyltransferases and mRNA levels to ganglioside expression in neuroblastoma and melanoma cells. *J Neurochem* 72: 514–521. <http://www.ncbi.nlm.nih.gov/pubmed/9930722>
102. Ruan S, Lloyd KO (1992) Glycosylation Pathways in the Biosynthesis of Gangliosides in Melanoma and Neuroblastoma Cells: Relative Glycosyltransferase Levels Determine Ganglioside Patterns. *Cancer Res* 52: 5725–5731.
103. Nakamura K, Koike M, Shitara K, Kuwana Y, Kiuragi K, et al. (1994) Chimeric Anti-Ganglioside GM2 Antibody with Antitumor Activity. *Cancer Res* 54: 1511–1516.
104. Yamaguchi H, Furukawa K, Fortunato SR, Livingston PO, Lloyd KO, et al. (1990) Human monoclonal antibody with dual GM2/GD2 specificity derived from an immunized melanoma patient. *Proc Natl Acad Sci U S A* 87: 3333–3337. <http://www.ncbi.nlm.nih.gov/pubmed/2159145>
105. Erttmann R (2008) Treatment of neuroblastoma with human natural antibodies. *Autoimmun Rev* 7: 496–500. <http://www.ncbi.nlm.nih.gov/pubmed/18558369>
106. Simon T, Hero B, Schulte JH, Deubzer H, Hundsdoerfer P, et al. (2017) 2017 GPOH Empfehlungen für Diagnostik und Therapie von Patienten mit neuroblastischen Tumoren (2017 GPOH Guidelines for Diagnosis and Treatment of Patients with Neuroblastic Tumors). *Klin Padiatr* 229: 147–167. <http://www.ncbi.nlm.nih.gov/pubmed/28561228>
107. Brinkman EK, Chen T, Amendola M, van Steensel B (2014) Easy quantitative assessment of genome editing by sequence trace decomposition. *Nucleic Acids Res* 42: e168. <http://www.ncbi.nlm.nih.gov/pubmed/25300484>
108. EMBL-EBI (2022) Clustal Omega: Search and sequence analysis tools services from EMBL-EBI in 2022, European Molecular Biology Laboratory.
109. Madeira F, Pearce M, Tivey ARN, Basutkar P, Lee J, et al. (2022) Search and sequence analysis tools services from EMBL-EBI in 2022. *Nucleic Acids Res* 50: W276–W279. <http://www.ncbi.nlm.nih.gov/pubmed/35412617>
110. Bio-Rad Laboratories I HuCAL Antibodies Technical Manual: HuCAL Technology. <https://www.bio-rad-antibodies.com/hucal-technical-manual.html> Accessed 21st July, 2023.
111. Ostendorp R, Frisch C, Urban M (2004) Generation, Engineering and Production of Human Antibodies Using Hucal®. In: Subramanian G (ed). *Antibodies, Volume 2: Novel Technologies and Therapeutic Use*, 1st ed. Springer, Boston, pp 13–52.
112. Knappik A, Ge L, Honegger A, Pack P, Fischer M, et al. (2000) Fully synthetic human combinatorial antibody libraries (HuCAL) based on modular consensus frameworks and CDRs randomized with trinucleotides. *J Mol Biol* 296: 57–86. <http://www.ncbi.nlm.nih.gov/pubmed/10656818>
113. Nishinaka Y, Ravindranath MH, Irie RF (1996) Development of a Human Monoclonal Antibody to Ganglioside GM2 with Potential for Cancer Treatment. *Cancer Res* 56: 5666–5671.
114. Shitara K, Fujiwara K, Igarashi S, Ohta S, Furuya A, et al. (1994) Immunoglobulin class switch of anti-ganglioside monoclonal antibody from IgM to IgG. *J Immunol Methods* 169: 83–92. <http://www.ncbi.nlm.nih.gov/pubmed/8133075>
115. Nakamura K, Tanaka Y, Fujino I, Hirayama N, Shitara K, et al. (2000) Dissection and optimization of immune effector functions of humanized anti-ganglioside GM2 monoclonal antibody. *Mol Immunol* 37: 1035–1046. <http://www.ncbi.nlm.nih.gov/pubmed/11399321>

## 10 References

---

116. Shitara K, Niwa R, Natsume A (24th 2008) Genetically Recombinant Antibody Composition Capable of Binding Specifically to Ganglioside GM2(US 2011/0236374 A1).
117. Fernandes DM, Baird AM, Berg LJ, Rock KL (1999) A Monoclonal Antibody Reactive with a 40-kDa Molecule on Fetal Thymocytes and Tumor Cells Blocks Proliferation and Stimulates Aggregation and Apoptosis. *The Journal of Immunology* 163: 1306–1314. <https://doi.org/10.4049/jimmunol.163.3.1306>
118. Fanger GR, Fanger NA, King DJ, Retter MW, Rock KL (28th 2006) Antibodies to treat cancer(US 7,781,569 B2).
119. Retter MW, Johnson JC, Peckham DW, Bannink JE, Bangur CS, et al. (2005) Characterization of a proapoptotic antiganglioside GM2 monoclonal antibody and evaluation of its therapeutic effect on melanoma and small cell lung carcinoma xenografts. *Cancer Res* 65: 6425–6434. <http://www.ncbi.nlm.nih.gov/pubmed/16024647>
120. Abanades B, Wong WK, Boyles F, Georges G, Bujotzek A, et al. (2023) ImmuneBuilder: Deep-Learning models for predicting the structures of immune proteins. *Commun Biol* 6: 575. <http://www.ncbi.nlm.nih.gov/pubmed/37248282>
121. Abanades B, Wong WK, Boyles F, Bujotzek A, Deane CM (2023) The antibody prediction toolbox: ABodyBuilder2. <https://opig.stats.ox.ac.uk/webapps/sabdab-sabpred/sabpred/abodybuilder2/> Accessed 21st July, 2023.
122. Dunbar J, Krawczyk K, Leem J, Marks C, Nowak J, et al. (2016) SAbPred: a structure-based antibody prediction server. *Nucleic Acids Res* 44: W474-8. <http://www.ncbi.nlm.nih.gov/pubmed/27131379>
123. Sasaki N, Hirabayashi K, Michishita M, Takahashi K, Hasegawa F, et al. (2019) Ganglioside GM2, highly expressed in the MIA PaCa-2 pancreatic ductal adenocarcinoma cell line, is correlated with growth, invasion, and advanced stage. *Sci Rep* 9: 19369. <http://www.ncbi.nlm.nih.gov/pubmed/31852956>
124. Suzuki M, Cheung N-KV (2015) Disialoganglioside GD2 as a therapeutic target for human diseases. *Expert Opin Ther Targets* 19: 349–362. <http://www.ncbi.nlm.nih.gov/pubmed/25604432>
125. Gillies SD (11th 2009) Anti-cancer antibodies with reduced complement fixation, USA.
126. Schaber B, Bruchelt G, Meyle J, Jeschke B, Handgretinger R, et al. (1994) Chemotactic activity of substances derived from antibody-loaded tumor cells on granulocytes. *Immunol Lett* 41: 67–71. <http://www.ncbi.nlm.nih.gov/pubmed/7959905>
127. Mayer P, Handgretinger R, Bruchelt G, Schaber B, Rassner G, et al. (1994) Activation of cellular cytotoxicity and complement-mediated lysis of melanoma and neuroblastoma cells in vitro by murine antiganglioside antibodies MB 3.6 and 14.G2a. *Melanoma Research* 4: 101.
128. Mabe NW, Huang M, Dalton GN, Alexe G, Schaefer DA, et al. (2022) Transition to a mesenchymal state in neuroblastoma confers resistance to anti-GD2 antibody via reduced expression of ST8SIA1. *Nat Cancer* 3: 976–993. <http://www.ncbi.nlm.nih.gov/pubmed/35817829>
129. Hunczek A (2012) Die Bedeutung humaner anti-Gangliosid-Antikörper für die Immuntherapie des Neuroblastoms, Tübingen.
130. Uhlén M, Fagerberg L, Hallström BM, Lindskog C, Oksvold P, et al. (2015) Proteomics. Tissue-based map of the human proteome. *Science* 347: 1260419. <http://www.ncbi.nlm.nih.gov/pubmed/25613900>
131. Pontén F, Jirstrom K, Uhlen M (2008) The Human Protein Atlas--a tool for pathology. *J Pathol* 216: 387–393. <http://www.ncbi.nlm.nih.gov/pubmed/18853439>
132. Schengrund CL, Repman MA (1982) Density-dependent changes in gangliosides and sialidase activity of murine neuroblastoma cells. *J Neurochem* 39: 940–947. <http://www.ncbi.nlm.nih.gov/pubmed/7119793>

## 10 References

---

133. Wiebel M, Kailayangiri S, Altvater B, Meltzer J, Grobe K, et al. (2021) Surface expression of the immunotherapeutic target GD2 in osteosarcoma depends on cell confluency. *Cancer Rep (Hoboken)* 4: e1394. <http://www.ncbi.nlm.nih.gov/pubmed/33811471>
134. Yin J, Hashimoto A, Izawa M, Miyazaki K, Chen G-Y, et al. (2006) Hypoxic culture induces expression of sialin, a sialic acid transporter, and cancer-associated gangliosides containing non-human sialic acid on human cancer cells. *Cancer Res* 66: 2937–2945. <http://www.ncbi.nlm.nih.gov/pubmed/16540641>
135. Bousquet PA, Sandvik JA, Jeppesen Edin NF, Kregel U (2018) Hypothesis: Hypoxia induces de novo synthesis of NeuGc gangliosides in humans through CMAH domain substitute. *Biochem Biophys Res Commun* 495: 1562–1566. <http://www.ncbi.nlm.nih.gov/pubmed/29196263>
136. Okuda T (2019) Dietary Control of Ganglioside Expression in Mammalian Tissues. *Int J Mol Sci* 21. <http://www.ncbi.nlm.nih.gov/pubmed/31887977>
137. Trindade VM, Daniotti JL, Raimondi L, Chazan R, Netto CA, et al. (2001) Effects of neonatal hypoxia/ischemia on ganglioside expression in the rat hippocampus. *Neurochem Res* 26: 591–597. <http://www.ncbi.nlm.nih.gov/pubmed/11519719>
138. Miyake M, Ito M, Hitomi S, Ikeda S, Taki T, et al. (1988) Generation of two murine monoclonal antibodies that can discriminate N-glycolyl and N-acetyl neuraminic acid residues of GM2 gangliosides. *Cancer Res* 48: 6154–6160. <http://www.ncbi.nlm.nih.gov/pubmed/3167861>
139. Hara S, Takemori Y, Yamaguchi M, Nakamura M, Ohkura Y (1987) Fluorometric high-performance liquid chromatography of N-acetyl- and N-glycolylneuraminic acids and its application to their microdetermination in human and animal sera, glycoproteins, and glycolipids. *Anal Biochem* 164: 138–145. <http://www.ncbi.nlm.nih.gov/pubmed/3674364>
140. Heiskanen A, Satomaa T, Tiitinen S, Laitinen A, Mannelin S, et al. (2007) N-glycolylneuraminic acid xenoantigen contamination of human embryonic and mesenchymal stem cells is substantially reversible. *Stem Cells* 25: 197–202. <http://www.ncbi.nlm.nih.gov/pubmed/17008421>
141. Lee J, Hwang H, Kim S, Hwang J, Yoon J, et al. (2019) Comprehensive Profiling of Surface Gangliosides Extracted from Various Cell Lines by LC-MS/MS. *Cells* 8. <http://www.ncbi.nlm.nih.gov/pubmed/31717732>
142. Yu J, Wu X, Yan J, Yu H, Xu L, et al. (2018) Anti-GD2/4-1BB chimeric antigen receptor T cell therapy for the treatment of Chinese melanoma patients. *J Hematol Oncol* 11: 1. <http://www.ncbi.nlm.nih.gov/pubmed/29298689>
143. Tsuchida T, Saxton RE, Morton DL, Irie RF (1987) Gangliosides of human melanoma. *Journal of the National Cancer Institute* 78. <http://www.ncbi.nlm.nih.gov/pubmed/3467129>
144. Kailayangiri S, Altvater B, Meltzer J, Pscherer S, Luecke A, et al. (2012) The ganglioside antigen G(D2) is surface-expressed in Ewing sarcoma and allows for MHC-independent immune targeting. *Br J Cancer* 106: 1123–1133. <http://www.ncbi.nlm.nih.gov/pubmed/22374462>
145. Yoshida S, Fukumoto S, Kawaguchi H, Sato S, Ueda R, et al. (2001) Ganglioside G(D2) in small cell lung cancer cell lines: enhancement of cell proliferation and mediation of apoptosis. *Cancer Res* 61: 4244–4252. <http://www.ncbi.nlm.nih.gov/pubmed/11358851>
146. Nguyen K, Yan Y, Yuan B, Dasgupta A, Sun J, et al. (2018) ST8SIA1 Regulates Tumor Growth and Metastasis in TNBC by Activating the FAK-AKT-mTOR Signaling Pathway. *Mol Cancer Ther* 17: 2689–2701. <http://www.ncbi.nlm.nih.gov/pubmed/30237308>
147. Zhang P, Ohkawa Y, Yamamoto S, Momota H, Kato A, et al. (2021) St8sia1-deficiency in mice alters tumor environments of gliomas, leading to reduced disease severity. *Nagoya J Med Sci* 83: 535–549. <http://www.ncbi.nlm.nih.gov/pubmed/34552288>

## 10 References

---

148. Paret C, Ustjanzew A, Ersali S, Seidmann L, Jennemann R, et al. (2022) GD2 Expression in Medulloblastoma and Neuroblastoma for Personalized Immunotherapy: A Matter of Subtype. *Cancers (Basel)* 14. <http://www.ncbi.nlm.nih.gov/pubmed/36551537>
149. Hedlund M, Padler-Karavani V, Varki NM, Varki A (2008) Evidence for a human-specific mechanism for diet and antibody-mediated inflammation in carcinoma progression. *Proc Natl Acad Sci U S A* 105: 18936–18941. <http://www.ncbi.nlm.nih.gov/pubmed/19017806>
150. Thirant C, Peltier A, Durand S, Kramdi A, Louis-Brennetot C, et al. (2023) Reversible transitions between noradrenergic and mesenchymal tumor identities define cell plasticity in neuroblastoma. *Nat Commun* 14: 2575. <http://www.ncbi.nlm.nih.gov/pubmed/37142597>
151. Gautier M, Thirant C, Delattre O, Janoueix-Lerosey I (2021) Plasticity in Neuroblastoma Cell Identity Defines a Noradrenergic-to-Mesenchymal Transition (NMT). *Cancers (Basel)* 13. <http://www.ncbi.nlm.nih.gov/pubmed/34200747>
152. Mc Nerney KO, Karageorgos S, Ferry GM, Wolpaw AJ, Burudpakdee C, et al. (2022) TH-MYCN tumors, but not tumor-derived cell lines, are adrenergic lineage, GD2+, and responsive to anti-GD2 antibody therapy. *Oncoimmunology* 11: 2075204. <http://www.ncbi.nlm.nih.gov/pubmed/35646475>
153. Liang Y-J, Ding Y, Lavery SB, Lobaton M, Handa K, et al. (2013) Differential expression profiles of glycosphingolipids in human breast cancer stem cells vs. cancer non-stem cells. *Proc Natl Acad Sci U S A* 110: 4968–4973. <http://www.ncbi.nlm.nih.gov/pubmed/23479608>
154. Shishido F, Uemura S, Kashimura M, Inokuchi J-I (2017) Identification of a new B4GalNAcT1 (GM2/GD2/GA2 synthase) isoform, and regulation of enzyme stability and intracellular transport by arginine-based motif. *Biochim Biophys Acta Biomembr* 1859: 2001–2011. <http://www.ncbi.nlm.nih.gov/pubmed/28709807>
155. Hettmer S, McCarter R, Ladisch S, Kaucic K (2004) Alterations in neuroblastoma ganglioside synthesis by induction of GD1b synthase by retinoic acid. *Br J Cancer* 91: 389–397. <http://www.ncbi.nlm.nih.gov/pubmed/15187999>
156. Bork K, Weidemann W, Berneck B, Kuchta M, Bennmann D, et al. (2017) The expression of sialyltransferases is regulated by the bioavailability and biosynthesis of sialic acids. *Gene Expr Patterns* 23-24: 52–58. <http://www.ncbi.nlm.nih.gov/pubmed/28351515>
157. Liu X-Y, Chen Y-L, Liu G-J, Deng X-N, Cui Y, et al. (2022) Development of a variant of dinutuximab with enhanced antitumor efficacy and reduced induction of neuropathic pain. *FEBS Open Bio* 12: 1644–1656. <http://www.ncbi.nlm.nih.gov/pubmed/35792784>
158. Tai T, Paulson JC, Cahan LD, Irie RF (1983) Ganglioside GM2 as a human tumor antigen (OFA-I-1). *Proc Natl Acad Sci U S A* 80: 5392–5396. <http://www.ncbi.nlm.nih.gov/pubmed/6193515>
159. Maria Yiallourous (2011) Häufigkeit: Wie oft kommt ein Neuroblastom vor? [https://www.gpoh.de/kinderkrebsinfo/content/erkrankungen/weitere\\_solide\\_tumoren/pohneuroblpatinfo120120611/allgemeine\\_informationen/haeufigkeit/index\\_ger.html](https://www.gpoh.de/kinderkrebsinfo/content/erkrankungen/weitere_solide_tumoren/pohneuroblpatinfo120120611/allgemeine_informationen/haeufigkeit/index_ger.html) Accessed 17th September, 2023.
160. Barry JA, Gawrisch K (1995) Effects of ethanol on lipid bilayers containing cholesterol, gangliosides, and sphingomyelin. *Biochemistry* 34: 8852–8860. <http://www.ncbi.nlm.nih.gov/pubmed/7612626>
161. Mathew J, Klemm WR (1989) Differences in susceptibility of rat liver and brain sialidases to ethanol and gangliosides. *Pharmacol Biochem Behav* 33: 797–803. <http://www.ncbi.nlm.nih.gov/pubmed/2616598>
162. Attar A (2014) Changes in the Cell Surface Markers During Normal Hematopoiesis: A Guide to Cell Isolation. *G.J. Hematol. Blood Trans.* 1: 20–28. <https://doi.org/10.15379/2408-9877.2014.01.01.4>
163. Zhong X, Zhang Y, Wang L, Zhang H, Liu H, et al. (2019) Cellular components in tumor microenvironment of neuroblastoma and the prognostic value. *PeerJ* 7: e8017. <http://www.ncbi.nlm.nih.gov/pubmed/31844563>

## 10 References

---

164. Yu AL, Gilman AL, Ozkaynak MF, Naranjo A, Diccianni MB, et al. (2021) Long-Term Follow-up of a Phase III Study of ch14.18 (Dinutuximab) + Cytokine Immunotherapy in Children with High-Risk Neuroblastoma: COG Study ANBL0032. *Clin Cancer Res* 27: 2179–2189. <http://www.ncbi.nlm.nih.gov/pubmed/33504555>
165. Kailayangiri S, Altvater B, Lesch S, Balbach S, Göttlich C, et al. (2019) EZH2 Inhibition in Ewing Sarcoma Upregulates GD2 Expression for Targeting with Gene-Modified T Cells. *Mol Ther* 27: 933–946. <http://www.ncbi.nlm.nih.gov/pubmed/30879952>
166. Bosse KR, Raman P, Zhu Z, Lane M, Martinez D, et al. (2017) Identification of GPC2 as an Oncoprotein and Candidate Immunotherapeutic Target in High-Risk Neuroblastoma. *Cancer Cell* 32: 295-309.e12. <http://www.ncbi.nlm.nih.gov/pubmed/28898695>
167. Pulido R, Nunes-Xavier CE (2023) Hopes on immunotherapy targeting B7-H3 in neuroblastoma. *Transl Oncol* 27: 101580. <http://www.ncbi.nlm.nih.gov/pubmed/36327699>
168. Dodev TS, Karagiannis P, Gilbert AE, Josephs DH, Bowen H, et al. (2014) A tool kit for rapid cloning and expression of recombinant antibodies. *Sci Rep* 4: 5885. <http://www.ncbi.nlm.nih.gov/pubmed/25073855>
169. Yang Y, Li Z, Li Q, Ma K, Lin Y, et al. (2022) Increase recombinant antibody yields through optimizing vector design and production process in CHO cells. *Appl Microbiol Biotechnol* 106: 4963–4975. <http://www.ncbi.nlm.nih.gov/pubmed/35788878>
170. Li J, Menzel C, Meier D, Zhang C, Dübel S, et al. (2007) A comparative study of different vector designs for the mammalian expression of recombinant IgG antibodies. *J Immunol Methods* 318: 113–124. <http://www.ncbi.nlm.nih.gov/pubmed/17161420>
171. Chung HH, Buck L, Daris K, Welborn B, Luo Q, et al. (2018) Investigation of the free heavy chain homodimers of a monoclonal antibody. *Biotechnol Prog* 34: 738–745. <http://www.ncbi.nlm.nih.gov/pubmed/29341500>
172. Ho SCL, Koh EYC, van Beers M, Mueller M, Wan C, et al. (2013) Control of IgG LC:HC ratio in stably transfected CHO cells and study of the impact on expression, aggregation, glycosylation and conformational stability. *J Biotechnol* 165: 157–166. <http://www.ncbi.nlm.nih.gov/pubmed/23583871>
173. Toporova VA, Argentova VV, Aliev TK, Panina AA, Dolgikh DA, et al. (2023) Optimization of recombinant antibody production based on the vector design and the level of metabolites for generation of Ig-producing stable cell lines. *J Genet Eng Biotechnol* 21: 23. <http://www.ncbi.nlm.nih.gov/pubmed/36811683>
174. Rahimpour A, Bayat H, Omid M, Peyrovan M, Mohammadian O, et al. (2016) Stable Expression of Anti-CD52 Monoclonal Antibody Using a Bicistronic Vector System. *Biol Med (Aligarh)* 08. <https://doi.org/10.4172/0974-8369.1000341>
175. Fallot S, Ben Naya R, Hieblot C, Mondon P, Lacazette E, et al. (2009) Alternative-splicing-based bicistronic vectors for ratio-controlled protein expression and application to recombinant antibody production. *Nucleic Acids Res* 37: e134. <http://www.ncbi.nlm.nih.gov/pubmed/19729510>
176. Kunes YZ, Gion WR, Fung E, Salfeld JG, Zhu R-R, et al. (2009) Expression of antibodies using single-open reading frame vector design and polyprotein processing from mammalian cells. *Biotechnol Prog* 25: 735–744. <http://www.ncbi.nlm.nih.gov/pubmed/19363814>
177. Gion WR, Davis-Taber RA, Regier DA, Fung E, Medina L, et al. (2013) Expression of antibodies using single open reading frame (sORF) vector design: Demonstration of manufacturing feasibility. *MAbs* 5: 595–607. <http://www.ncbi.nlm.nih.gov/pubmed/23774760>

## 10 References

---

178. Kim DW, Uetsuki T, Kaziro Y, Yamaguchi N, Sugano S (1990) Use of the human elongation factor 1 alpha promoter as a versatile and efficient expression system. *Gene* 91: 217–223.  
<http://www.ncbi.nlm.nih.gov/pubmed/2210382>
179. Qin JY, Zhang L, Clift KL, Hulusi I, Xiang AP, et al. (2010) Systematic comparison of constitutive promoters and the doxycycline-inducible promoter. *PLoS One* 5: e10611.  
<http://www.ncbi.nlm.nih.gov/pubmed/20485554>
180. Frenzel A, Hust M, Schirrmann T (2013) Expression of recombinant antibodies. *Front Immunol* 4: 217.  
<http://www.ncbi.nlm.nih.gov/pubmed/23908655>
181. Chan CEZ, Lim APC, Chan AHY, MacAry PA, Hanson BJ (2010) Optimized expression of full-length IgG1 antibody in a common *E. coli* strain. *PLoS One* 5: e10261.  
<http://www.ncbi.nlm.nih.gov/pubmed/20422027>
182. Simmons LC, Reilly D, Klimowski L, Raju TS, Meng G, et al. (2002) Expression of full-length immunoglobulins in *Escherichia coli*: rapid and efficient production of aglycosylated antibodies. *J Immunol Methods* 263: 133–147. <http://www.ncbi.nlm.nih.gov/pubmed/12009210>
183. Backliwal G, Hildinger M, Kuettel I, Delegrange F, Hacker DL, et al. (2008) Valproic acid: a viable alternative to sodium butyrate for enhancing protein expression in mammalian cell cultures. *Biotechnol Bioeng* 101: 182–189. <http://www.ncbi.nlm.nih.gov/pubmed/18454496>
184. Chromikova V, Mader A, Steinfellner W, Kunert R (2015) Evaluating the bottlenecks of recombinant IgM production in mammalian cells. *Cytotechnology* 67: 343–356.  
<http://www.ncbi.nlm.nih.gov/pubmed/24615530>
185. Tchoudakova A, Hensel F, Murillo A, Eng B, Foley M, et al. (2009) High level expression of functional human IgMs in human PER.C6 cells. *MAbs* 1: 163–171.  
<http://www.ncbi.nlm.nih.gov/pubmed/20061826>
186. Sellick CA, Croxford AS, Maqsood AR, Stephens G, Westerhoff HV, et al. (2011) Metabolite profiling of recombinant CHO cells: designing tailored feeding regimes that enhance recombinant antibody production. *Biotechnol Bioeng* 108: 3025–3031. <http://www.ncbi.nlm.nih.gov/pubmed/21769861>
187. Garidel P, Eiperle A, Blech M, Seelig J (2020) Thermal and Chemical Unfolding of a Monoclonal IgG1 Antibody: Application of the Multistate Zimm-Bragg Theory. *Biophys J* 118: 1067–1075.  
<http://www.ncbi.nlm.nih.gov/pubmed/32049058>
188. Ionescu RM, Vlasak J, Price C, Kirchmeier M (2008) Contribution of variable domains to the stability of humanized IgG1 monoclonal antibodies. *J Pharm Sci* 97: 1414–1426.  
<http://www.ncbi.nlm.nih.gov/pubmed/17721938>
189. Ito T, Tsumoto K (2013) Effects of subclass change on the structural stability of chimeric, humanized, and human antibodies under thermal stress. *Protein Sci* 22: 1542–1551.  
<http://www.ncbi.nlm.nih.gov/pubmed/23963869>
190. Liu H, Bulseco G-G, Sun J (2006) Effect of posttranslational modifications on the thermal stability of a recombinant monoclonal antibody. *Immunol Lett* 106: 144–153.  
<http://www.ncbi.nlm.nih.gov/pubmed/16831470>
191. Hristodorov D, Fischer R, Joerissen H, Müller-Tiemann B, Apeler H, et al. (2013) Generation and comparative characterization of glycosylated and aglycosylated human IgG1 antibodies. *Mol Biotechnol* 53: 326–335. <http://www.ncbi.nlm.nih.gov/pubmed/22427250>
192. Kayser V, Chennamsetty N, Voynov V, Forrer K, Helk B, et al. (2011) Glycosylation influences on the aggregation propensity of therapeutic monoclonal antibodies. *Biotechnol J* 6: 38–44.  
<http://www.ncbi.nlm.nih.gov/pubmed/20949542>

## 10 References

---

193. Simons K, Toomre D (2000) Lipid rafts and signal transduction. *Nat Rev Mol Cell Biol* 1: 31–39. <http://www.ncbi.nlm.nih.gov/pubmed/11413487>
194. Simons K, Sampaio JL (2011) Membrane organization and lipid rafts. *Cold Spring Harb Perspect Biol* 3: a004697. <http://www.ncbi.nlm.nih.gov/pubmed/21628426>
195. Raju TS, Briggs JB, Borge SM, Jones AJ (2000) Species-specific variation in glycosylation of IgG: evidence for the species-specific sialylation and branch-specific galactosylation and importance for engineering recombinant glycoprotein therapeutics. *Glycobiology* 10: 477–486. <http://www.ncbi.nlm.nih.gov/pubmed/10764836>
196. Raju TS, Jordan RE (2012) Galactosylation variations in marketed therapeutic antibodies. *MAbs* 4: 385–391. <http://www.ncbi.nlm.nih.gov/pubmed/22531450>
197. The Royal Swedish Academy of Sciences (2018) The Nobel Prize in Chemistry 2018 was divided, one half awarded to Frances H. Arnold "for the directed evolution of enzymes", the other half jointly to George P. Smith and Sir Gregory P. Winter "for the phage display of peptides and antibodies": The Nobel Prize in Chemistry 2018. <https://www.nobelprize.org/prizes/chemistry/2018/summary/>. Accessed 28th July, 2023.
198. Frenzel A, Schirrmann T, Hust M (2016) Phage display-derived human antibodies in clinical development and therapy. *MAbs* 8: 1177–1194. <http://www.ncbi.nlm.nih.gov/pubmed/27416017>
199. Briney B, Inderbitzin A, Joyce C, Burton DR (2019) Commonality despite exceptional diversity in the baseline human antibody repertoire. *Nature* 566: 393–397. <http://www.ncbi.nlm.nih.gov/pubmed/30664748>
200. Schroeder HW (2006) Similarity and divergence in the development and expression of the mouse and human antibody repertoires. *Dev Comp Immunol* 30: 119–135. <http://www.ncbi.nlm.nih.gov/pubmed/16083957>
201. Clausen H, Wandall HH, DeLisa MP, Stanley P, Schnaar RL (2022) *Essentials of Glycobiology: Glycosylation Engineering*. (4th), Cold Spring Harbor (NY).
202. Jones ML, Alfaleh MA, Kumble S, Zhang S, Osborne GW, et al. (2016) Targeting membrane proteins for antibody discovery using phage display. *Sci Rep* 6: 26240. <http://www.ncbi.nlm.nih.gov/pubmed/27189586>
203. Barnidge DR, Dasari S, Ramirez-Alvarado M, Fontan A, Willrich MAV, et al. (2014) Phenotyping polyclonal kappa and lambda light chain molecular mass distributions in patient serum using mass spectrometry. *J Proteome Res* 13: 5198–5205. <http://www.ncbi.nlm.nih.gov/pubmed/25134970>
204. Xiao H, Guo T, Yang M, Qi J, Huang C, et al. (2019) Light chain modulates heavy chain conformation to change protection profile of monoclonal antibodies against influenza A viruses. *Cell Discov* 5: 21. <http://www.ncbi.nlm.nih.gov/pubmed/30993000>
205. Townsend CL, Laffy JMJ, Wu Y-CB, Silva O'Hare J, Martin V, et al. (2016) Significant Differences in Physicochemical Properties of Human Immunoglobulin Kappa and Lambda CDR3 Regions. *Front Immunol* 7: 388. <http://www.ncbi.nlm.nih.gov/pubmed/27729912>
206. Ponomarenko N, Chatziefthimiou SD, Kurkova I, Mokrushina Y, Stepanova A, et al. (2014) Role of  $\kappa \rightarrow \lambda$  light-chain constant-domain switch in the structure and functionality of A17 reactibody. *Acta Crystallogr D Biol Crystallogr* 70: 708–719. <http://www.ncbi.nlm.nih.gov/pubmed/24598740>
207. Irie RF, Sze LL, Saxton RE (1982) Human antibody to OFA-I, a tumor antigen, produced in vitro by Epstein-Barr virus-transformed human B-lymphoid cell lines. *Proc Natl Acad Sci U S A* 79: 5666–5670. <http://www.ncbi.nlm.nih.gov/pubmed/6291057>

## 10 References

---

208. Nishinaka Y, Hoon DS, Irie RF (1998) Human IgM antibodies to tumor-associated gangliosides share VHIII (V3-23) and VKIV family subgroups. *Immunogenetics* 48: 73–75. <http://www.ncbi.nlm.nih.gov/pubmed/9601948>
209. Patel K, Rossell RJ, Pemberton LF, Cheung NK, Walsh FS, et al. (1989) Monoclonal antibody 3F8 recognises the neural cell adhesion molecule (NCAM) in addition to the ganglioside GD2. *Br J Cancer* 60: 861–866. <http://www.ncbi.nlm.nih.gov/pubmed/2481486>
210. Itonori S, Hidari K, Sanai Y, Taniguchi M, Nagai Y (1989) Involvement of the acyl chain of ceramide in carbohydrate recognition by an anti-glycolipid monoclonal antibody: the case of an anti-melanoma antibody, M2590, to GM3-ganglioside. *Glycoconj J* 6: 551–560. <http://www.ncbi.nlm.nih.gov/pubmed/2535499>
211. Ząbczyńska M, Polak K, Kozłowska K, Sokołowski G, Pocheć E (2020) The Contribution of IgG Glycosylation to Antibody-Dependent Cell-Mediated Cytotoxicity (ADCC) and Complement-Dependent Cytotoxicity (CDC) in Hashimoto's Thyroiditis: An in Vitro Model of Thyroid Autoimmunity. *Biomolecules* 10. <http://www.ncbi.nlm.nih.gov/pubmed/31979029>
212. Mujoo K, Cheresch DA, Yang HM, Reisfeld RA (1987) Disialoganglioside GD2 on human neuroblastoma cells: target antigen for monoclonal antibody-mediated cytolysis and suppression of tumor growth. *Cancer Res* 47: 1098–1104. <http://www.ncbi.nlm.nih.gov/pubmed/3100030>
213. Yamada T, Bando H, Takeuchi S, Kita K, Li Q, et al. (2011) Genetically engineered humanized anti-ganglioside GM2 antibody against multiple organ metastasis produced by GM2-expressing small-cell lung cancer cells. *Cancer Sci* 102: 2157–2163. <http://www.ncbi.nlm.nih.gov/pubmed/21895875>
214. Chen RL, Reynolds CP, Seeger RC (2000) Neutrophils are cytotoxic and growth-inhibiting for neuroblastoma cells with an anti-GD2 antibody but, without cytotoxicity, can be growth-stimulating. *Cancer Immunol Immunother* 48: 603–612. <http://www.ncbi.nlm.nih.gov/pubmed/10663607>
215. Raju TS (2008) Terminal sugars of Fc glycans influence antibody effector functions of IgGs. *Curr Opin Immunol* 20: 471–478. <http://www.ncbi.nlm.nih.gov/pubmed/18606225>
216. Hodoniczky J, Zheng YZ, James DC (2005) Control of recombinant monoclonal antibody effector functions by Fc N-glycan remodeling in vitro. *Biotechnol Prog* 21: 1644–1652. <http://www.ncbi.nlm.nih.gov/pubmed/16321047>
217. Luo C, Chen S, Xu N, Wang C, Sai WB, et al. (2017) Glycoengineering of pertuzumab and its impact on the pharmacokinetic/pharmacodynamic properties. *Sci Rep* 7: 46347. <http://www.ncbi.nlm.nih.gov/pubmed/28397880>
218. Yu J, Song Y, Tian W (2020) How to select IgG subclasses in developing anti-tumor therapeutic antibodies. *J Hematol Oncol* 13: 45. <http://www.ncbi.nlm.nih.gov/pubmed/32370812>
219. Brüggemann M, Williams GT, Bindon CI, Clark MR, Walker MR, et al. (1987) Comparison of the effector functions of human immunoglobulins using a matched set of chimeric antibodies. *J Exp Med* 166: 1351–1361. <http://www.ncbi.nlm.nih.gov/pubmed/3500259>
220. Natsume A, Niwa R, Satoh M (2009) Improving effector functions of antibodies for cancer treatment: Enhancing ADCC and CDC. *Drug Des Devel Ther* 3: 7–16. <http://www.ncbi.nlm.nih.gov/pubmed/19920917>
221. Lua W-H, Ling W-L, Yeo JY, Poh J-J, Lane DP, et al. (2018) The effects of Antibody Engineering CH and CL in Trastuzumab and Pertuzumab recombinant models: Impact on antibody production and antigen-binding. *Sci Rep* 8: 718. <http://www.ncbi.nlm.nih.gov/pubmed/29335579>
222. Kendra K, Malkovska V, Allen M, Guzman J, Albertini M (1999) In vivo binding and antitumor activity of Ch14.18. *J Immunother* 22: 423–430. <http://www.ncbi.nlm.nih.gov/pubmed/10546158>

223. Martinez Sanz P, van Rees DJ, van Zogchel LMJ, Klein B, Bouti P, et al. (2021) G-CSF as a suitable alternative to GM-CSF to boost dinutuximab-mediated neutrophil cytotoxicity in neuroblastoma treatment. *J Immunother Cancer* 9. <http://www.ncbi.nlm.nih.gov/pubmed/34049929>
224. Barker E, Mueller BM, Handgretinger R, Herter M, Yu AL, et al. (1991) Effect of a chimeric anti-ganglioside GD2 antibody on cell-mediated lysis of human neuroblastoma cells. *Cancer Res* 51: 144–149. <http://www.ncbi.nlm.nih.gov/pubmed/1988079>
225. Nguyen R, Zhang X, Sun M, Abbas S, Seibert C, et al. (2022) Anti-GD2 antibodies conjugated to IL15 and IL21 mediate potent anti-tumor cytotoxicity against neuroblastoma. *Clin Cancer Res* 28: 3785–3796. <http://www.ncbi.nlm.nih.gov/pubmed/35802683>
226. Ishikawa F, Yasukawa M, Lyons B, Yoshida S, Miyamoto T, et al. (2005) Development of functional human blood and immune systems in NOD/SCID/IL2 receptor  $\gamma$  chainnull mice. *Blood* 106: 1565–1573. <http://www.ncbi.nlm.nih.gov/pubmed/15920010>
227. Nicolini FE, Cashman JD, Hogge DE, Humphries RK, Eaves CJ (2004) NOD/SCID mice engineered to express human IL-3, GM-CSF and Steel factor constitutively mobilize engrafted human progenitors and compromise human stem cell regeneration. *Leukemia* 18: 341–347. <http://www.ncbi.nlm.nih.gov/pubmed/14628073>
228. Shultz LD, Lyons BL, Burzenski LM, Gott B, Chen X, et al. (2005) Human lymphoid and myeloid cell development in NOD/LtSz-scid IL2R gamma null mice engrafted with mobilized human hemopoietic stem cells. *J Immunol* 174: 6477–6489. <http://www.ncbi.nlm.nih.gov/pubmed/15879151>
229. Morris KM, Aden DP, Knowles BB, Colten HR (1982) Complement biosynthesis by the human hepatoma-derived cell line HepG2. *J Clin Invest* 70: 906–913. <http://www.ncbi.nlm.nih.gov/pubmed/6288774>
230. Alper CA, Johnson AM, Birtch AG, Moore FD (1969) Human C'3: evidence for the liver as the primary site of synthesis. *Science* 163: 286–288. <http://www.ncbi.nlm.nih.gov/pubmed/4883617>
231. Botto M, Lissandrini D, Sorio C, Walport MJ (1992) Biosynthesis and secretion of complement component (C3) by activated human polymorphonuclear leukocytes. *J Immunol* 149: 1348–1355. <http://www.ncbi.nlm.nih.gov/pubmed/1500721>
232. Lipitsä T, Naukkarinen A, Laitala J, Harvima IT (2016) Complement C3 is expressed by mast cells in cutaneous vasculitis and is degraded by chymase. *Arch Dermatol Res* 308: 575–584. <http://www.ncbi.nlm.nih.gov/pubmed/27465068>
233. Lubbers R, van Essen MF, van Kooten C, Trouw LA (2017) Production of complement components by cells of the immune system. *Clin Exp Immunol* 188: 183–194. <http://www.ncbi.nlm.nih.gov/pubmed/28249350>
234. Blümich S, Zdimerova H, Münz C, Kipar A, Pellegrini G (2021) Human CD34+ Hematopoietic Stem Cell-Engrafted NSG Mice: Morphological and Immunophenotypic Features. *Vet Pathol* 58: 161–180. <http://www.ncbi.nlm.nih.gov/pubmed/32901581>
235. Verma MK, Clemens J, Burzenski L, Sampson SB, Brehm MA, et al. (2017) A novel hemolytic complement-sufficient NSG mouse model supports studies of complement-mediated antitumor activity in vivo. *J Immunol Methods* 446: 47–53. <http://www.ncbi.nlm.nih.gov/pubmed/28390927>
236. Li Q, Wang W, Machino Y, Yamada T, Kita K, et al. (2015) Therapeutic activity of glycoengineered anti-GM2 antibodies against malignant pleural mesothelioma. *Cancer Sci* 106: 102–107. <http://www.ncbi.nlm.nih.gov/pubmed/25421609>
237. Baz RC, Zonder JA, Gasparetto C, Reu FJ, Strout V (2016) Phase I Study of Anti-GM2 Ganglioside Monoclonal Antibody BIW-8962 as Monotherapy in Patients with Previously Treated Multiple Myeloma. *Oncol Ther* 4: 287–301. <http://www.ncbi.nlm.nih.gov/pubmed/28261656>

## 10 References

---

238. Amos Bairoch (2018) The Cellosaurus, a Cell-Line Knowledge Resource. *Journal of Biomolecular Techniques* : JBT 29: 25. <http://www.ncbi.nlm.nih.gov/pubmed/29805321>
239. Heckl D, Kowalczyk MS, Yudovich D, Belizaire R, Puram RV, et al. (2014) Generation of mouse models of myeloid malignancy with combinatorial genetic lesions using CRISPR-Cas9 genome editing. *Nat Biotechnol* 32: 941–946. <http://www.ncbi.nlm.nih.gov/pubmed/24952903>
240. Labuhn M, Adams FF, Ng M, Knoess S, Schambach A, et al. (2018) Refined sgRNA efficacy prediction improves large- and small-scale CRISPR-Cas9 applications. *Nucleic Acids Res* 46: 1375–1385. <http://www.ncbi.nlm.nih.gov/pubmed/29267886>
241. Stemmer M, Thumberger T, Del Sol Keyer M, Wittbrodt J, Mateo JL (2015) CCTop: An Intuitive, Flexible and Reliable CRISPR/Cas9 Target Prediction Tool. *PLoS One* 10: e0124633. <http://www.ncbi.nlm.nih.gov/pubmed/25909470>
242. Weber K, Bartsch U, Stocking C, Fehse B (2008) A multicolor panel of novel lentiviral "gene ontology" (LeGO) vectors for functional gene analysis. *Molecular therapy : the journal of the American Society of Gene Therapy* 16. <http://www.ncbi.nlm.nih.gov/pubmed/18362927>
243. Fehse B, Kustikova OS, Bubenheim M, Baum C (2004) Pois(s)on--it's a question of dose. *Gene Ther* 11: 879–881. <http://www.ncbi.nlm.nih.gov/pubmed/15057265>
244. EuroMabNet (1st 2023) Monoclonal Antibody Production Process: Transient transfection protocol for HEK293T cells. <https://www.euromabnet.com/protocols/transient-transfection-HEK293T-cells.php>
245. Kim S, Chen J, Cheng T, Gindulyte A, He J, et al. (2023) PubChem 2023 update. *Nucleic Acids Res* 51: D1373-D1380. <http://www.ncbi.nlm.nih.gov/pubmed/36305812>

## 11 List of figures

FIGURE 1: THE ILLUSTRATION ADAPTED FROM TAS <i>ET AL.</i> SHOWS THE KAPLAN-MEIER CURVES OF THE 5-YEAR OVERALL SURVIVAL OF NEUROBLASTOMA PATIENTS AT DIFFERENT STAGES IN THE NETHERLANDS BETWEEN 1990 AND 2014 [9].	5
FIGURE 2: STRUCTURAL COMPONENTS OF AN ANTIBODY AND DIFFERENT ANTIBODY ISOTYPES.	10
FIGURE 3: IN THE BIOSYNTHESIS PATHWAY OF GANGLIOSIDES, MONOSACCHARIDES AND SIALIC ACIDS ARE SUCCESSIVELY ADDED TO LACTOSYLCERAMIDE BY GLYCOSYLTRANSFERASES	15
FIGURE 4: GRAPHICAL SUMMARY OF THE OBJECTIVES ADDRESSED IN THIS WORK.	19
FIGURE 5: GANGLIOSIDES GM2 AND GD2 WERE EXPRESSED ON THE SURFACE OF NEUROBLASTOMA AND VARIOUS OTHER TUMOR CELL LINES.	21
FIGURE 6: NEUROBLASTOMA CELL LINES WITH A KNOCKOUT OF <i>B4GALNT1</i> WERE DEPLETED FROM GM2 AND GD2.	25
FIGURE 7: THE AMINO ACID SEQUENCES OF THE VARIABLE HEAVY AND LIGHT CHAINS OF DIFFERENT ANTI-GM2 ANTIBODIES WERE ALIGNED.	26
FIGURE 8: ANTIBODY STRUCTURE MODELS SHOWING VARIABLE HEAVY AND LIGHT CHAINS WITH COMPLEMENTARY DETERMINING REGIONS WERE PREDICTED USING A BODYBUILDER2 [120–122].	28
FIGURE 9: PRODUCTION OF ANTI-GM2 ANTIBODIES BY TRANSFECTION OF HEK293T CELLS WAS SUCCESSFUL.	30
FIGURE 10: THERMAL UNFOLDING PROFILES OF TESTED ANTI-GM2 IgG ANTIBODY CLONES, REVEALED DIFFERENCES IN THEIR THERMOSTABILITY, BUT STORAGE AT DIFFERENT TEMPERATURES DID NOT AFFECT STABILITY OF ANTI-GM2-AB3 IgG OVER TIME.	32
FIGURE 11: ANTI-GM2 IgG ANTIBODIES SPECIFICALLY RECOGNIZED GM2 AND MAINTAINED THEIR SPECIFICITY UPON SWITCHING TO IgM ISOTYPE.	34
FIGURE 12: ANTI-GM2 ANTIBODIES DEMONSTRATED VARIABLE BINDING SPECIFICITY TO GM2 <sup>+</sup> NEUROBLASTOMA CELLS	35
FIGURE 13: GM2-AB3 IgG DEMONSTRATED VARIABLE BINDING SPECIFICITY TO DIFFERENT TUMOR TYPES.	36
FIGURE 14: SEVERAL ANTI-GM2 ANTIBODIES SELECTIVELY INDUCED COMPLEMENT-DEPENDENT CYTOTOXICITY <i>IN VITRO</i> AGAINST GM2-EXPRESSING NEUROBLASTOMA CELLS, BUT NOT AGAINST <i>B4GALNT1</i> KNOCKOUT CELLS, LACKING GM2 AND GD2.	38
FIGURE 15: GM2-AB3 IgG WAS ABLE TO INDUCE ANTIBODY-DEPENDENT CELLULAR CYTOTOXICITY AGAINST NEUROBLASTOMA CELLS <i>IN VITRO</i> .	39
FIGURE 16: TREATMENT OF POORLY HUMANIZED MICE WITH GM2-AB3 IgG DID NOT SHOW ANY EFFECTS ON TUMOR GROWTH.	41
FIGURE 17: MULTIPLE TREATMENTS WITH GM2-AB3 IgG SLOWED DOWN TUMOR GROWTH <i>IN VIVO</i> .	43
FIGURE 18: CLONING STRATEGY FOR INSERTION OF KM966 VARIABLE SEQUENCES INTO THE pVITRO-IgG1/k EXPRESSION PLASMID.	77

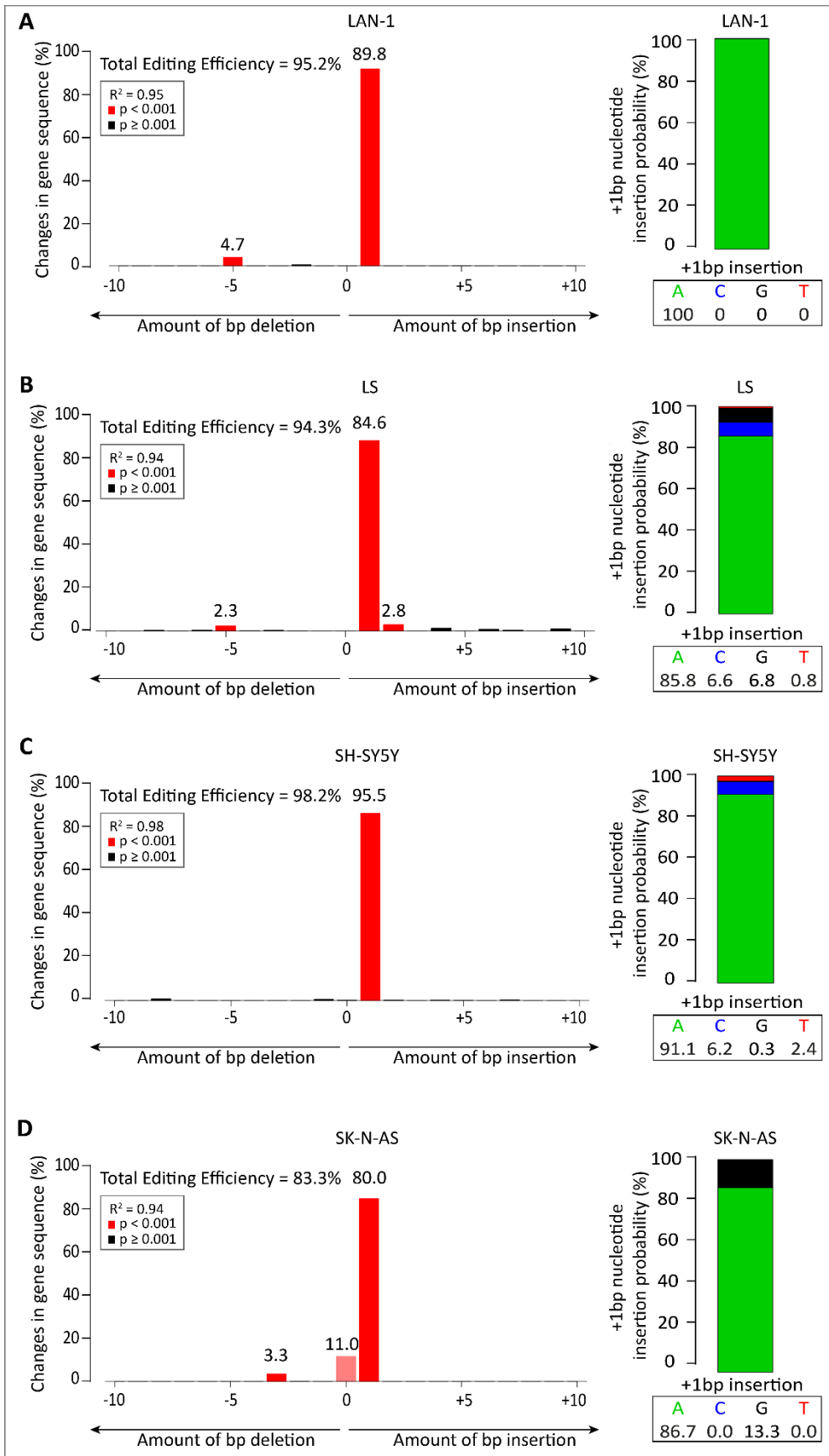
## 12 List of Tables

TABLE 1: NEUROBLASTOMA PATIENT DATA AND SAMPLE CHARACTERISTICS.....	22
TABLE 2: GD2 AND GM2 EXPRESSION LEVELS ON CELLS FROM NEUROBLASTOMA PATIENT SAMPLES.....	23
TABLE 3: INSTRUMENTS USED FOR ANALYSIS AND EXPERIMENTAL SETUP.....	64
TABLE 4: CONSUMABLES USED FOR <i>IN VITRO</i> AND <i>IN VIVO</i> EXPERIMENTS.....	64
TABLE 5: CHEMICALS, REAGENTS AND SOLUTIONS USED FOR <i>IN VITRO</i> EXPERIMENTS.....	65
TABLE 6: DIFFERENT COMPOSITIONS OF THE GROWTH MEDIA AND BUFFERS USED FOR CELL CULTURE.....	66
TABLE 7: OVERVIEW OF CELL LINES USED IN THIS WORK AND APPROPRIATE CULTURE MEDIUM.....	67
TABLE 8: UTILIZED COMMERCIAL KITS.....	68
TABLE 9: ENZYMES AND BUFFERS USED FOR CLONING.....	68
TABLE 10: OLIGONUCLEOTIDE SEQUENCES USED FOR CLONING OF ANTIBODY EXPRESSION PLASMIDS OR FOR CRISPR/CAS9 KNOCKOUT PLASMIDS.....	69
TABLE 11: ORIGINAL PLASMIDS USED FOR CLONING AND THE NEW PLASMIDS GENERATED IN THIS WORK WITH THEIR PROPERTIES AND USE.....	71
TABLE 12: ANTIBODIES USED FOR FLOW CYTOMETRIC OR WESTERN BLOT ANALYSIS.....	72
TABLE 13: SOFTWARE USED FOR ANALYSIS OF DATA.....	73

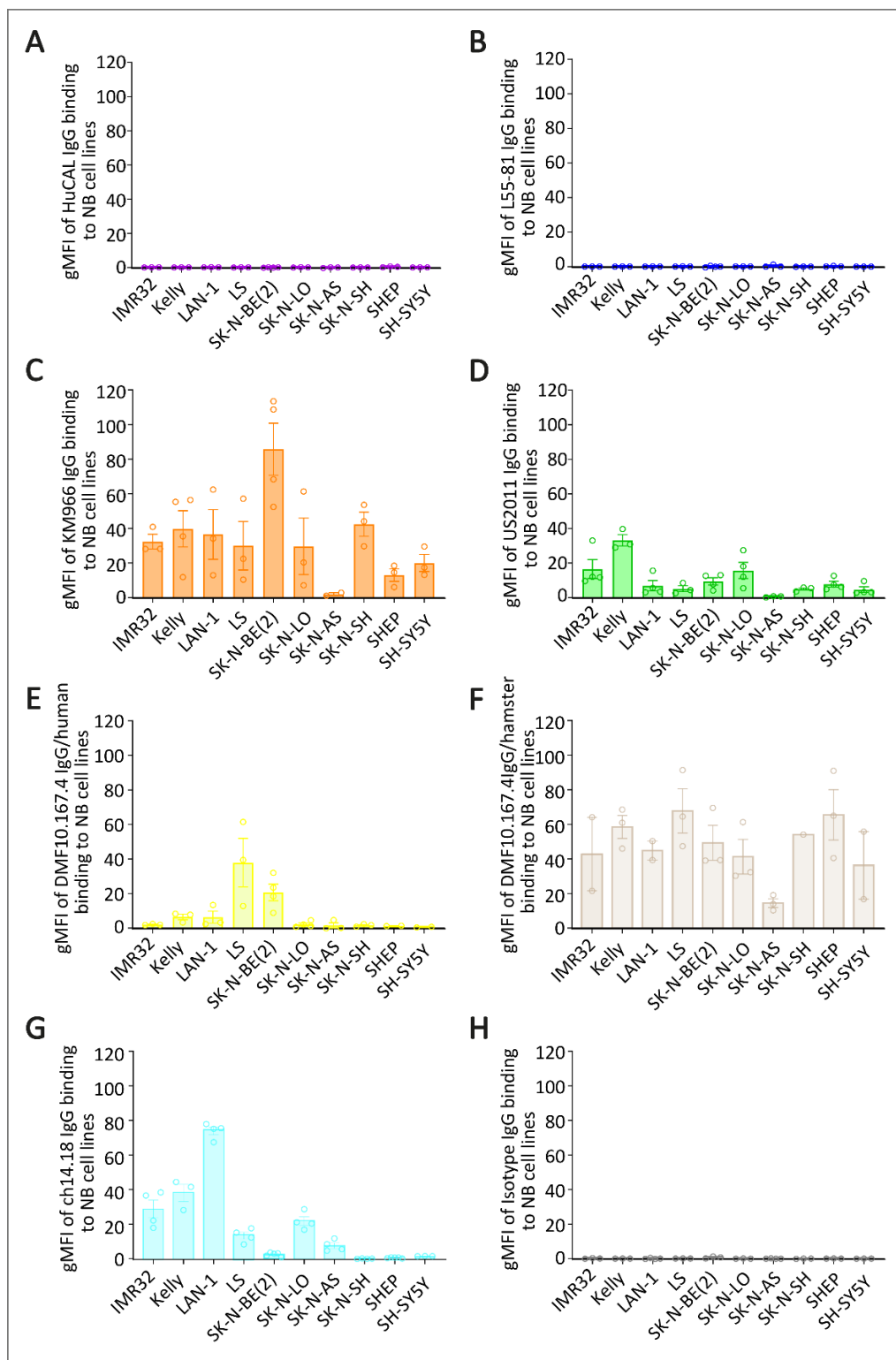
## **13 Appendix**

### **13.1 Appendix A: Supplementary Data**

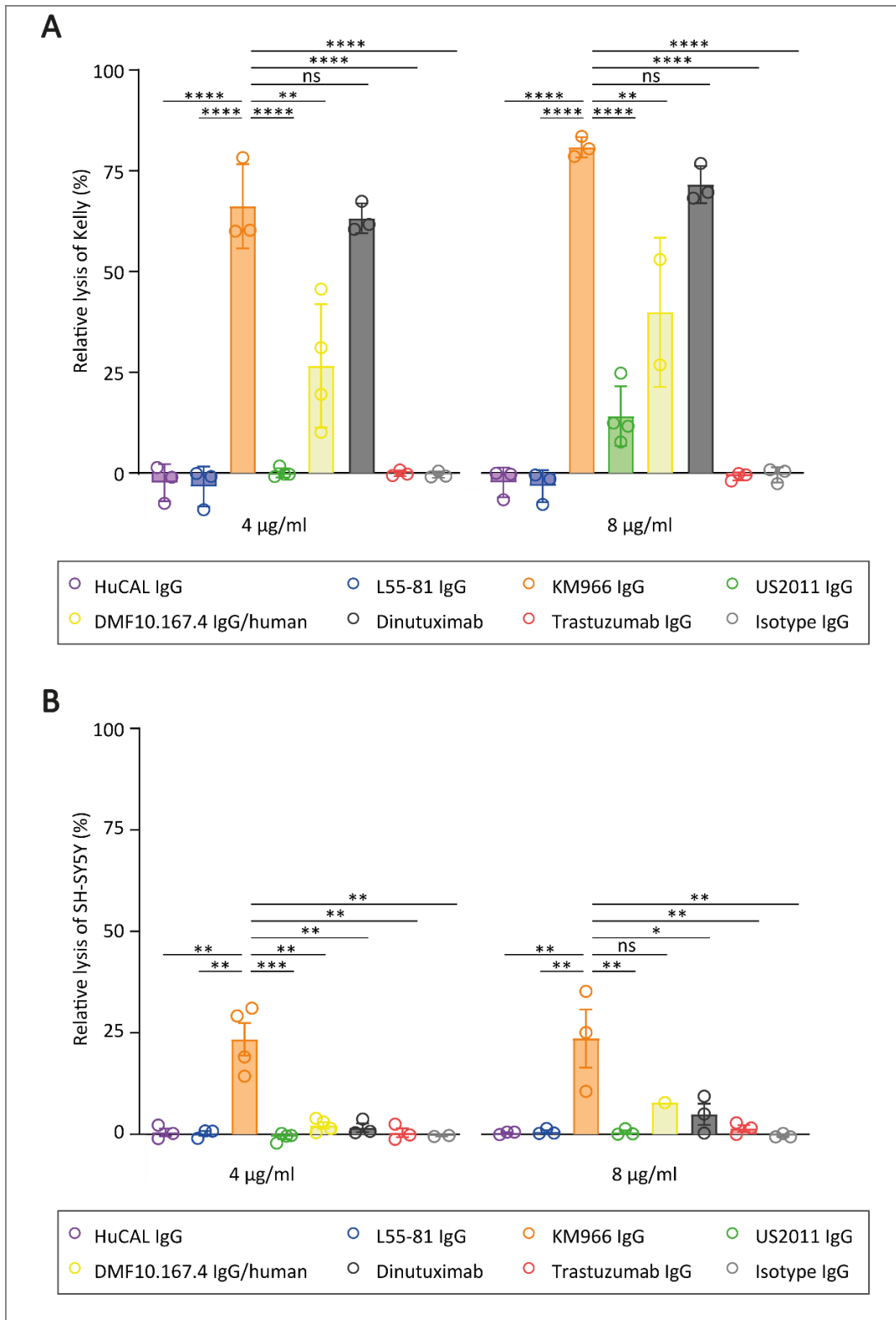
This chapter presents some supplementary experiments that further elaborate on the results presented in the results section. This additional information serves to provide a more comprehensive understanding of the results of this thesis.



**Appendix A-1: The spectrum of genome editing after CRIPSR/Cas9-based knockout of the *B4GALNT1* gene.** The percentage of indels and the probability of nucleotides at the +1bp insertion site is depicted for LAN-1 (A), LS (B), SH-SY5Y (C), and SK-N-AS (D). bp: base pair.



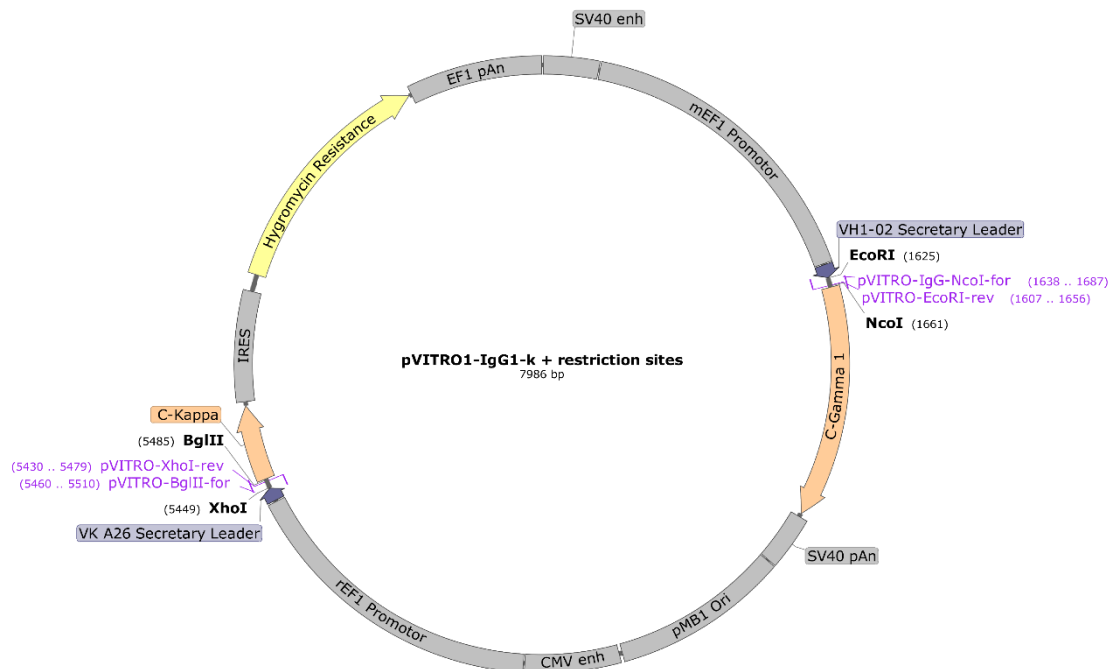
**Appendix A-2: The analysis of the binding of each anti-GM2 antibody tested to neuroblastoma cell lines revealed distinct differences in their binding specificities.** Flow cytometric staining was utilized to assess the binding of GM2-AB1 IgG (A), GM2-AB2 IgG (B), GM2-AB3 IgG (C), GM2-AB4 IgG (D), GM2-AB5 (E), and hamster DMF10.167.4 IgG (F), using 1  $\mu$ g of the respective antibody. Additionally, the binding of the anti-GD2 antibody ch14.18 IgG (G) and the Isotype IgG (H) were also determined. The geometric mean fluorescent intensities (gMFI) of individual measurements, along with the SEM, were depicted and normalized to the secondary control (an APC-labeled anti-human IgG antibody). At least one independent representative experiment was performed to obtain these results. gMFI: geometric mean fluorescence intensity; NB: neuroblastoma.



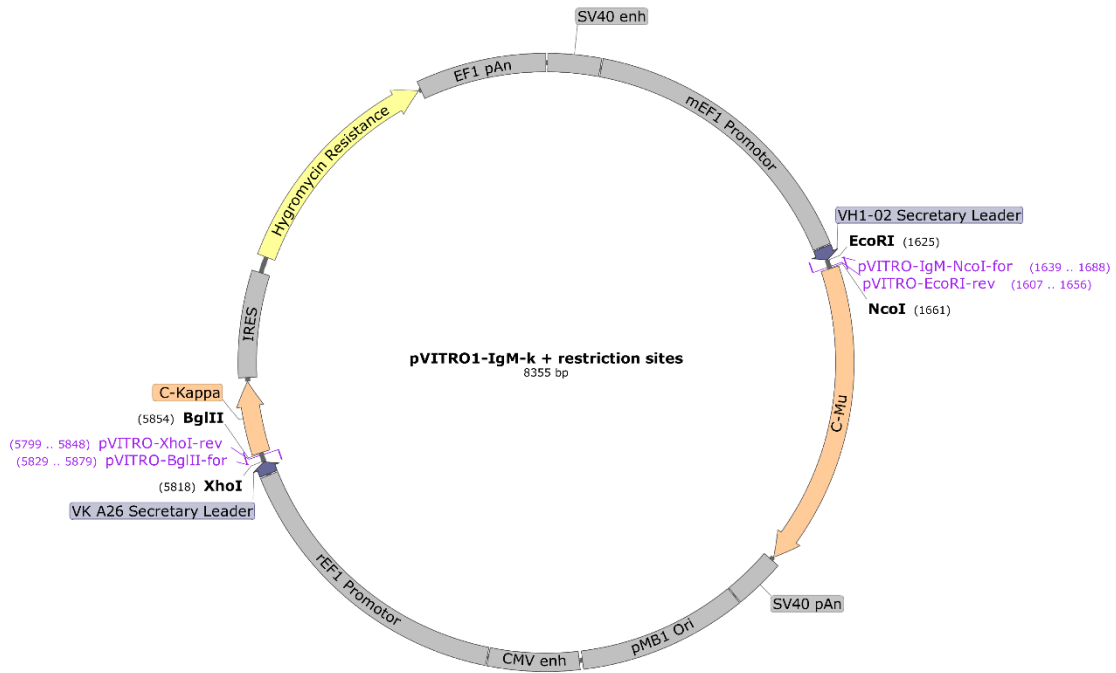
**Appendix A-3: Anti-GM2 antibodies showed different levels of complement-dependent cytotoxicity against various neuroblastoma cell lines.** The complement-dependent cytotoxic activity of GM2-AB1 IgG, GM2-AB2 IgG, GM2-AB3 IgG, GM2-AB4 IgG and GM2-AB5 IgG was assessed for Kelly (**A**) and SH-SY5Y (**B**) using the InCuCyte Live Cell Imaging system. The neuroblastoma cells were incubated with 12.5% human serum and either 4 µg/ml or 8 µg/ml of the respective antibody for 2 h. Trastuzumab IgG and Isotype IgG were used as negative controls while the anti-GD2 antibody Dinutuximab was used as a positive control. The columns show the mean percentage of relative lysis from at least  $n = 3$  independent representative experiments and SEM. Statistics represent multiple unpaired t-tests with \*\*\*\*  $P < 0.0001$ , \*\*\*  $P < 0.001$ , \*\*  $P < 0.01$ , \*  $P < 0.05$ ; ns =  $P \geq 0.05$ .

## 13.2 Appendix B: Plasmid Gene Cards

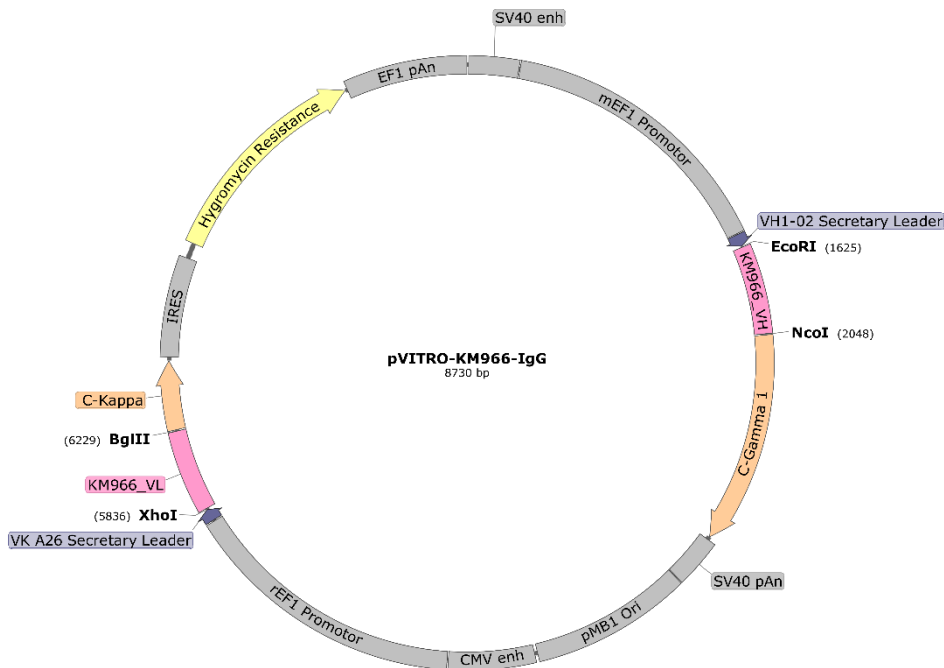
Exemplary plasmid maps of the plasmids 10, 11, 18, 20, and 25 generated in this work are shown in this section.



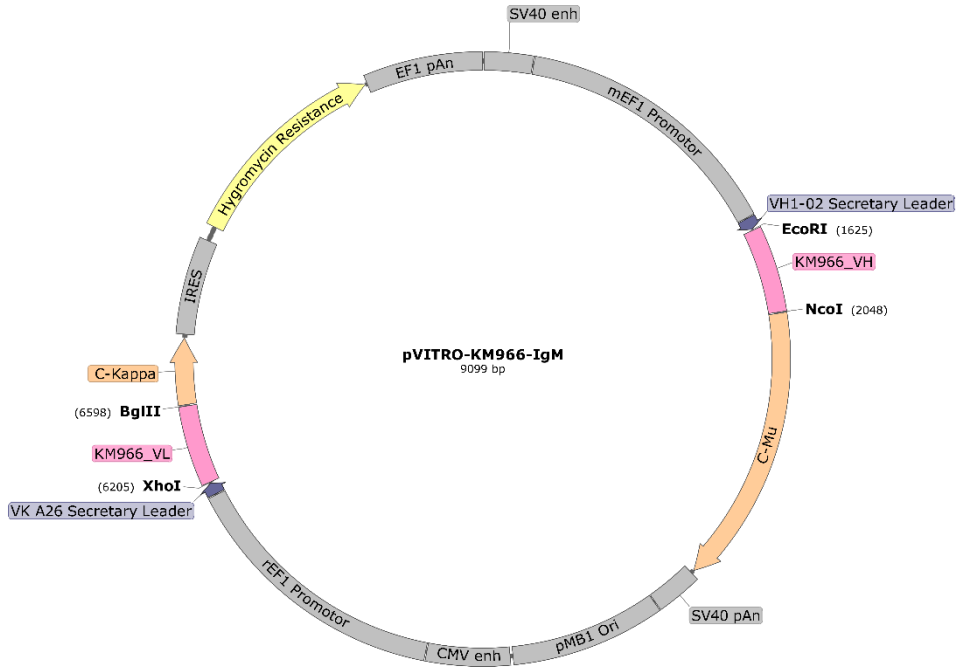
**Appendix B-1: Plasmid map of pVITRO1-IgG1-k + restriction sites.** The additionally inserted restriction sites EcoRI, NcoI, BglIII, and XhoI are highlighted (black) and used primer pairs are shown (purple). The plasmid encodes the constant heavy and constant light sequences (orange) of an IgG1 antibody. A hygromycin resistance cassette (yellow) is present and was used for selection in *E. coli* bacterial cultures. This construct was used for insertion of variable anti-GM2 antibody sequences.



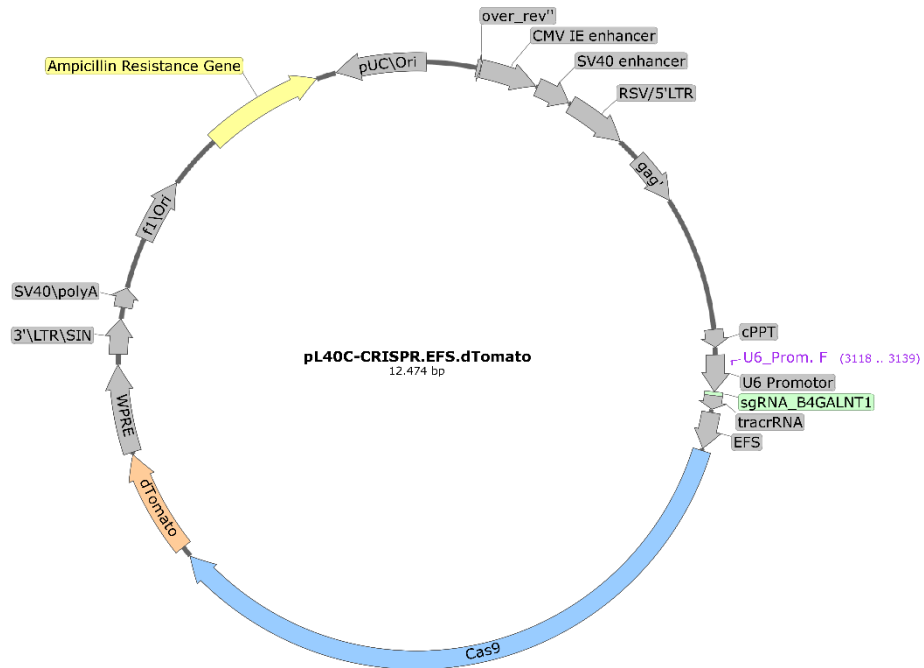
**Appendix B-2: Plasmid map of pVITRO1-IgM-k + restriction sites.** The additionally inserted restriction sites EcoRI, NcoI, BglIII, and XhoI are highlighted (black) and used primer pairs are shown (purple). The plasmid encodes the constant heavy and constant light sequences (orange) of an IgM antibody. A hygromycin resistance cassette (yellow) is present and was used for selection in *E. coli* bacterial cultures. This construct was used for insertion of variable anti-GM2 antibody sequences.



**Appendix B-3: Plasmid map of pVITRO1-KM966-IgG.** The variable heavy and light sequences of KM966 were inserted after restriction of the plasmid and inserts with restriction enzymes (black). Upstream of the variable sequences is a secretary leader sequence (blue) which is responsible for the secretion of the antibody. The plasmid encodes the constant heavy and constant light sequences (orange) of an IgG1 antibody. A hygromycin resistance cassette is present and was used for selection in *E. coli* bacterial cultures. This construct was used for IgG antibody expression.



**Appendix B-4: Plasmid map of pVITRO1-KM966-IgM.** The variable heavy and light sequences of KM966 were inserted after restriction of the plasmid and inserts with restriction enzymes (black). Upstream of the variable sequences is a secretary leader sequence (blue) which is responsible for the secretion of the antibody. The plasmid encodes the constant heavy and constant light sequences (orange) of an IgM antibody. A hygromycin resistance cassette is present and was used for selection in *E. coli* bacterial cultures. This construct was used for IgM antibody expression.



**Appendix B-5: Plasmid map of pL40C-CRISPR.EFS.dTomato.** The single guide RNA for knockout of the *B4GALNT1* gene was inserted downstream of the U6 promoter. The plasmid encodes Cas9 (blue), the dTomato fluorescent reporter (orange) and an ampicillin resistance cassette (yellow) for selection in *E. coli* bacterial cultures. The final plasmid was sequenced using the indicated primer (purple) to verify correct insertion.

### 13.3 Appendix C: Hazardous substances

**Appendix C-1: Hazardous substances according to GHS.** GHS Symbols and H and P statements are listed according to PubChem chemical information online database or to the safety datasheet supplied by the manufacturer of the substance [245].

Name	GHS symbol	H and P statements
Ampicillin	07, 08	H317, H334, P261, P272, P280, P285, P302+P352, P304+P341, P321, P333+P313, P342+P311, P363, P501
CaCl <sub>2</sub>	07	H319, P264, P280, P305+P351+P338, P337+P3137
Chloroquine	07	H302, P264, P270, P301+P312, P330, P501
DTT	07	H302, H315, H319, H335, P261, P264, P264+P265, P270, P271, P280, P301+P317, P302+P352, P304+P340, P305+P351+P338, P319, P321, P330, P332+P317, P337+P317, P362+P364, P403+P233, P405, P501
DMSO	07	H315, H319, H335, P261, P264, P271, P280, P302+P352, P304+P340, P305+P351+P338, P312, P321, P332+P313, P337+P313, P362, P403+P233, P405, P501
EDTA	07	H319, P264, P280, P305+P351+P338, P337+P313
Ethanol	02	H225, P210, P233, P240, P241, P242, P243, P280, P303+P361+P353, P370+P378, P403+P235, P501
Ethidium bromide	06, 07, 08	H302, H330, H341, P201, P202, P260, P264, P270, P271, P281, P284, P301+P312, P304+P340, P308+P313, P310, P320, P330, P403+P233, P405, P501
Hygromycin	05, 06, 08	H300+H310+H330, H318, H334, P260, P261, P262, P264, P264+P265, P270, P271, P280, P284, P301+P316, P302+P352, P304+P340, P305+P354+P338, P316, P317, P320, P321, P330, P342+P316, P361+P364, P403+P233, P405, P501
Isoflurane	07, 08	H336, H373, P260, P261, P271, P304+P340, P319, P403+P233, P405, P501
Isopropanol	02, 07	H225, H319, H336, P210, P233, P240, P241, P242, P243, P261, P264, P271, P280, P303+P361+P353, P304+P340, P305+P351+P338, P312, P337+P313, P370+P378, P403+P233, P403+P235, P405, P501
Methanol	02, 06, 08	H225, H301, H311, H331, H370, P210, P233, P240, P241, P242, P243, P260, P261, P264, P270, P271, P280, P301+P316, P302+P352, P303+P361+P353, P304+P340, P308+P316, P316, P321, P330, P361+P364, P370+P378, P403+P233, P403+P235, P405, P501
Paraformaldehyde	05, 06, 07, 08	H301, H311, H314, H317, H331, H341, H350, P201, P202, P260, P261, P264, P270, P271, P272, P280, P281, P301+P310, P301+P330+P331, P302+P352, P303+P361+P353, P304+P340, P305+P351+P338, P308+P313, P310, P311, P312, P321, P322, P330, P333+P313, P361, P363, P403+P233, P405, P501
pNPP	07	H302, P264, P270, P301+P317, P330, P501
Penicillin/Streptomycin	07, 08	H317, H334, H360, P201, P202, P261, P280, P284, P302 + P352, P333 + P313, P342 + P311, P308 + P313, P362, P304 + P340
Polybrene	07	H302, P264, P270, P301+P312, P330, P501
Proteinase K	08	H334, P261, P280, P284, P304 + P340, P342
SDS	02, 05, 07	H228, H302, H315, H318, H319, H332, H335, H412, P210, P240, P241, P261, P264, P270, P271, P273, P280, P301+P312, P302+P352, P304+P312, P304+P340, P305+P351+P338, P310,

		P312, P321, P330, P332+P313, P337+P313, P362, P370+P378, P403+P233, P405, P501
Sodium pyruvate	07	H317, H319, P261, P264, P272, P280, P302+P352, P305+P351+P338, P321, P333+P313, P337+P313, P363, P501
Tris	07	H315, H319, H335, P261, P264, P264+P265, P271, P280, P302+P352, P304+P340, P305+P351+P338, P319, P321, P332+P317, P337+P317, P362+P364, P403+P233, P405, P501
Triton X 100	05, 07, 09	H302, H318, H411, P270, P273, P280, P305+P351+P338, P310
Trypan blue	09	H350, P203, P280, P318, P405, P501

---

### 14 Acknowledgement

At this point of my thesis, I want to express my gratitude to all the wonderful people who supported me during my time at the Research Institute Children's Cancer Center Hamburg over the last years.

First and foremost, I would like to thank Prof. Dr. Ingo Müller for giving me the opportunity to be part of this amazing research group. It has been an exciting journey that has already started when I joined the team for my master's thesis. I am thankful that you made it possible for me to conduct my PhD project in this laboratory, working on this interesting and challenging project. Your feedback during lab meetings, journal clubs, or our neuroblastoma meetings was always helpful and constructive. There were many ideas that moved the project forward. I am grateful for the opportunity to learn to work in a self-organized manner and being able to develop my skills in the field of scientific research.

Next, I would like to thank Prof. Dr. Wolfram Brune for supervising my practical work and evaluating the written part of my thesis. Even though our regular meetings were an extra effort, I really appreciate that you took the time to listen to my progress and discuss scientific issues with me.

I would like to express my gratitude to the 'Werner Otto Stiftung' and the 'Fördergemeinschaft Kinderkrebs-Zentrum Hamburg' for their financial support. Without them, this project wouldn't have been possible.

Special shoutout is directed to PD Dr. Kerstin Cornils and Dr. Benjamin Schattling the best lab supervisors I could have wished for. Your doors and ears were always open for me, and your support and encouragement helped me to overcome many obstacles and keep going when things got tough. Your patience, composure and expertise always helped to find new ideas when the frustration level was at its highest. You provided me with constructive feedback and advice and helped to move the project forward. Another thanks goes out to you Ben for teaching me how to work with mice, so that I managed not to be afraid of them and not to be bitten (yet). I learned a lot from you, which encompassed not only project-related knowledge, but also various new aspects of football.

A huge thank you is directed to Isabelle Bley, my fellow team member in 'Team Neuroblastoma'. Your open-mindedness and helpful attitude made every discussion productive and enjoyable. Mostly, very good ideas emerged from our conversations, and we motivated each other, were happy about both our successes and comforted each other in the face of failures. Working with you was always a pleasure, and I will miss our fun times together. You helped me to grow with this project and I am sure that you will also succeed and find THE antibody! I hope we'll stay in touch, and you're always welcome to paint another wall at my place or taste Lukas' delicious food. You know the way to my home is not far to go.

I want to acknowledge all my colleagues at the Research Institute Children's Cancer Center Hamburg for creating a friendly and supportive work environment. Lunch breaks in N63 were always a highlight, and I enjoyed our little chats when I came over to use the IncuCyte. Thanks to Vanessa Thaden for always answering my messages and providing the materials I needed. And to my AG Müller colleagues, Anne Kruchen, Anna-Katharina Franke, Marianne Klokow, and Julia Spötter, your advice and technical support were invaluable. You always had an open ear when it came to challenging cloning strategies, problems with the MACSQuant, experimental setups, or even just small talk about weekend plans. Another special thanks is directed to Frauke Gotzhein, Lena Martin and Luise Hecht, who introduced me to lab work when I joined the team. I am also thankful that I was able to support and co-supervise several projects from our students. It was a pleasure to meet and work with you, Wiebke Jünemann, Yandamé Möller, Lynn Stückemann, and Sarah Gottwald. I enjoyed working closely together with each of you and I hope that I was also able to be of assistance to you. Our conversations at least helped me to expand my knowledge of different topics and I will remember a lot of funny and exciting moments with you in the lab and after closing time.

To Susanne Witt, Philipp Lewe, and Ronald Maitschke-Rajasekharan from the 'Centre for Structural Systems Biology', thank you for supplying me with tons of antibody. Most of this work wouldn't have been possible without your expertise and support in antibody production. Special thanks to the animal caretakers from the research animal facility who always kept an eye on the mice. Thank you, Nicole Lüder, for your help with animal handling and blood collection.

Finally, I would like to mention my family and friends and thank them from the bottom of my heart. Your support means the world to me, even if I haven't always shown it. Mama, Papa, Chiara, and Lukas, thank you for being by my side throughout my scientific journey with its ups and downs. It means a lot to me that you have paved the way for me to study and now be at this point in my science career. Even if you have not understood much of my work and what I do all day long, you always listened to my challenges and tried to offer help and encouraged me. Lukas, thank you for being patient during all those mouse-checking weekends when you waited for me in the car. Elisa and Luise, you've been amazing friends. I am happy that I have become close friends with both of you. Elisa, even though you live in the wrong half of Germany, it never feels like we're far apart when we talk on the phone (thanks to J5-Gauß). Your understanding of the challenges of scientific work and your encouraging words have been a constant source of strength for me.

### 15 Declaration of authorship

I hereby declare under oath that I have independently written the present dissertation and have not used any aids other than those stated. The submitted written version corresponds to the version on the electronic storage medium. I further affirm that this dissertation was not submitted in a previous doctoral procedure.

Hamburg, 18<sup>th</sup> September 2023

---

City, Date

---

Signature

